NASA/ TM–20240005376

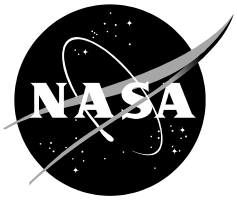

Advances in Thermoplastic Composites Over Three Decades – A Literature Review

Ronald Krueger
National Institute of Aerospace, Hampton, Virginia, USA

Andrew Bergan
NASA Langley Research Center, Hampton, Virginia, USA

May 2024

NASA STI Program Report Series

Since its founding, NASA has been dedicated to the advancement of aeronautics and space science. The NASA scientific and technical information (STI) program plays a key part in helping NASA maintain this important role.

The NASA STI program operates under the auspices of the Agency Chief Information Officer. It collects, organizes, provides for archiving, and disseminates NASA's STI. The NASA STI program provides access to the NTRS Registered and its public interface, the NASA Technical Reports Server, thus providing one of the largest collections of aeronautical and space science STI in the world. Results are published in both non-NASA channels and by NASA in the NASA STI Report Series, which includes the following report types:

- TECHNICAL PUBLICATION. Reports of completed research or a major significant phase of research that present the results of NASA Programs and include extensive data or theoretical analysis. Includes compilations of significant scientific and technical data and information deemed to be of continuing reference value. NASA counterpart of peer-reviewed formal professional papers but has less stringent limitations on manuscript length and extent of graphic presentations.

- TECHNICAL MEMORANDUM. Scientific and technical findings that are preliminary or of specialized interest, e.g., quick release reports, working papers, and bibliographies that contain minimal annotation. Does not contain extensive analysis.

- CONTRACTOR REPORT. Scientific and technical findings by NASA-sponsored contractors and grantees.

- CONFERENCE PUBLICATION. Collected papers from scientific and technical conferences, symposia, seminars, or other meetings sponsored or co-sponsored by NASA.

- SPECIAL PUBLICATION. Scientific, technical, or historical information from NASA programs, projects, and missions, often concerned with subjects having substantial public interest.

- TECHNICAL TRANSLATION. English-language translations of foreign scientific and technical material pertinent to NASA's mission.

Specialized services also include organizing and publishing research results, distributing specialized research announcements and feeds, providing information desk and personal search support, and enabling data exchange services.

For more information about the NASA STI program, see the following:

- Access the NASA STI program home page at http://www.sti.nasa.gov

- Help desk contact information:

https://www.sti.nasa.gov/sti-contact-form/
and select the "General" help request type.

NASA/TM–20240005376

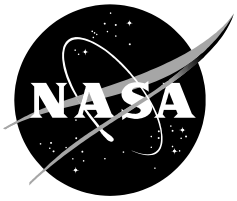

Advances in Thermoplastic Composites Over Three Decades – A Literature Review

Ronald Krueger
National Institute of Aerospace, Hampton, Virginia, USA

Andrew Bergan
NASA Langley Research Center, Hampton, Virginia, USA

National Aeronautics and
Space Administration

Langley Research Center
Hampton, Virginia, USA

May 2024

Available from:

NASA STI Program / Mail Stop 050
NASA Langley Research Center
Hampton, VA 23681-2199

Advances in Thermoplastic Composites Over More Than Three Decades - A Literature Review

Ronald Krueger
National Institute of Aerospace, Hampton, Virginia, USA

Andrew Bergan
NASA Langley Research Center, Hampton, Virginia, USA

ABSTRACT

Recently, there has been a renewed interest in thermoplastic composites driven mainly by advances in automation which can lead to significant cost reductions by increasing manufacturing rates while simultaneously reducing the part count and energy consumption relative to the manufacturing of thermoset composites. At the same time, new material systems have been developed and the thermoplastic composites prepreg material quality has improved over time. Additionally, thermoplastic composites have nearly infinite room-temperature shelf life and production scraps can be reused and retired parts can be recycled, providing opportunities for more sustainable operations and downstream markets. These factors have contributed to a strong interest in advancing thermoplastic composites for aerospace, automotive, and other industrial applications.

The objective of the present study is to assess the state of the art regarding the maturity and performance of thermoplastic composite materials and to document the advances made in manufacturing and assembly of thermoplastic composite structures. Therefore, more than 200 NASA reports, conference proceedings and journal papers spanning three and a half decades (1986-2022) were reviewed and the findings summarized. The current study, however, is limited in scope with a focus on the application of thermoplastic composites to aircraft structures. Further, the study does not provide a comprehensive assessment of the available literature but rather offers an overview of past and present research being conducted in the field of thermoplastic composites. The information provided may be used to identify gaps and help guide future research and development.

In this report, the opportunities offered by the use of thermoplastic composites in general and challenges encountered in particular are presented first. Second, an overview of thermoplastic materials is presented, manufacturing methods are discussed, and new methods for fastener-less assembly such as welding are introduced. Third, tests that have been performed on different levels of the building block, ranging from coupon to structural level, are presented. In particular, fracture toughness results for different thermoplastic composite materials are used to demonstrate their performance compared to state-of-the-art thermoset composites. Fourth, several examples of analyses are discussed including process modelling and progressive damage analysis (PDA). An extensive list of references and appendices with tables support the narrative. Lastly, a brief summary with outlook and recommendations for future research is provided.

LIST OF ABBREVIATIONS, ACRONYMS, AND SYMBOLS

Abbreviations and Acronyms

AFP	Automated Fiber Placement
ARMD	Aeronautics Research Mission Directorate
ASTM	ASTM International, standards organization
ATL	Automated Tape Laying
ATP	Automated Tow Placement
BE	Boundary Element
BK	Mixed-mode fracture criterion proposed by Benzeggagh and Kenane
CAI	Compression After Impact
CCM	Center for Composite Materials
CCM	Continuous Compression Molding
CDM	Continuum Damage Mechanics
C-ELS	Calibrated End-Loaded Split test/specimen
CEN	Center-Notched Tension test/specimen
CF	Carbon Fiber
CFRP	Carbon Fiber Reinforced Plastic
CTE	Coefficient of Thermal Expansion
CZM	Cohesive Zone Modeling
DCB	Double Cantilever Beam test/specimen
DEN	Double-Edge-Notched Tension test/specimen
DIC	Digital Image Correlation
DLR	German Aerospace Center
DoE	Design of Experiments
EDT	Edge Delamination Test
ELS	End-Loaded Split test/specimen
ENF	End-Notched Flexure test/specimen
EVP	Elastic-visco-plastic
FAA	Federal Aviation Administration
FCC	Face Centered Cubic
FE	Finite Element
FST	Fire, Smoke, and Toxicity
GF	Glass Fiber
GMC	Generalized Method of Cells
HG	Homogenization
HDPE	High-density polyethylene
HiCAM	Hi-Rate Composite Aircraft Manufacturing
HSR	High Speed Research
ICI	Imperial Chemical Industries
ILSS	Inter-Laminar Shear Strength
ISC	In-Situ Consolidation
ISO	International Organization for Standardization
JIS	Japanese Industrial Standard
LAMMPS	Large-scale Atomic/Molecular Massively Parallel Simulator
LaRC	Langley Research Center
LATP	Laser-Assisted Tape Placement
LM-PAEK	Low-Melt Polyaryletherketone
MASC	Modeling for Affordable Sustainable Composites
MD	Molecular dynamics
MFFD	Multifunctional Fuselage Demonstrator
MMA	Methylmethacrylate

MMB	Mixed-Mode Bending test/specimen
NASA	National Aeronautics and Space Administration
NCAMP	National Center for Advanced Materials Performance
NCF	Non-Crimp Fabric
NIAR	National Institute for Aviation Research
NLR	Royal Netherlands Aerospace Centre
OOA	Out of Autoclave
PA	Polyamid
PAEK	Polyaryletherketone
PC	Polycarbonate
PDA	Progressive Damage Analysis
PEEK	Polyetheretherketone
PEI	Polyetherimide
PEKK	Polyetherketoneketone
PETI	Phenylethynyl-terminated imide
PI	Polyimides
PMMA	PolyMethyl-MethAcrylate
PP	Polypropylene
PPS	Polyphenylene-sulphide
PPSU	Polyphenylsufone
PS	Polysulfones
PW	Plain Weave fabric
SBS	Short Beam Shear test/specimen
SEM	Scanning electron microscope
SENB	Single-Edge Notched Bending test/specimen
SENT	Single-Edge-Notch Tensile test/specimen
SLB	Single-Leg Bending test/specimen
SLS	Single-Lap Shear test/specimen
TP	Thermoplastic
TPC	Thermoplastic Composite
TRL	Technical Readiness Level
TS	Thermoset
TSC	Thermoset Composites
TuFF	Tailored Universal Feedstock for Forming
UAM	Urban Air Mobility
UD	Unidirectional
UHMWPE	Ultra-high-molecular-weight polyethylene
UMAT	User Material Subroutine in Abaqus/Standard®
ULI	University Leadership Initiative
VE	Viscoelastic
VCCT	Virtual Crack Closure Technique
VP	Viscoplastic
VUMAT	User Material Subroutine in Abaqus/Explicit®
WSU	Wichita State University
2D	Two-dimensional
3D	Three-dimensional

Symbols

G	Energy release rate
G_c	Critical energy release rate, fracture toughness
G_{Ic}	Mode I fracture toughness
G_{IIc}	Mode II fracture toughness
H	Magnetic field intensity
J	Induced current density
η	Exponent for mixed-mode fracture criterion curve fit

INTRODUCTION

Glass and carbon fiber reinforced polymer matrix composite materials have emerged as the materials of choice for increasing the performance and reducing the weight and cost of military aircraft, general aviation aircraft, transport aircraft, and space launch vehicles. Many different organizations worldwide, including NASA Langley Research Center (LaRC), have conducted research on composites over the past several decades which led to major advancements in the ability to design, fabricate, and analyze large complex aerospace structures [1-3]. Ultimately, this research made the successful development and production of today's commercial composite transport aircraft such as the Boeing B-787, Airbus A-220 and A-350 possible. Today, large structural components for these airliners such as the fuselage, wing and empennage are primarily made of high-performance composites consisting of laminated carbon fiber unidirectional plies or fabric embedded in a thermoset polymer matrix. Typically, these components are cured in an autoclave in a highly controlled process cycle that specifies temperature ramp-up, hold and cool-down as well as applied pressure to achieve consolidated parts of high quality.

At present, the production rate using these established processes for thermoset composites is low. To reach the same output currently achieved for single-aisle commercial aircraft made of aluminum, the manufacturing rate of composite aircraft needs to be increased by 400–600%. Thus mature, affordable, high-rate composite manufacturing and assembly technologies for thermoset and thermoplastic composites need to be developed as planned in NASA's Hi-Rate Composite Aircraft Manufacturing (HiCAM) project [4-6]. One approach to achieve an increase in production rate is to develop new thermoset resins that allow for out-of-autoclave (OOA) processing [7]. Another approach favors the use of thermoplastic matrix based composites which promise advantages of unlimited shelf life of the prepreg and rapid, inexpensive processing, such as in-situ consolidation during automated fiber placement (AFP) as well as fastener-less assembly using newly developed welding techniques [8-10].

The objective of the present study is to assess the state of the art regarding the maturity and performance of thermoplastic composite materials and to document the advances made in manufacturing and assembly of thermoplastic composite structures. More than 200 NASA reports, conference proceedings and journal papers spanning three and a half decades (1986–2022) were reviewed and the findings summarized. A first peak in research activities was observed during the late 1980s and 1990s. Already then, the high cost of manufacturing and assembly of high-performance composites was identified as an obstacle for the widespread use of composite materials in primary aircraft structures [11]. Thus, a major reason for the interest in thermoplastic matrix-based composites was their potential advantage of inexpensive processing and their promise of much greater fracture toughness relative to the typical epoxy resins. Improvement in resin toughness was deemed desirable as one approach to improving delamination resistance and damage tolerance in composite structures [12] and led to focused research in thermoplastic matrix based composites in the US and Europe [13-18]. An obstacle encountered was the *boardiness* of the thermoplastic tape material at room temperature [19]. This *boardiness* produces a stiff, occasionally uneven tape that is prone to producing gaps and splits and can also cause in-plane waviness of the material. The waviness may in turn lead to some tape width inconsistency which subsequently causes problems during tape slitting, which relies on consistent tape widths to stay within specifications. Further, unlike a thermoset prepreg, which has tack at room temperature that facilitates ply-to-ply adhesion during layup, a thermoplastic prepreg is dry and tack-less [9, 20]. The *boardiness* caused particular problems in the manufacturing of thin, double-curved shell-type structures [19]. Following reduced defence spending in the 1990s and the development of second-generation toughened epoxies which subsequently led to an increase in fracture toughness of the composite, the research refocused on thermosets and the interest in thermoplastic composites for subsonic transport aircraft declined [19-20]. Research and development of thermoplastic composites, however,

continued with a focus on high-temperature applications such as high-speed and supersonic aircraft [1].

With a targeted rate of 60 aircraft per month or more for new designs, there has been renewed interest in using thermoplastic composites for transport aircraft since they offer cycle times, materials storage, toughness, and recyclability advantages that could until recently not be matched by thermosets [20]. Thus, another wave of research activities started in the late 2000s in Europe [21-23] and is still ongoing due to national aerospace consortia (e.g. *TAPAS1* and *TAPAS2* in The Netherlands) and large research and development projects (e.g. *STUNNING*) funded by the European Union under the *Clean Sky* (2008–2016), *Clean Sky 2* (2017–2021) and *Horizon 2020* (2014–2021) programs [24-28]. An overview of different projects is given in Figure 1.

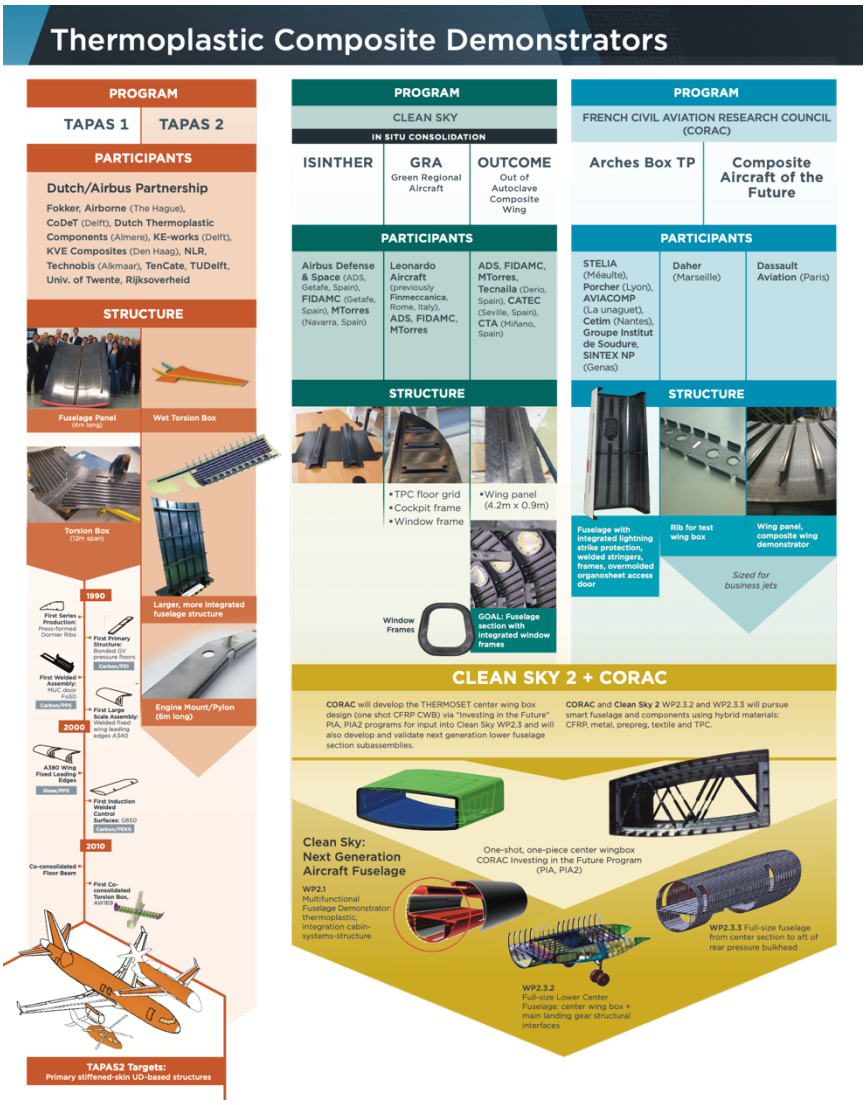

Figure 1: European research and development projects.[1]

[1] Image source *CompositesWorld* [25], used with permission.

In the United States, the National Center for Advanced Materials Performance (NCAMP) at Wichita State University (WSU) works with the FAA and industry partners to qualify material systems and populate a shared materials database that can be viewed publicly. Recently, the first two thermoplastic composite materials were NCAMP-qualified [29-38]. Further, the National Institute for Aviation Research (NIAR) at WSU has developed material and process specifications for automated fiber placement (AFP) systems following NCAMP protocols. This effort is a part of the *Modeling for Affordable Sustainable Composites* (MASC) program, sponsored by the Air Force Research Laboratory (Wright-Patterson Air Force Base, Ohio, U.S.). The MASC program focuses on developing a certification framework for enabling novel materials and advanced structural concepts used for automated manufacturing technologies [38]. NASA's Aeronautics Research Mission Directorate (ARMD) is funding the University of South Carolina and several partner institutions through the University Leadership Initiative (ULI) for the development of thermoplastic technologies for urban air mobility (UAM) vehicles. The project is titled *Synthetic Design Synthesis of 'Thermoplastic UD Tape based, Fastener-free Assemblies' for Urban Air Mobility Vehicles* with a focus on welding [39-42]. Also through the NASA/ARMD/ULI, the Center for Composite Materials (CCM) at the University of Delaware is continuing the development of their new high-performance material referred to as *Tailored Universal Feedstock for Forming* (TuFF) preforms, which can be combined with thermoset or thermoplastic resin to produce a prepreg that can be stamped into complex shapes [43-44].

The current study is limited in scope and does not provide a complete review and comprehensive assessment of the available literature but rather offers an overview and summary of past and present research being conducted in the field of thermoplastic composites. The information provided may be used as a stepping stone and motivation for future research. The current focus is on the application to aircraft structures. Although there are significant overlaps, thermoplastic composites as an enabling technology for space applications is discussed in detail elsewhere [45]. In this report, the opportunities offered by the use of thermoplastic composites in general, and challenges encountered in particular, are presented first. Second, an overview of thermoplastic materials is presented. Manufacturing methods are discussed and new methods for fastener-less assembly such as welding are introduced. Third, tests that have been performed on different levels of the building block, ranging from coupon to structural level, are presented. Coupon-level tests referenced were typically used to assess material properties while tests on the element and structural level were performed to assess the structural performance of the thermoplastic composite and for model evaluation. In particular, fracture toughness results for different thermoplastic composite materials were used to demonstrate their performance compared to state-of-the-art thermoset composites. Fourth, several examples of analyses are discussed, including buckling simulations, process modelling and progressive damage analysis (PDA). Lastly, a brief summary with outlook and recommendations for future research is provided. Three appendices with tables support the narrative.

OPPORTUNITIES AND CHALLENGES FOR THERMOPLASTIC COMPOSITES

Motivation To Use Thermoplastic Matrix Based Composites

High cost of manufacture and assembly was identified as a major obstacle to the widespread use of high-performance composites in primary aircraft structures [1, 11]. Thus, the demand for cost-effective techniques for the fabrication and joining of primary airframe structure led to the investigation of thermoplastic composite (TPC) materials [11]. Thermoplastic composites are attractive materials due to their potential advantages of unlimited shelf life and rapid, inexpensive processing, an advantage due to their intrinsic characteristic which allows them to be melted and molded several times without suffering significant property losses. Unlike composites made with a thermoset matrix, curing TPCs requires neither complex chemical reactions or lengthy curing processes. Thus, a major advantage of TPC over thermoset composites (TSC) is cycle time reduction. However, TPC parts cannot compete cost-wise simply by using the same automated layup and autoclave consolidation process currently used for thermoset composite primary structures [46]. Press and diaphragm forming methods are lowering production costs for mass-produced TPC structures. Although press and diaphragm forming methods can provide a cost improvement over autoclave processing, setup and new tooling costs are only suitable for large production runs [46]. The capability of TPC materials to be melted and molded several times creates the ability to join components via fusion bonding or welding which presents an attractive alternative to the conventional methods such as mechanical fastening and adhesive bonding which are used to join TSC parts today [8, 26, 47]. Melting and remelting also improve recycling, repair and maintenance capabilities compared to their TSC counterparts [48]. Further, TPC materials are considered to be more damage tolerant than TSC materials. The semi-crystalline nature of the TP polymers offers several advantages over conventional TS resins such as excellent damage and impact resistance and they may be used over a wide range of temperatures. These improvements in resin toughness are desirable as one approach to improving delamination resistance and damage tolerance in composite structures [12, 15, 49-50]. The increased toughness makes TPCs an excellent choice for thin-walled structures such as aircraft fuselages, which can then be designed with lower weights and novel design features that reduce cost [25]. Certain polymers (PPS, PEI and PEEK) also offer excellent thermal stability which makes them suitable for high-temperature applications in military, aeroengine and prospective supersonic business jet programs where aero-frictional heating can generate continuous service temperatures that exceed the capabilities of structural epoxies [51-52]. Additionally, thermoplastics generally exhibit superior fire/smoke/toxicity performance and chemical resistance compared to their TSC counterparts [46, 51, 53]. To assess the economic advantage of TPCs, the specific strength was plotted versus the cost in Figure 2 [54]. A list of perceived advantages of TPCs relative to TSCs is provided in Table 1.

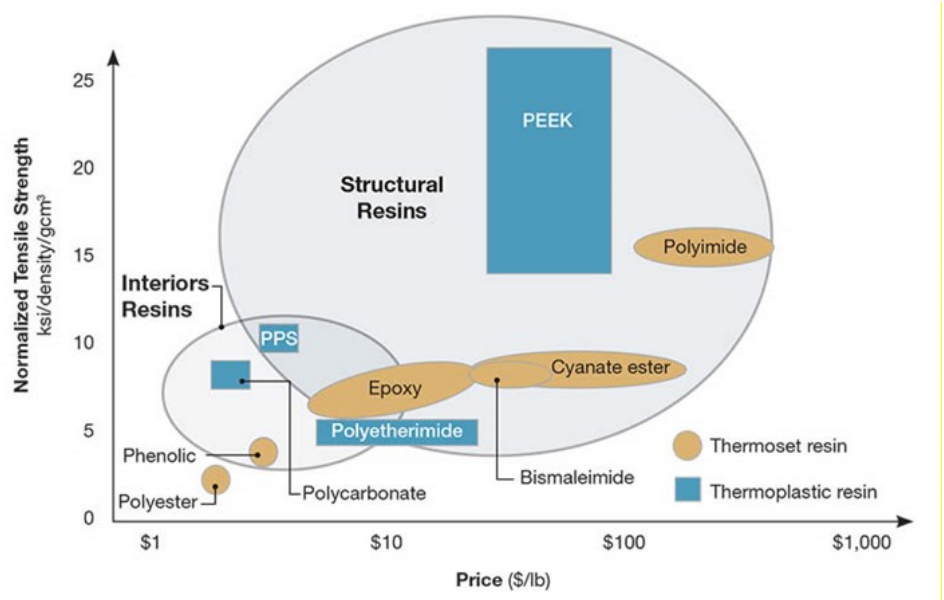

Figure 2: Performance versus cost for several classes of thermoset and thermoplastic composites.[2]

Difficulties And Challenges to Overcome When Considering Thermoplastic Composites

Thermoplastic composites still have significant barriers to overcome before they can be widely used in complex, contoured primary structures, particularly for aircraft produced in smaller volumes. The main drawback of high-performance TPCs (like PEEK, PEKK and PPS) concerns their processability that is more difficult than that of TSC systems [51]. Difficulties arise with regards to fiber impregnation due to higher viscosity, leading to a poor fiber-matrix interface, porosity and partial impregnation during production [55]. Further, the lack of tack and drapability of unidirectional TP-based prepreg tape makes it difficult to use on highly curved surfaces. Use of a material or preform on curved surfaces requires that the material be drapable and conform easily to the surface [56]. Other barriers include automated processing speed and quality, as well as a lack of developed repair technologies and cost [53]. Ideally, in-situ consolidation of the TPC part should be achieved, without requiring any secondary processing. However, additional research is needed to achieve true out-of-autoclave processing and ensure 100 percent consolidation and sufficient crystallization [53]. Achieving the desired level of crystallinity is critical in high-performance applications to attain the optimum combination of strength and toughness. Controlling the crystallinity requires stringent control of thermal cycles and a precise understanding of the crystallization kinetics and of the impact of crystallinity level on the performance of the component [55, 57-58]. Due to the elevated processing temperatures and the high matrix/fiber thermal expansion mismatch, substantial residual thermal stresses may develop in TPC parts. These thermally induced residual stresses may represent a significant fraction of the failure stress of the material, possibly leading to premature failure under mechanical load in the form of delamination and transverse cracking. The buildup of residual stresses during processing of amorphous resins begins only below the glass transition temperature, whereas for semicrystalline matrices it begins during the

[2] Image source *CompositesWorld* [54], used with permission.

crystallization process. In semicrystalline thermoplastics, crystallization causes a large volumetric shrinkage in addition to the usual coefficient of thermal expansion (CTE) induced thermal contraction and causes the buildup of additional residual stresses. As the composite's mechanical properties are dependent on the matrix constituents and the reinforcing phase, the development of thermal stresses is directly affected by the variations in temperature and degree of crystallinity occurring during processing [59, 60]. Also, thermoplastic tapes required for automated tape laying (ATL) and AFP lack the maturity of thermoset tapes and are more expensive than the epoxies with which they compete [9, 20].

During operation, different sensitivities to temperature have been observed for TPCs and TSCs. Thermoplastics may flow at elevated temperature while crosslinks in thermosets would prevent such irreversible creep behavior. The temperature and strain rate sensitivity therefore needs to be studied [61-62]. Also during operation, certain resins (PEIs) have shown to be susceptible to attack by anti-icing fluids and to moisture absorption, which limits their use in aircraft skins [52]. A list of observed disadvantages of TPCs relative to TSCs was added to Table 1.

Table I: Advantages and disadvantages of thermoplastic composites compared to thermoset composites.

Advantages	Disadvantages
• Higher production rate (reduced cycle time) • Welded joints have complete material fusion (no interface), potentially streamlining certification compared with bonded joints certification • Automated assembly via welding and/or co-consolidation can reduce assembly costs through unitization • Processing via remelting allows for post-forming, reconfiguration, and recycling • Higher fracture toughness results in improved durability, damage tolerance, and microcracking resistance • Good fatigue resistance • Essentially no shelf-life limitation (or out-time concern). Room-temperature storage saves cost. • Better performance in hot/wet conditions • Hydrolytic stability; low water absorption • Excellent fire, smoke, and toxicity (FST) performance • Semicrystalline TPCs have good chemical resistance • Stable glass transition temperature (T_g), even under hot/wet conditions • No toxicity/hazardous chemical issues • Low coefficient of friction • High abrasion resistance • Minimal outgassing; low contaminating mass loss ($1/5^{th}$ mass loss of epoxy [3])	• High processing temperatures and pressures required, higher-cost tooling (often heated Invar tools) → challenging economics for low volume production • Higher residual stresses make dimensional tolerances more difficult to achieve; failure locations may deviate from expectations based on TSCs • Slightly higher raw material cost • Lower TRL, especially OOA processes such as in-situ consolidation • Structural properties and chemical resistance are sensitive to crystallinity (i.e., cooldown profile); amorphous TPCs have lower chemical resistance compared to semi-crystalline TPCs • Difficult to contour to highly curved shapes, require thermal tacking during layup • Higher melted viscosity (more fiber misalignment → lower compressive strength), difficult to get good impregnation with uniform fiber distribution (although material quality has improved since 2015) • Crystallinity may change during part lifecycle

THERMOPLASTIC COMPOSITE MATERIALS FOR AIRCRAFT STRUCTURES

In the following sections an overview of thermoplastic composite materials that have been of interest to the aircraft community is presented. Processing and its effects on the mechanical properties of the material are discussed. Manufacturing techniques and currently pursued options for assembly are summarized.

Thermoplastic Composite Materials for Aircraft Applications – An Overview

Historically, NASA LaRC pioneered the development of resins and adhesives for potential application to space vehicles, supersonic and high-speed aircraft. The research included molecular modeling, resin formulation, processing studies, and characterization. Studies included laminates made of carbon fiber reinforced polycarbonate (PC) [12, 63]. Additionally, numerous formulations have been registered under LARC™. A major technology worked at LaRC under the High-Speed Research (HSR) program was the development of high-temperature composites for the airframe. Key contributions made under this research effort are discussed in reference [1].

Today, six general classes of thermoplastics are used most frequently: Polycarbonates (PC) Polyamides (nylon, PA-6, PA-12), Polyphenylene Sulfide (PPS), Polyetherimide (PEI), Poly-ether-ether-ketone (PEEK) and Poly-ether-ketone-ketone (PEKK) [52]. Of those PEEK, PEKK, as well as LM-PAEK belong to the poly-aryl-ether-ketone (PAEK) family. The polymers primarily used in aerospace thermoplastic composites are PPS, PEI, as well as PEEK, PEKK, and LM-PAEK. These TPCs offer high damage tolerance in the finished parts, as well as moisture and chemical resistance and, thus, do not degrade in hot/wet conditions. The vast majority of research publications is on PEEK, often reinforced with AS4 fiber creating a product known as ACP-2 originally manufactured by Imperial Chemical Industries (ICI) [15, 64-65]. A selection of TPC materials is listed in Table A-I in the appendix.

Several aircraft components have already been manufactured using TPC and are in service today. These parts are mainly made from PPS and PEI matrix composites. A historical timeline is shown in Figure 3. An example of the application of fiber reinforced PPS is the J-Nose, a wing fixed leading edge structure for the Airbus A340-500/600 series. PPS-based composites are mainly used in ribs and panels, e.g. ailerons and the keel beam for the Airbus A340-500/600 series [66] and have been mentioned particularly for the chemical resistance to hydraulic fluids like Skydrol® [22]. Another example is the tail section control surfaces on the Gulfstream G650 (made by Fokker/GKN Netherlands) which are welded thermoplastic structures [67]. Further, the Airbus A400 cockpit floor was made of Carbon/PEEK [54, 67]. A list of currently flying parts made of TPC is provided in Table A-II.

Recently PEKK and LM-PAEK reinforced materials have become more of a focus [26, 68-69, 70-71]. The compressive strength of PEKK was found to be much higher compared to PEEK, which is a substantial advantage [69]. LM-PAEK has a lower melt (LM) temperature and much better flow than PEKK and PEEK. It also can be processed at higher speeds than PEKK and PEEK [70]. Recently, two thermoplastic LM-PAEK-based composite materials Cetex® TC1225 (LM PAEK) T700GC 12K T1E Unidirectional Tape [30-33] and VICTREX AE™ 250, Hexcel AS4 12k Unidirectional Tape [34-37] were qualified through the NCAMP process.

A relatively new material is Elium® — a reactive Methyl-methacrylate (MMA) thermoplastic resin considered to be the first liquid thermoplastic resin designed for manufacturing composite parts with mechanical properties similar to thermoset parts. The major advantage of Elium® is it acts like a thermoplastic, which means it is uniquely designed for thermoforming, recycling and welding [61, 72-73].

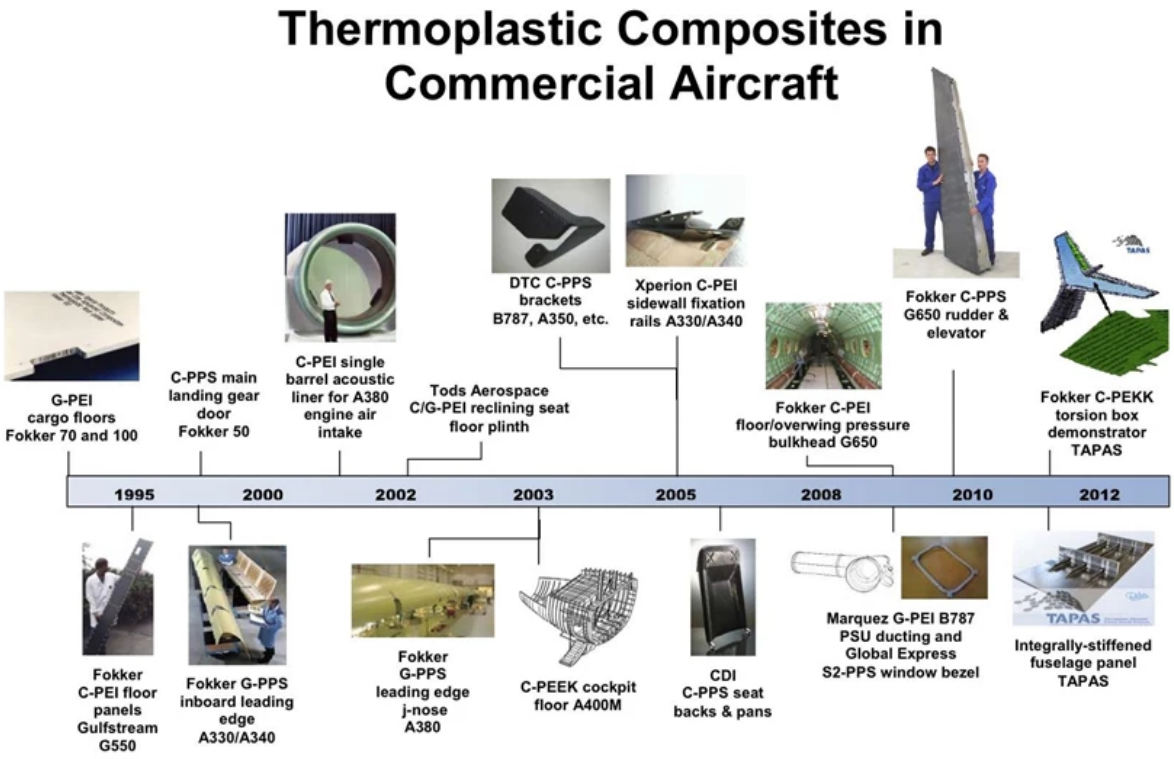

Figure 3: Thermoplastic Composites in Commercial Aircraft: A Timeline.[3]

Effects of Processing Parameters on the Mechanical Properties

Contrary to thermosets, thermoplastics can be melted and reformed without permanent damage or degradation when proper care is taken during processing to avoid thermal degradation. This capability improves recycling, repair and maintenance capabilities and opens up new manufacturing opportunities such as fusion bonding or welding. Thermoplastics can be classified into either amorphous or semi-crystalline. Amorphous thermoplastics (e.g., PEI, PPSU) are composed of randomly oriented polymer chains and typically have a broad softening range, low shrinkage, low chemical resistance, and poor fatigue resistance. In contrast to amorphous polymers, semi-crystalline polymers (e.g., PAEK, PEEK, PEKK, PPS) contain regions of both ordered and non-ordered molecular structures, which results in some unique material characteristics including a sharp melting point, high shrinkage, high chemical resistance, and good fatigue and wear properties. Due to these properties, the recent focus for high-performance composites has primarily been on semi-crystalline thermoplastics [74].

Due to the elevated processing temperatures and the high matrix/fiber thermal expansion mismatch, substantial residual thermal stresses may be developed in thermoplastic composites. The buildup of residual stresses during processing of amorphous resins begins only below the glass transition temperature, whereas for semicrystalline matrices it begins during the crystallization process. In semicrystalline thermoplastics, crystallization causes a large volumetric shrinkage in addition to the usual, CTE-dependent, thermal contraction and causes the buildup of additional residual stresses. As the composite's mechanical properties are

[3] Image source *CompositesWorld* [53], used with permission.

dependent on the matrix constituents and the reinforcing phase, the development of thermal stresses is directly affected by the variations in temperature and degree of crystallinity occurring during processing [60]. Residual stress also arises due to the mismatch in CTE between layers of different ply orientations and non-isothermal cooling of the layers (thermal gradients through thickness that vary with time) which represent additional loading on the microstructure. Process-induced residual stress can initiate microstructural damage (e.g., microcracking) and have significant effects on the dimensional stability/warpage and assembly of components.

In semi-crystalline polymers it is generally advantageous to achieve a high degree of crystallinity to improve solvent resistance and strength and reduce creep. These improvements come at the cost of lower ductility and fracture toughness as will be discussed later. Rapid cooling typically results in low crystallinity [46, 59, 75]. In general, slower cooling rates (e.g., 5°C/min) increase crystallinity, which results in higher strength properties and chemical resistance in the finished laminate. The higher cooling rates start to reduce crystallinity (e.g., 100°C/min and faster). For example, PEEK must be cooled at >2000°C/min to eliminate crystallinity. It was reported that the strength properties change slightly, as does the chemical resistance, when the crystallinity is 5–6% or more below the maximum crystallinity (about 37% for PEEK) [25]. The trend for other thermoplastics is expected to be the same. The exact values, however, may vary with for different chemistries.

Tempering or annealing of a TPC part during post-processing at a temperature above the crystallization temperature allows for the removal of process-induced thermal stresses and an unwanted crystallinity distribution. Thus, during the subsequent cooling of the part, a cool-down rate may be selected that results in the level of crystallinity throughout the part to achieve the mechanical properties desired [75-80]. A tempering or annealing step may be particularly attractive after a part has been made using automated fiber placement (AFP) or tow placement (ATP) with many passes of the deposition head over the same area. The many repeated heating and cooling cycles in the same area of an ATP/AFP part results in an undefined crystallinity distribution through the thickness. Similarly, when parts are joined using fusion bonding or welding the crystallinity through the thickness may be unknown and annealing may provide an opportunity to obtain the desired level and distribution of crystallinity. It is possible, and often much more practical, to anneal a polymer well below the melt temperature (T_m) and at or above the glass-transition temperature (T_g). By doing so, the crystallinity can be increased, but not decreased. The sub-T_m anneal is more practical than the full melt because the part will need to be supported completely when brought to melt, whereas an anneal process around the T_g will not require complete support from tooling on all surfaces of the part.

Manufacturing and joining techniques are discussed in the following section. New advances in process simulation which may be able to simulate the temperature distribution through a part and predict its crystallinity are discussed in the analysis section.

Part Manufacturing and Assembly Techniques for Structures

This section provides a brief summary of the TPC manufacturing and assembly technologies relevant to aircraft applications. The discussion includes the most critical identified advantages and limitations of each technology. Many of the processes result in complex thermal histories and so analysis may be required to map the process history to mechanical performance and predict structure performance when process history may vary throughout a part. A challenge is that there is limited data available characterizing mechanical properties as a function of process history [81].

Automated fiber and tow placement

AFP and ATP are additive manufacturing processes for high-performance composite structures. In-situ AFP is a true out-of-autoclave process that has been used in serial production for over 25 years [46]. Research efforts are underway to improve process models

and expand process capabilities using synergistic technologies such as lasers and ultrasonics [46]. During AFP a deposition head includes a tape feed and cut mechanism, a compaction roller and a heater. Diode lasers are now the norm for heating TPCs during AFP. As the prepreg tape is fed through the AFP head and onto the part, the laser heats the incoming tape and substrate surfaces up to and often above the melt temperature of the thermoplastic matrix. In cases when a second consolidation step will be undertaken, the heating enables a partial weld (where the interface is not completely consolidated and healed) to the previously deposited ply. A fully consolidated interface is necessary for the single-step in-situ consolidation (ISC) application. One key characteristic that impacts process efficiency is void content. Most parts fabricated using PEEK have a void content of 4–6%, while most aerospace parts can be as low as 3–4%. For a complex part, 96% consolidation (3–4% porosity) can be achieved and for a flat part, porosity is less than 2%. Another key concern is crystallinity, as discussed above, as the tape cools from melt temperature to a solid [9-10]. It would seem apparent that the rapid cooling as the laminate leaves the heat affected zone would result in low crystallinity in semi-crystalline polymers such as PEEK. However, crystallinity of 25% to 30% is achieved in the first layer and can be as high as 34% in the laminate as subsequent plies raise the temperature in the laminate enough to promote further crystallization. Thus with AFP, it is possible to achieve crystallization levels approaching the maximum crystallinity level (about 37% for PEEK) at the ideal crystal growth temperature [46].

Detailed research was performed in [82], using PEKK and PEEK UD-thermoplastic composite materials made from a 1⁄4-inch-wide tape laminated with a single-tow deposition machine and laser scanning as the heating source to study the evolution of crystallinity with multiple lamination steps during in-situ consolidation. The laminate was fabricated in stair steps. Thus, it was possible to extract test specimens composed of one layer, two layers, … and so on. When an unheated tool was employed, a marked phenomenon of cold crystallization was observed especially in the first layers. This cold crystallization occurs between the glass transition temperature and the melting temperature of the polymer. In contrast, the extent of crystallinity remained nearly constant when the automated lay-up was performed over a self-heated tool. Microscopic evaluation showed that when the number of layers increased during the automated lay-up and in-situ consolidation process, a marked decrease in the internal porosity was observed both for self-heated and non-self-heated tools so the degree of intimate contact increased with the number of consolidation steps [82].

Others investigated the influence of the four main process parameters for the in-situ AFP process: tooling temperature, nip-point temperature, layup speed and consolidation pressure [80]. A novel CF/LM-PAEK material with T700 fiber was used. A Face Centered Cubic (FCC) Design of Experiments (DoE) method was used to combine the different process parameters in a way that would yield the most useful results with the least number of samples. The weighting assigned to each process parameter was assessed based on the experience of the researchers as well as comparisons with the current literature. Single Lap Shear (SLS) specimens manufactured on a heated tool showed increased crystallinity and bonding strength over specimens manufactured on an unheated tool. Overall, an increase in nip-point temperature produced higher bonding strength, as did an increase in consolidation pressure, although the effect of pressure was less significant. Further, the researchers concluded that the layup speed had no apparent impact on either bonding strength or crystallinity, which from their understanding is contrary to other established thermoplastic materials and was attributed to the polymer's inherently low melt viscosity. A subsequent tempering process was found to increase bonding strength by 76% and yielded a final crystallinity of 32%. An initial material comparison revealed bonding strength values for the investigated CF/LM-PAEK material in the same order of magnitude as CF/PEEK and CF/PPS. The material's insensitivity to layup speed could potentially be an advantage over established thermoplastic materials, enabling higher production rates using the in-situ AFP process [80].

Forming processes

One of the most basic processes of forming thermoplastic composites is press consolidation, which has been used widely by researchers over several decades [14, 18, 48, 83-84]. The composite is consolidated under prescribed processing conditions (temperature and pressure) in a hot press. Researchers reported using ACP-2 tape [15], unidirectional prepreg tapes made of comingled yarn of GF/PP in a 50:50% weight mixture [77-78] and commingled uni-fabric AS4 3K/PEEK [85]. Others reported on using PEEK film and bidirectional plane weave graphite cloth such that the panels were fabricated by stacking film and cloth in alternate layers and then consolidated [86].

Thermoforming offers great potential in reducing manufacturing costs. Thermoforming is derived from stamping processes that were developed for sheet metal forming. However, the laminate deformation physics are different from that of metals. The most important fabric forming mechanisms are intra-ply shear and inter-ply slip [22]. Typically, thermoplastic tapes are cut to a prescribed shape and then stacked. The stack is inserted into a preheating oven to be softened and pre-consolidated. This stack-up is then transferred to a forming press, which usually consists of a matched metal tool that fully consolidates and cools the tapes under high pressure (250–500 psi). With thermoplastics, the part is typically not consolidated in the mold, but instead a pre-heated, pre-consolidated laminate is formed, and the tool is used to form and cool the pre-heated part [20]. Several manufacturing techniques are available, such as diaphragm forming, hydroforming, matched metal die forming, rubber pad pressing and rubber forming. On a particular project, a rib of a trailing-edge tab of a double slotted Fowler flap from a regional jet aircraft size was fabricated using rubber forming because it allows the manufacturing of complex shapes, while a near hydrostatic pressure can be maintained during consolidation. In addition, rubber forming reduces tooling manufacturing costs and the cycle times are on the order of 5 to 10 minutes. A six-ply Cetex® woven (5H satin fabric) CF/PPS laminate was selected due to its exceptional specific strength and stiffness properties, impact resistance, and its chemical resistance to hydraulic fluids like Skydrol® [22].

Although it is not widely used today, one of the most promising processes towards reducing porosity (<0.5% target) is continuous compression molding (CCM). Here, continuous tapes are passed through forming tools that heat and shape the material and create, effectively, a range of shapes, including T, C, H, hat and Omega profiles and others. This process has particular promise for the manufacture of stringers and frames for commercial aircraft [20].

Press-forming is a hybrid process in which forming the composite laminate and the injection molding processes are performed simultaneously in the same operation [68].

Fusion bonding and welding

A main driver for developing TPC for commercial aircraft is the ability to join components via fusion bonding or welding. This technique presents an attractive alternative to the conventional methods of mechanical fastening and adhesive bonding which are typically used to join TSC parts [8, 52]. Instead of bonding with a dedicated adhesive material, the matrix material in the composite plies themselves is used to form the bond in a welded joint. The polymer is locally heated until it liquifies, and pressure is applied so that an interface layer of liquid polymer emerges between the two components to be welded. After solidification both components are joined permanently, forming a cohesive bond [87]. The strength of the welded joints relies on the performance of the thermoplastic matrix which may be influenced by the welding process [26, 88-89].

Compared to riveting and adhesive bonding, the welding process has further advantages such as:

- Reducing the amount of parts needed for joining components compared to fasteners
- Reduction of surface treatment time required for adhesive bonding
- Short process cycle time, usually in the range of minutes
- Possibility of field repair

- Rewelding does not degrade the performance.

Further, specific technologies exist to weld and de-weld with resistance welding to disassemble by injecting current [8, 52, 66]. The frequent uneven heating of laminates, which can lead also to delamination and distortion of the fibers in the joining zone, is a disadvantage [66].
An overview of different welding techniques is shown in Figure 4.

	Resistance Welding	Induction Welding	Ultrasonic Welding	Laser Welding
	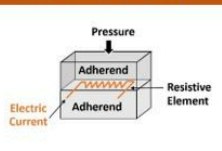	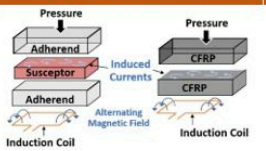	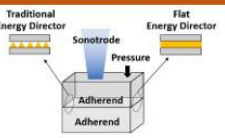	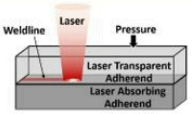
	Electric current passes through resistive element causes heat and melting	• Electromagnetic coil produces alternating electromagnetic fields which induce eddy currents in conductive (carbon fiber) laminate • Eddy currents produce heat which melts the thermoplastic	• Sonotrode coupled to a transducer produces high frequency (20-40 kHz) vibration that causes frictional heat and melting at interface • Energy director is required at interface	• Laser radiation passes through a laser transparent part (e.g., unreinforced PEEK bracket) and generates heat in a laser absorbent part which contains carbon fiber or conductive additive
Pros	▪ Heat generated only at weld interface ▪ Good for long welds — process time is independent of weld length	▪ Susceptor only required with non-conductive fiber composites (e.g., glass, aramid)	▪ Good for spot welds ▪ Very fast	▪ High speeds possible (400 mm/s)
Cons	▪ Requires a resistive element (metal or carbon fiber) which stays in the weld	▪ Harder to focus heat at weldline ▪ Well-suited for carbon fabric but more challenging with unidirectional and noncrimp fabric laminates	▪ Continuous welding still in development	▪ Weld seam affected by type and layout of reinforcements
Thickness	No limit	< 5mm per side		Demonstrated 2.4mm
Speed	≈1 m/min DLR ZLP Augsburg	0.5 m/min KVE	4-6 m/min	24 m/min
Applications	CF fabric/PPS main landing gear door for Fokker 50 turboprop aircraft GKN Fokker GF fabric/PPS fixed leading edge Airbus A340/A350 and A380 aircraft GKN Fokker CF fabric/PPS 8-section rear pressure bulkhead for Airbus A320 demonstration DLR ZLP Augsburg	CF fabric/PPS rudder Gulfstream G650 GKN Fokker CF fabric/PPS elevator Dassault Falcon 5X GKN Fokker CF fabric/PPS rudder Gulfstream G650 Aviacomp CF/PEKK UD tape stringers to skin for STELIA "Arches TP" demonstration fuselage Composite Integrity	Injection molded CF fabric/PEI parts to CF/PEI floors for G650 GKN Fokker Clean Sky 2 EcoDesign demonstrator CF/CF/PEEK hinge and CF/PEKK clips to CF/PEEK C-frames TU Delft CF/PPS and CF/PEKK up to 1m, robot based in progress DLR ZLP Augsburg	LaWocs demonstrators: ▪ UD glass/ PEEK L bracket to CF fabric/PEEK laminate ▪ Unreinforced PA 6,6 aerospace attachment pin to CF/PA 6,6 baseplate ▪ Glass/PEI, PPS hat-stringer stiffeners to glass/PEI, PPS skins. Element Materials, KVE, LZH, TenCate, Unitech Aerospace, et. al.

Figure 4: Welding techniques used for thermoplastic composites.[4]

Resistance welding is based on the principle of the ohmic resistance. An electrically conductive welding aid (of metal or carbon fiber laminate) is positioned in the welding zone and connected to a generator on both ends. After switching on the generators and applying a certain pre-pressure the current flows through the welding aid. Due to the electrical resistance of the welding aid, heat is generated in the welding zone. An advantage of the process is the local heat generation in the welding zone. A disadvantage of resistance welding is the relatively long cycle time relative to other welding processes [26, 66, 89-90].

Induction welding is a joining technique that is based on magnetic induction. An alternating current, which generates an alternating magnetic field, flows through an inductor (usually a water-cooled copper tube). This magnetic field penetrates the material, where it generates a secondary electric circuit and heats up the materials due to resistance losses. The resistance losses of metal or carbon fiber reinforced thermoplastics are sufficient to melt the matrix. If two continuous fiber reinforced thermoplastics in a melted condition are pressed together, a composite is developed. Induction welding is a cost-effective process because the equipment can be easily adopted for joining several geometries and because of low equipment investment costs. This process is mainly of interest for the production of small and medium-sized components since the magnetic field has to penetrate the structure [26, 66, 89]. Recently this process has been extensively modeled as discussed later in the section on *Process Modeling and Manufacturing Simulations.*

[4] Image source *CompositesWorld* [8], used with permission.

Conduction welding is based on heating the surface of the part through an induction heated tool and generating the weld bath by heat conduction through the laminate. The benefit of this technique is that it does not require addition of welding specific materials such as energy directors or conductive strips. Furthermore, the technique is scalable and therefore more suitable than the other welding techniques for welding of large parts [8, 88, 91].

Ultrasonic welding uses a sonotrode to generate high-frequency (20–40 kHz) vibrations that cause frictional heat and melting at the weld surfaces. It is generally considered good for spot welds and can be very fast and highly automated. The technique has been used with plastics for several decades, typically with energy directors at the weld interface. Energy directors are typically triangular or rectangular ridges of neat resin, molded into the surfaces to be welded, and increase local heat generation. Recent studies have shown that 0.08-mm-thick, unreinforced thermoplastic films may be used in their place [8, 26, 89, 92-94].

Laser welding applications are mostly limited to metals. However, laser beams can also be used to weld TPC parts. Typically, the two parts are pressed together as the laser beam passes along the bond line. The laser beam decomposes (burns) some of the polymer along its path but leaves behind a thin layer of molten polymer at the bond line of the two parts, which are brought together under pressure to solidify, thereby resulting in a weld. In an advanced process, laser light is first passed through a part that is transparent or partially transparent in the near infrared spectral range (e.g., an unreinforced thermoplastic or glass fiber TPC). The light is then absorbed by the carbon fibers or conductive additives in a second adjacent part, transforming the laser energy into heat, which creates the weld between the two materials. Since many injection-molded aircraft brackets are laser transparent there is great potential for using laser welding to achieve assembly of these brackets to Carbon Fiber Reinforced Plastic (CFRP) fuselage structures without holes, dust, or fasteners. Though both reinforcement type and laminate thickness affect the weld quality, the technology has demonstrated good results with glass fiber and carbon fiber reinforced PPS and polyetherimide (PEI) laminates [8, 26, 68, 89, 95].

Additive deposition processes for complex geometry

Northrop Grumman started development of a free-form additive deposition manufacturing system for TPCs around 2010. The system aims to combine the capability and benefits of TPCs and thermoplastic additive manufacturing. The system was developed in partnership with *Electroimpact*. The scalable composite robotic additive manufacturing (SCRAM) system is a multi-material manufacturing system for deposition of aerospace-grade TPC structures. Both continuous fiber (AFP-like) and short-fiber or particulate filled material can be consolidated to form complex structures in a single tool-less operation. This manufacturing capability is focused on highly complex structures and geometries. NIAR has acquired a system [96-97].

Additive manufacturing

Additive manufacturing (AM), commonly referred to as 3D printing, has also become a topic of intensive research. Fused Filament Fabrication (FFF) is one of the popular additive manufacturing (AM) techniques, which has been regarded as an effective method for the creation of complex geometries [79-98]. Researchers report the use of 1.75-mm-diameter PA 12 (Nylon FX 256) reinforced by short carbon fibers (15 vol.%), with approximately 100 μm in length and 10 μm diameter, obtained in filament form [98].

Another AM technique described is Fused Deposition Modeling (FDM) where a FDM 3D printer was fed with CF/PEEK filaments to fabricate flexural and short beam shear test specimens. All samples were printed at 400°C and 15 mm/s speed, using a nozzle with 0.4-mm diameter creating 0.1-mm layer thickness [75].

Resin infusion

Recently, a novel composite system was developed using a cost-effective vacuum assisted resin infusion process. The matrix system used in the study was a liquid PMMA thermoplastic resin (Elium® 280 from ARKEMA). The Elium® resin, although it is a liquid thermoplastic resin can be cured at room temperature with a fast demolding time of four hours, which includes two hours of post-curing at 80°C. As reinforcement, thin carbon non-crimp fabric (NCF) bi-angle ply C-Ply™ (200 g/m^2) and thick carbon NCF bi-angle C-Ply™ (400 g/m^2) were used where the plies were sized specially to be used with epoxy and thermoplastic matrices [72]. In other studies, Elium® 150 was used in combination with carbon [73] and glass fibers [61-62].

Injection molding and overmolding

Injection molding is used with neat thermoplastic material and in conjunction with very short fibers (~1 mm long) [68, 99]. The process has been used by researchers to fabricate specimens and investigate the behavior of glass fiber and carbon fiber TPCs [100-101]. The *Multifunctional Fuselage Demonstrator* (MFFD) [27, 102] plan in Europe calls for fabricating all of the brackets by injection molding short fiber compounds made from scrap produced during primary structure manufacture to develop recycling capability. The recycled material has degraded properties and is only suited for lightly loaded applications [26]. Several injection molded parts are currently in service and are listed in Table A-II in the appendix.

Overmolding is a technology in which a thermoplastic composite laminate is thermoformed and subsequently injection overmolded. This near-net-shape manufacturing process is well-suited for automated large series production of complex 3D structures with excellent structural performance and a high level of functional integration [100, 103-104].

Large-scale manufacturing demonstration projects

The *Thermoplastic Affordable Primary Aircraft Structure* (TAPAS) consortium was a collaboration between Airbus, several Dutch companies, and the Dutch government. One activity was the development to TRL 6 of a 12-m torsion box for horizontal tails with induction welded butt-joint stiffening ribs [53, 67]. The post-buckled design was enabled due to welding and was based on a Gulfstream G650 horizontal stabilizer. The design was developed with Solvay UD carbon fiber/PEKK-FC and co-consolidation in a press. Ultimately, the torsion box was 10% lighter than the TSC baseline as a result of the selected post-buckling design. The torsion box successfully sustained static and fatigue loadings. The team won the 2010 JEC innovation award for this work. Another activity in TAPAS developed a unitized fuselage panel technology. The technology was used to create a TPC ortho-grid structure via co-consolidation and is now employed in a Gulfstream panel as shown in Figure 5. The approach is described as a *butt joint orthogonally stiffened skin with welded frames* [91, 105] which highlights three key design features and manufacturing developments needed to implement them: (1) the ortho-grid, (2) the butt joint, and (3) welding technology. Testing included multi-stringer panel compression tests and damage tolerance testing [91].

The Multifunctional Fuselage Demonstrator (MFFD) is one of three fuselage demonstrators to be fabricated and tested as part of the European Clean Sky 2 initiative. The goals of the MFFD are to enable production rates of 70–100 aircraft/month, reduce weight by 1000 kg, and reduce recurring costs by 20% compared to state-of-the-art aircraft. MFFD is an 8-m-long fuselage barrel made from welded TPC parts. The MFFD is broken into fabrication of the upper and lower halves of the fuselage and includes resistance, ultrasonic, conduction, and induction welding techniques for fuselage assembly. The plan calls for joining the upper and lower halves of the MFFD with a welded multi-step lap joint [26-27, 102, 106]. In addition, the MFFD plan calls for fabricating all of the brackets by injection molding short fiber compounds made from scrap produced during primary structure manufacture to develop recycling capability, as described previously.

Two unidirectional material systems are being evaluated for the fabrication of the upper fuselage structure: carbon fiber/LM-PAEK supplied by Toray and carbon fiber/PEKK supplied by

Solvay. MFFD includes dozens of individual projects contributing to different aspects of the fuselage demonstrator. The lower half of the MFFD is being fabricated in a project called *STUNNING* led by GKN Fokker. The effort is focused on high-TRL developments and structural integration. The demonstrator includes the fuselage panels, sub-structure, floor beams, parts of the cabin, and cargo doors [24]. The materials considered are carbon fiber PEEK, LM-PAEK, and PEKK. The Royal Netherlands Aerospace Centre (NLR) used AFP to lay down the 8.5-m-by-4-m-diameter skin – the largest known single piece TPC fabricated by AFP. The MFFD skin was laid down in two 90° halves and will be consolidated in a large autoclave, and then GKN will do assembly and integration [24]. The upper half of the MFFD is being produced by in-situ consolidated (ISC) AFP in an effort led by the German Aerospace Center (DLR). The stringers will be attached with continuous ultrasonic welding. The frames will be joined with resistance welding (a discontinuous process). The use of the resistance element or weld-aid allows for reduced shimming with tooling used to push the parts together while they are soft to take up the assembly tolerance while simultaneously producing a strong joint [67, 102, 107].

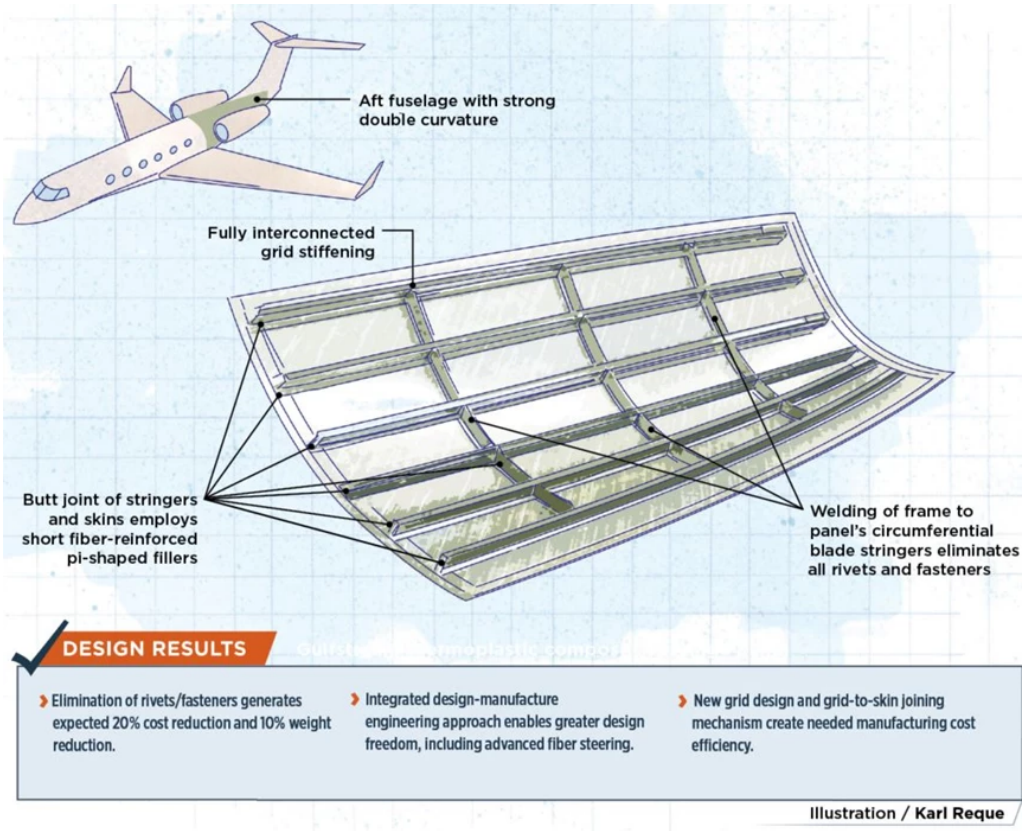

Figure 5: Orthogrid fuselage panel.[5]

An activity completed under MFFD is the MECATESTERS project that aimed to validate induction welding and conduction welding of TPC laminates and T-joints for aircraft applications [26, 71]. The 2.5-year project led by GKN Fokker started in 2019. The goal of the project was to develop best practices for induction welding autoclave-cured adherends made from UD carbon fiber/LM PAEK (Toray TC1225) material. The project objectives were:

[5] Image source *CompositesWorld* [105], used with permission.

- evaluate the effect of surface conditions on the welded interface
- examine the effects of aging on durability
- establish process windows for the two welding methods,
- and perform mechanical testing to validate joint performance.

Test configurations included static and fatigue of

- lap shear
- pull-off, shear, and combined load tests for skin/stiffener joints,
- and mode I and II fracture toughness tests.

The test matrix included two skin thicknesses (2.2 and 2.8 mm), different ply orientations at the weld interface, and three environments (room temperature, −55°C, 80°C, and a subset at 120°C). Process parameters evaluated in the test matrix included three release agents, surface preparation (sanding, abrasives, and plasma treatment), and the addition of an extra layer of neat resin film at the interface. Tests were planned to evaluate welded interfaces between UD laminate skin and short-fiber material used for brackets [26, 71].

Airbus Nantes exhibited a fuselage panel with integrated stiffeners at the 2013 Paris Air Show to successfully demonstrate fabrication of an aircraft structure. It was fabricated using the CF/LM-PAEK tape supplied by TenCate (TC1225), with press-formed omega and butt-jointed T-stringer elements that were welded to the AFP skin [70, 89].

A project at the University of Limerick, funded through the Science Foundation Ireland and supported by local industry, was focused on the development of a variable-stiffness unitized integrated-stiffener thermoplastic composite wing box [108]. The manufactured wing box segment, which was based on the design loads and the approximate geometry of the wing box of a B737/A320 size aircraft at 85% of the wing semi-span, was a demonstrator of several novel technologies and was not intended to be fully representative of an actual aircraft component. The wing box demonstrator was designed to buckle elastically at the design load. Variable stiffness in the wing box top and bottom skins was achieved by fiber steering, which increased the skin buckling load. The results of the project highlighted the potential advances that become possible in primary aerospace structures by combining fiber steering and in situ consolidation of carbon-fiber thermoplastic composites together with new blended, unitized structural concepts [108-113].

TESTING - FROM SIMPLE COUPONS TO STRUCTURAL COMPONENTS

Over the last three decades a multitude of tests have been performed on thermoplastic composites and results have been reported in the literature. Tests have been performed on different levels of the building block shown in Figure 6. Starting on the coupon level, tests were performed for material characterization, such as the Double Cantilever Beam (DCB), End-Notched Flexure (ENF) and Mixed-Mode Bending (MMB) tests for fracture toughness measurements and the Short Beam Shear (SBS) test to determine the interlaminar shear strength of the composite. A more detailed overview with material and layup tested as well as references is provided in Table B-I in Appendix B. On the sub-element level, curved beam tests, open hole tension, center-notched tension, and lap-shear tests were performed amongst others. A more detailed overview is provided in Table B-II. Element-level tests included stiffener pull-off and single-stringer tests with more details provided in Table B-III. Testing on the sub-component, component, and sub-structure levels includes stiffened panels, a rudder leading edge, and a wing box, amongst others, as well as a full-scale fuselage demonstrator with more details and references offered in Table B-IV.

In the following sections more information is provided regarding material data. Tabulated material property data (i.e., elastic constants) for baseline TSC and selected TPC materials are provided in Tables C-I and C-II in Appendix C. The focus in the narrative below is on fracture toughness as an example since an abundance of information is available. Fracture toughness is also an important input to modern finite element (FE)-based progressive damage analysis tools and thus deserves particular attention. The superior fracture toughness of TPC materials in comparison with traditional TSC materials is demonstrated. Further, the influence of crystallinity on fracture toughness is presented. The influence of loading rate on measured fracture toughness is also briefly discussed. Tabulated fracture toughness data for baseline TSC and selected TPC materials are provided Tables C-III and C-IV in Appendix C.

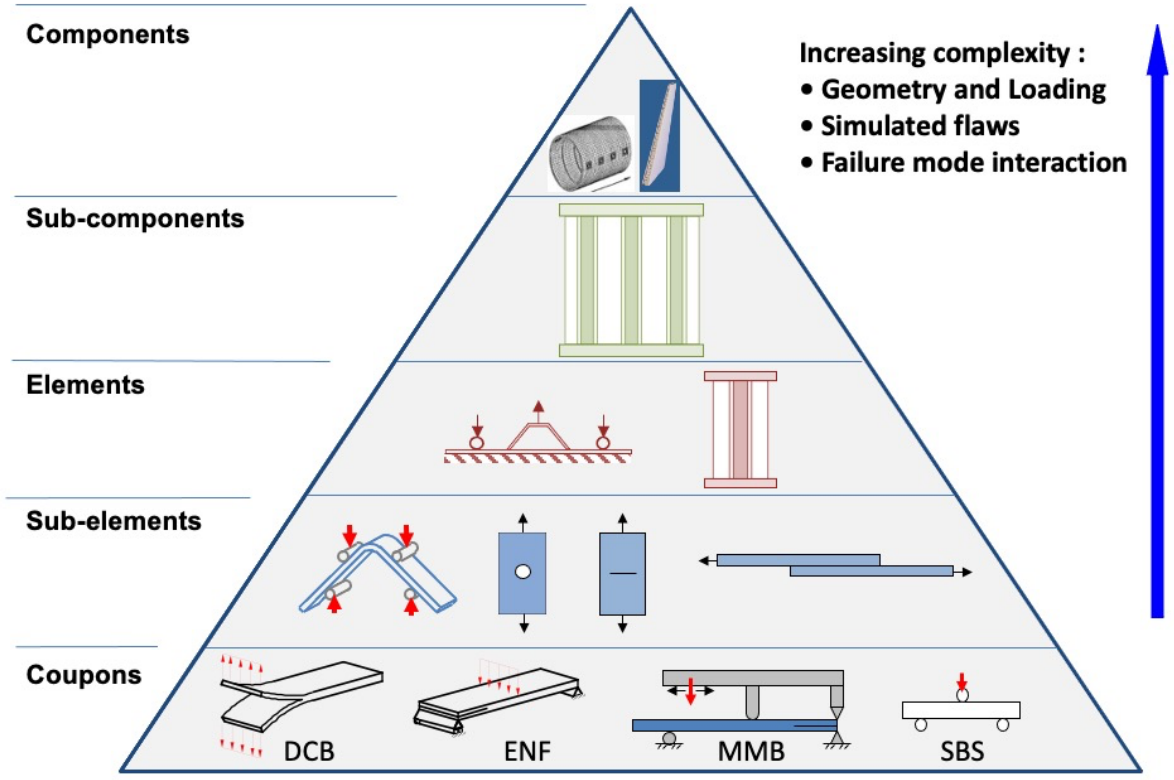

Figure 6: Building block approach.

Fracture Toughness of Thermoplastic Composites

A major reason for the interest in thermoplastic matrix-based composites was their promise of much greater fracture toughness relative to the typical epoxy resins. Improvements in resin toughness was deemed desirable as one approach to improving delamination resistance and damage tolerance in composite structures [12] and led to focused research in the US and Europe [13-18].

A comparison of mode I fracture toughness G_{Ic} values for typical thermoset materials with those for thermoplastic materials is shown in Figure 7. As expected, the values for the thermosets (IM7/8552, AS4/3501-6, IM7/E7T1, IM7/977-2) shown as solids bars on the left are considerably lower than those for the AS4/PEEK shown in the center and for other thermoplastic composites (C/PPS, AS4-3K-PEI, T300 FIT PEEK, IM7/PEEK, AS4/PEKK, Toray TC1225 PAEK, T700G LM-PAEK) shown on the right. A significant variation for the AS4/PEEK material can be observed. In spite of the variation, the superior fracture toughness for all thermoplastic composites is obvious. The variation may be due to the fact that different suppliers provided AS4/PEEK with slightly altered chemical formulations and processing parameters over several decades.

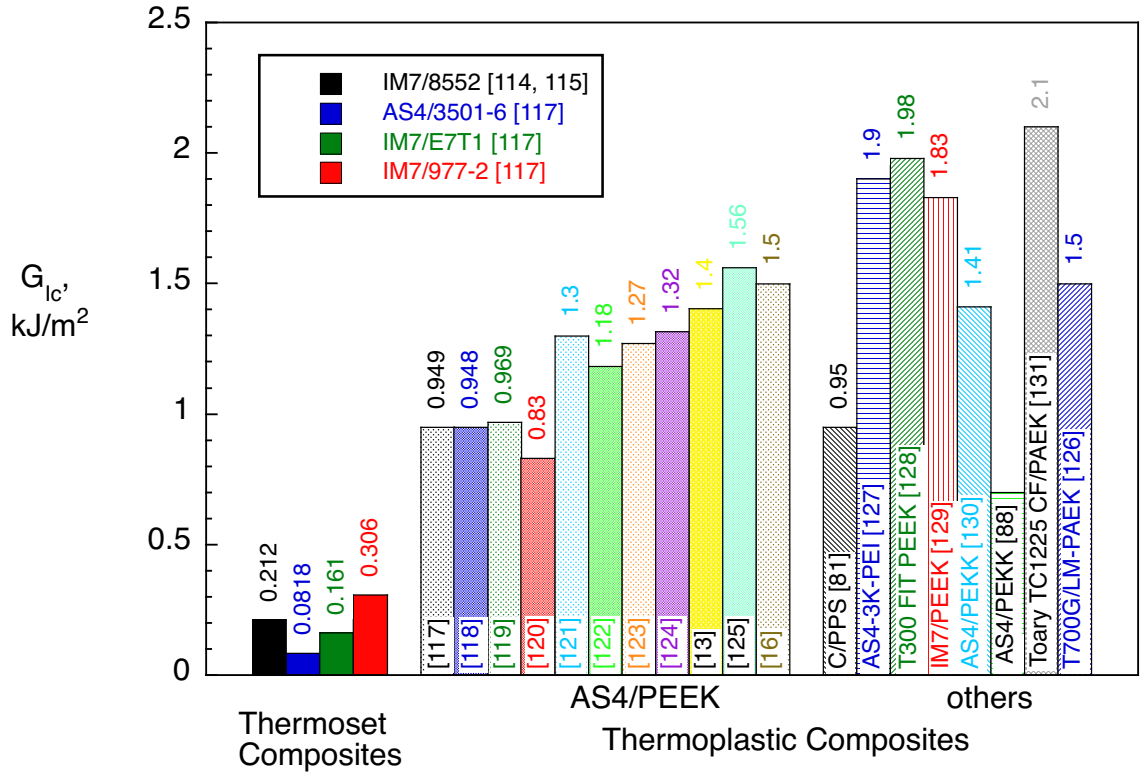

Figure 7: Mode I fracture toughness for thermoset and thermoplastic composites.

Further, tests were performed by different researchers using different equipment. Additionally, the DCB test was not standardized in the early days of testing and in particular the insert material to create the initial delamination and its thickness were not well defined for these thermoplastic materials which get processed at higher temperatures than the thermosets. One study recommended polyimide (Upilex®) films for materials with high cure (or consolidation) temperatures e.g., AS4/PEEK – ACP-2. These polyimide films were recommended over the aluminum films for use as inserts because problems with crimping, tears, and folds in aluminum inserts were noted in the first international round robin [122]. This recommendation was

followed by others [132]. Also a 25 μm Upilex® film insert, coated with a release agent, was used to produce a pre-crack of 60 mm length in the midplane of the composite panels (uni-fabric UD AS4 3K/ PEEK), which were used for mode I and II interlaminar fracture tests [85]. Other researchers used Kapton® film (13 μm, 76 μm,) for the same material (ACP-2) [120, 124], 133]. Most recently a 51 μm thick Kapton® film was used in order to obtain a starter crack in CF/PI fabric composite (T650-35/HFPE-II-52 – 8HS). It was reported that two layers of film were required because the Kapton® partially bonded to the polyimide matrix during cure [134]. As mentioned above aluminum foil was also used to create the starter delamination [15, 129, 135]. Additionally, thin steel foils, 25 μm and 30 μm thick, coated with release agent, were used in order to obtain a starter crack in an ACP-2 and GF/PP composite, respectively [13, 77]. Further studies may be required before a definite recommendation can be made in a standard.

A comparison of mode II fracture toughness G_{IIc} values for typical thermoset materials with those for thermoplastic materials is shown in Figure 8. As before, the values for the thermosets (IM7/8552, AS4/3501-6, IM7/E7T1, IM7/977-2) are shown as solids bars on the left, values for the AS4/PEEK TPC are shown in the center and values for other thermoplastic composites (IM7/PEEK, AS4/PEKK, Toray TC1225 PAEK, T700G LM-PAEK) are shown on the right. The modern TPCs (e.g., Toray TC1225 PAEK, T700G LM-PAEK) exhibit a higher mode II fracture toughness compared to TSCs, however, in general, the difference is less pronounced than for mode I.

While mode I fracture toughness data is available in abundance, data that allow full characterization from pure mode I over mixed mode I/II to pure mode II are limited. Often the BK-criterion, suggested by Benzeggah and Kenane [136], is used to characterize the mixed-mode fracture behavior of a composite. A BK-fit through experimental data for a typical thermoset composite IM7/8552 (solid grey line and open circles) is shown in Figure 9, where the fracture toughness, G_c, is plotted versus the mixed-mode ratio G_{II}/G_T. While early data for the thermoplastic composite AS4/PEEK (solid dark blue line) clearly show improvements over the entire mixed-mode range compared to the thermoset fracture toughness values, the difference between mode I and mode II values is small compared to the thermoset data. Later results for AS4/PEEK (dashed light blue line) show nearly the same mode I fracture toughness as the earlier result but a much-improved mode II fracture toughness. Currently available data for the newer AS4D/PEKK (red line) lie between the thermoset and the older AS4/PEEK data.

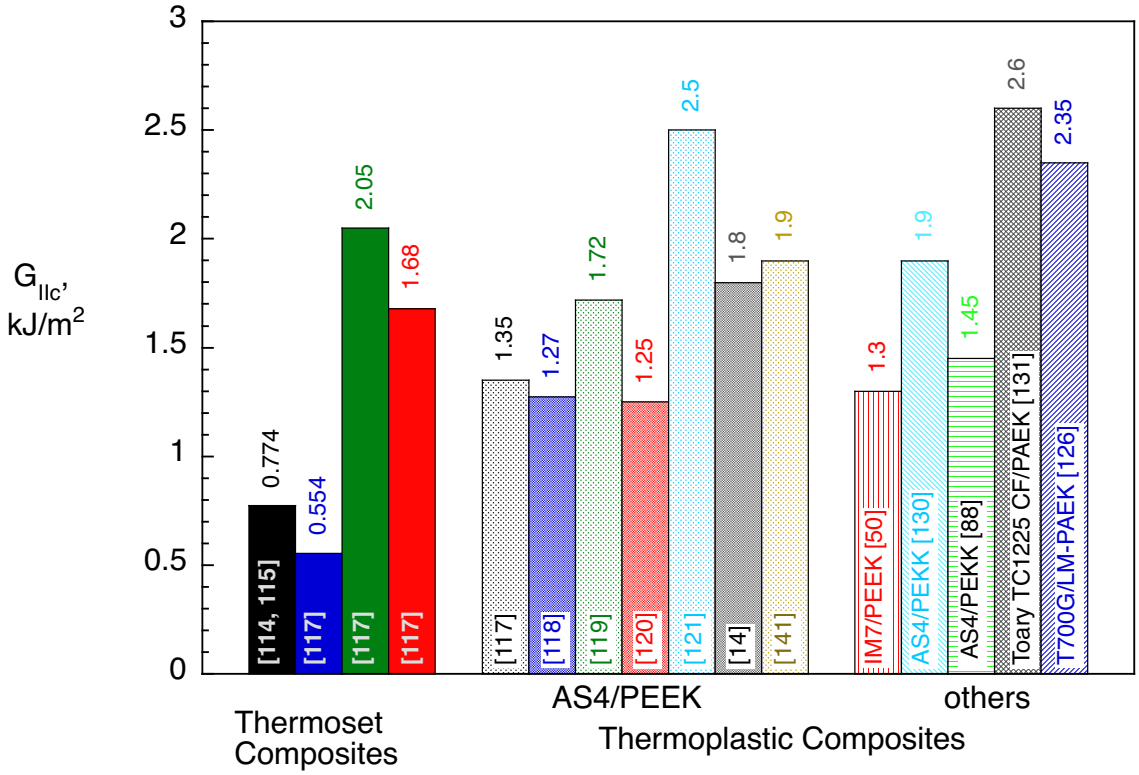

Figure 8. Mode II fracture toughness for thermoset and thermoplastic composites.

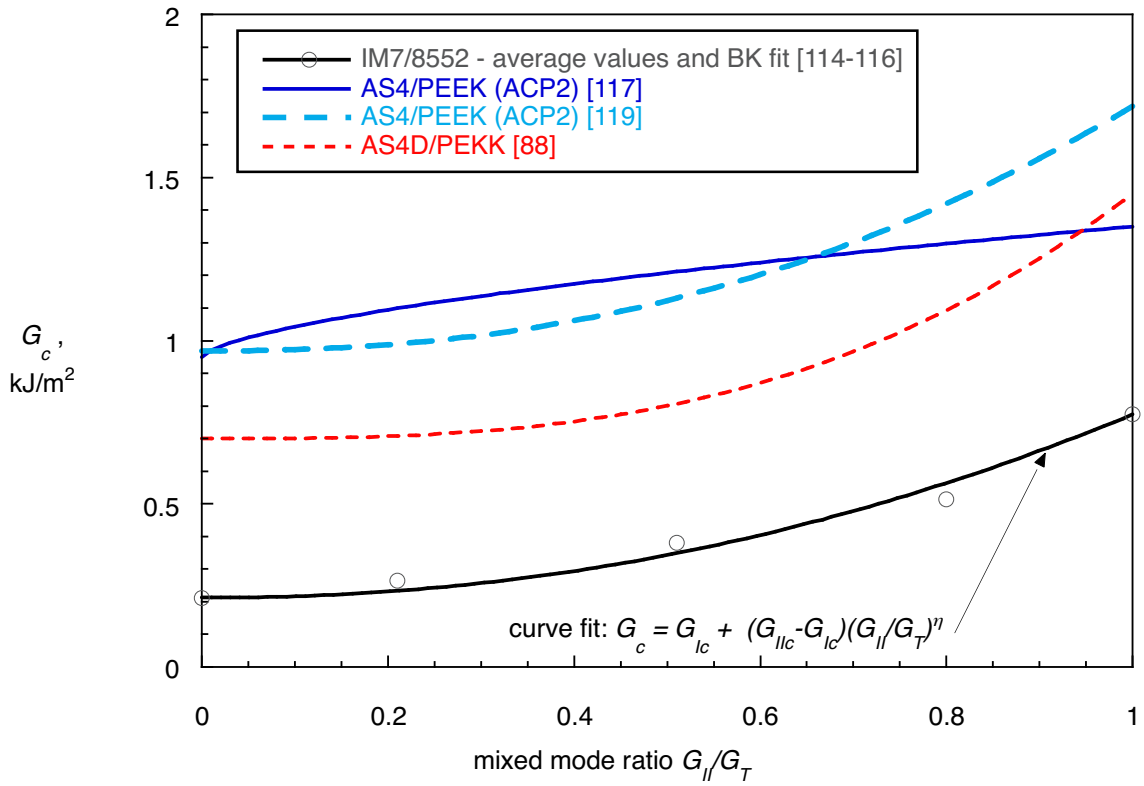

Figure 9: Mixed-mode fracture data for IM7/8552, AS4/PEEK and AS4D/PEKK.

Effect of Cooling Rate on Crystallinity and Fracture Toughness

Achieving the desired level of crystallinity is critical in high-performance applications to attain the optimum combination of strength and toughness, as already mentioned in the section on thermoplastic composites. Therefore controlled processing conditions are required with optimum thermal cycles based on a precise understanding of the crystallization kinetics and its impact on the performance of the composite [55, 57-58]. Several researchers studied the influence of cooling rate on crystallinity and the subsequent effect on fracture toughness. It was observed that rapid cooling conditions resulted in a lower degree of crystallinity, smaller spherulite size, and greater values of the interlaminar fracture toughness, G_{Ic}, in a GF/PP laminate [77-78]. Slow cooling and isothermal crystallization caused the formation of voids, larger spherulites in the resin-rich areas, and lower values of G_{Ic} [77-78]. Thus, the major reason for changes in fracture toughness with processing conditions was not due to the crystallinity itself, but more due to the various meso-structures, i.e. the existence of resin-rich regions with different spherulitic morphology between clusters of fibers, and due to the changes in the fiber/matrix adhesion as a result of variations in processing history [77-78].

A strong correlation between fracture toughness and degree of crystallinity was also found in a CF/PPS composite. A decrease in the degree of crystallinity from 33.3% (reference sample) to 12.1% (stamp-formed sample with the lowest mold temperature) was found to result in a doubling of the interlaminar fracture toughness. The samples with a low degree of crystallinity showed a high interlaminar fracture toughness and large plastic deformation of the matrix during fracture [81, 83].

As a quantitative example, the influence of crystallinity on the measured mode II fracture toughness of a carbon fiber/PPS plain weave fabric is shown in Figure 10. As discussed above the fracture toughness is lower for higher levels of crystallinity.

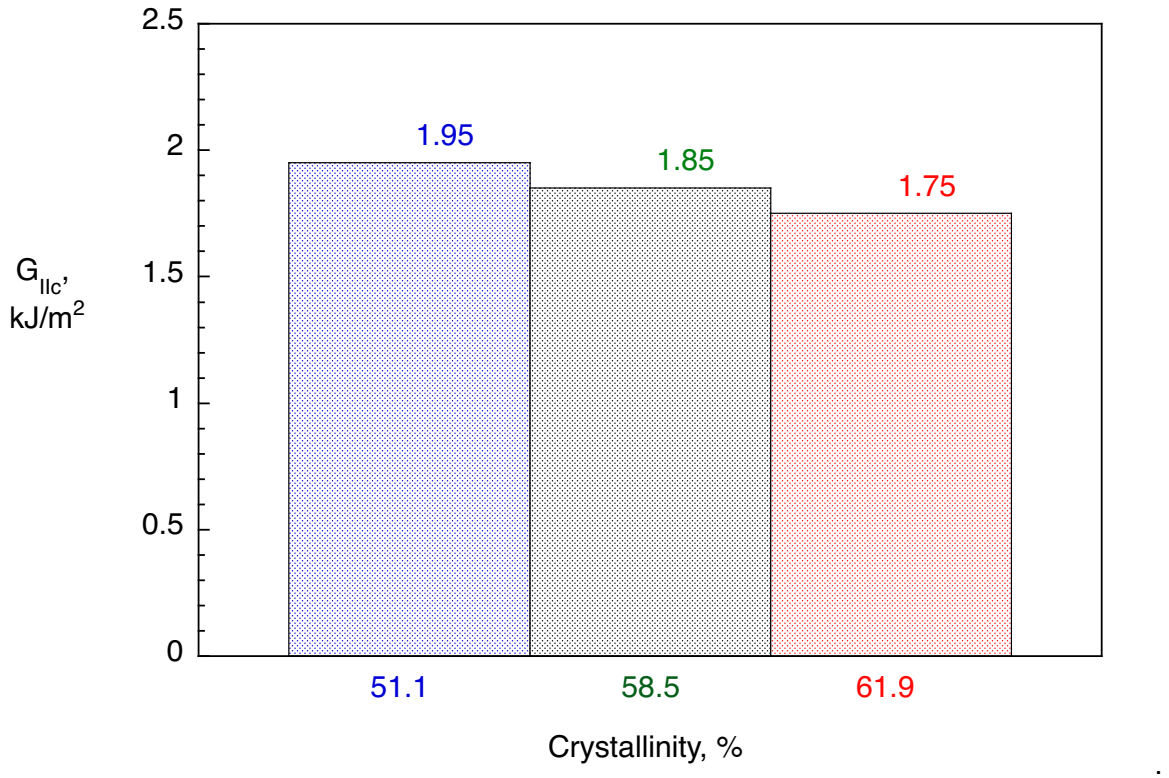

Figure 10: Influence of crystallinity on mode II facture toughness of a plain weave PPS [84].

Other researchers found that the fracture toughness of AS4/PEEK relies on both interfacial interactions and matrix morphology [137]. The fracture toughness perpendicular to the fibers (measured using a Single-Edge Notched Bending test (SENB)) was found to be closely related to the bulk crystallinity of the composite, which is in turn determined by the short-range and long-range effects of the fiber during processing. The fracture toughness along the fiber direction depends more significantly on interfacial adhesion and polymeric chain orientation. Thus, the fracture toughness of the AS4/PEEK studied depends on both crystallinity and crystallites texture of the matrix polymer in which interfacial interaction plays an important role, but not merely on crystallinity as suggested previously for ACP-2 laminates. This complex dependence on morphology leaves space for optimizing both the elastic properties and the fracture toughness in the processing of the thermoplastic composites [137]. Hence, for future application of TPC in aircraft structures the appropriate level of crystallinity needs to be determined that satisfies both strength and toughness requirements.

Loading Rate and Crack Speed Effects on Fracture Toughness

Fracture toughness measurements using the DCB test are performed under displacement control. Typical displacement rates found in the literature for thermoplastic composites varied from as low as 0.3 mm/min [134] to as high as 5 mm/min [98, 138] with most tests performed at intermediate rates (1 mm/min [139]; 1.27 mm/min [133]; 2 mm/min [129, 140]; 2.5 mm/min [132]). A range from 1 to 5 mm/min was reported for an international round robin [13]. For the ENF test typical displacement rates reported varied between 0.2 to 2 mm/min for the international round robin testing [13]. Several researchers performed tests at 0.5 mm/min [132, 135, 138] however, displacement rates as high as 2.54 mm/min [133] were also reported.

Several researchers studied the influence of loading rate on fracture toughness. DCB specimens made with C/PEEK (AS4/PEEK-ACP-2) were tested over a range of crosshead displacement rates from 0.252 mm/min to 40,200 mm/min. Results indicate that the fracture toughness is rate-sensitive and G_{Ic} decreases from 1.5 to 0.35 kJ/m^2 over five decades of opening rate [16]. Mode II ENF tests were performed by the same researchers at crosshead displacement rates ranging from 0.252 mm/min to 5,520 mm/min. The ENF specimens exhibited a rate-dependent, non-linear load displacement response as a result of subcritical crack growth prior to crack propagation. The extent of non-linearity decreased with increasing crosshead rates and was virtually non-existent at rates larger than 19.2 mm/min. Studies using a Scanning Electron Microscope (SEM) showed that for low loading rates the polymer deformation behavior was ductile in nature with extensive plastic deformation. At the high rates, a linear elastic behavior was observed, and the microscopic polymer deformation behavior was brittle in nature. The loading rate at which the transition between plastic deformation and brittle behavior occurs was not reported. The observed decrease in G_{IIc} with increasing crosshead rates was attributed to a decrease in the development of plastic deformation during loading [141]. Another group studied both DCB and ENF tests which were performed under different loading rates (0.25; 2.5; 25 and 250 mm/min) [14, 18, 125]. Subcritical crack growth and 'stick-slip' phenomena were found to be highly rate-dependent and were attributed to plastic and viscoelastic (VE) effects in the process zone around the crack tip. The decrease in G_{Ic} with rate was attributed to a ductile to brittle transition of the polymer in the process zone. Nonlinear rate dependent load-displacement response prior to unstable fracture was also observed, with higher crosshead rates leading to a more linear elastic behavior. The nonlinearities were attributed to a combination of subcritical crack growth preceding unstable crack growth and material inelastic behavior in the process zone around the crack tip. The rate dependency of the composite toughness is similar to that of the matrix material. Fiber bridging may increase the interlaminar toughness in mode I and mode II loading, but does not explain the observed rate effects or stick-slip growth observed in mode I [14, 18, 125]. The observed trends were independently confirmed by other researchers who tested DCB specimens made of CF/PEEK

and used various crossheads rates ranging from 0.5 mm/min to 1000 mm/min. The interlaminar fracture toughness of the tested thermoplastic composite was found to decrease with increasing loading rate, and this decrease was up to 65% over the range considered [86].

About a decade later, the same observations were made when researchers tested DCB specimens made of C/PEEK (BASF AS4-3K-PEEK) loaded at constant load-point displacement rates ranging from 0.05 to 500 mm/min at temperatures ranging from −50°C to 130°C. A fairly regular, decreasing trend of fracture toughness, G_{Ic}, with increasing loading rate was observed [142]. However, for DCB tests performed at constant displacement rates ranging from 6,000 mm/min to 300,000 mm/min on IM7/PEEK UD specimens, the significant rate effects reported by other researchers previously were not observed [129]. Also for new materials (Glass fiber/Elium 150) tested at four different loading rates (0.05, 5.0, 500 and 30,000 mm/min) using the DCB test significant displacement rate effects were not observed [61].

Several researchers focused on the measurement of the crack growth velocity and its effects on the fracture toughness. For a AS4-3K-PEI composite, the mode I toughness values showed a tendency to increase with increasing crack growth velocity (0.5 to 500 mm/min) and with decreasing temperature (23°C, 75°C, 130°C). Composite fracture toughness shows a smooth, regular increase with increasing crack speed. By shifting the data along the logarithmic crack speed axis, as previously done for the neat resin, a master curve for a reference temperature of 23°C was derived [127]. Others performed mode II tests on a IM7/PEEK composite. ENF tests were performed at a loading rate of 1.68 mm/min. During the tests the unstable crack propagation was filmed with an ultra-high-speed camera in order to determine the crack growth velocity. The mean velocity for the tests varied between 807 m/s to 962 m/s with a maximum velocity measured at 1200 m/s. Initial fracture toughness varied from 0.6 to 1.3 kJ/m^2. Afterwards, stable propagation was observed until the point of maximum force, when G_{IIC} increased to a value between 1.4 and 3 kJ/m^2. Infra-Red Thermography (IRT) enabled fracture toughness to be assessed using the heat energy dissipated by the crack growth. This technique was used to estimate fracture toughness during ENF tests with unstable propagation. From its maximum force peak value, G_{IIC} decreased to a value between 0.9 and 1.5 kJ/m^2. This high variation in the fracture toughness with crack growth velocity is most likely due to the transition between a ductile fracture mode for low velocity (stable process) and a brittle fracture mode for high velocity (unstable propagation) [49-50].

A set of quantitative examples is presented in Figure 11 where the mode I and mode II facture toughness values for AS4/PEEK are shown on the left side of the bar chart for different crosshead loading rates. For both mode ratios the fracture toughness appears to decrease with increasing crosshead rate. This trend is also observed for the mode I fracture toughness of T300 FIT/PEEK shown on the right for two different crack speeds. With increasing crack speed, the fracture toughness drops. Another set of examples is presented in Figure 12 where the mode I facture toughness values for AS4-3K-PEI on the left and AS4-3K-PEEK on the right of the bar chart are shown for different crack speeds. For AS4-3K-PEI the toughness appears to be increasing with crack speed. For AS4-3K-PEEK the results suggest that the fracture toughness is almost constant over several decades of crack speed. Thus, no conclusive statement can be made at this point with regard to fracture toughness and crack speed.

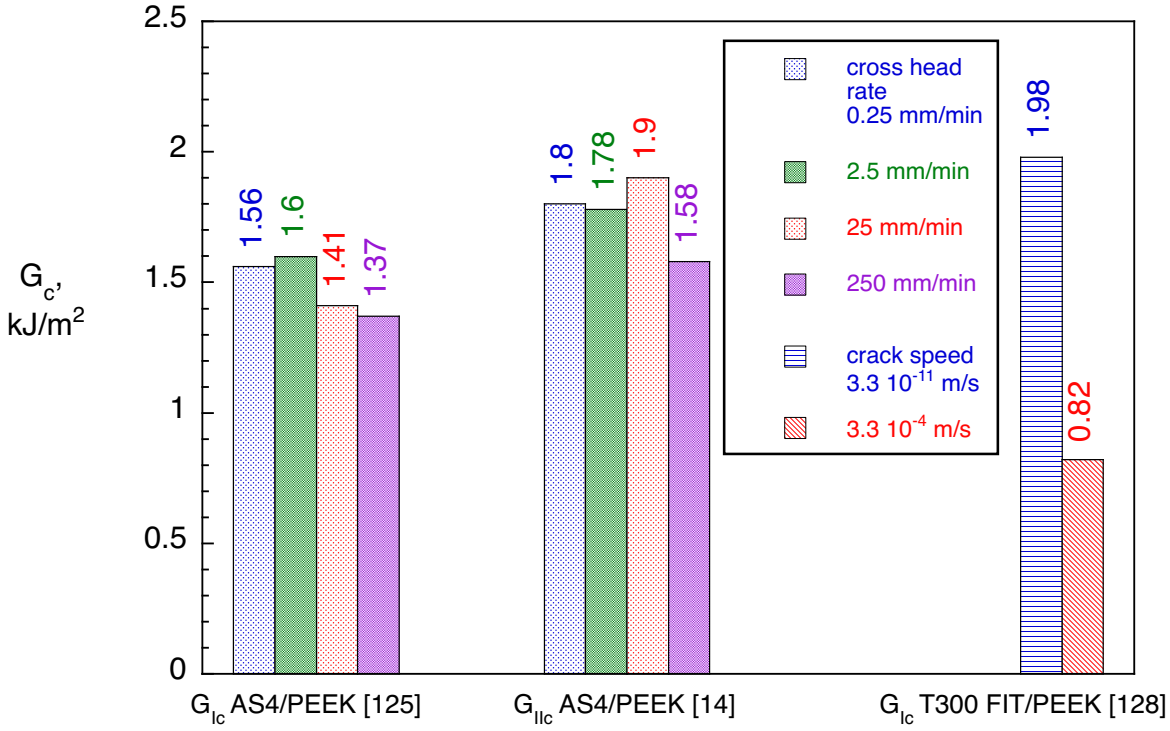

Figure 11: Influence of loading rate and crack speed on fracture toughness [14, 125, 128].

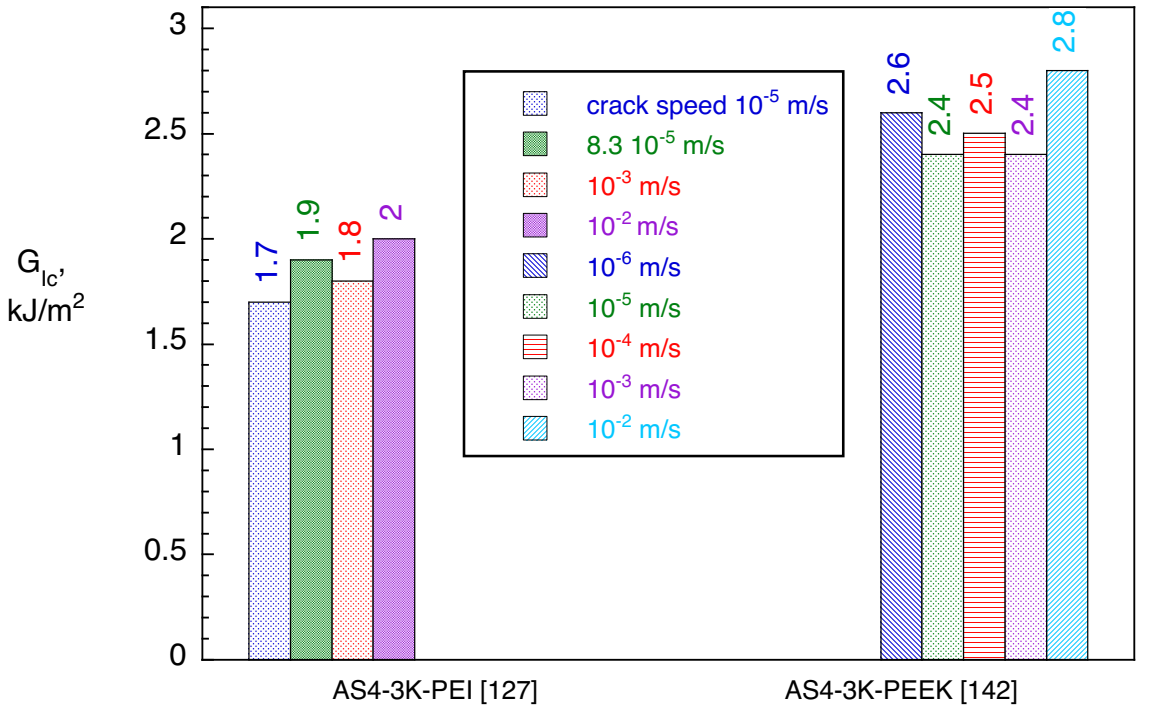

Figure 12: Influence of crack speed on Mode I fracture toughness [127, 142].

ANALYSIS

In the following section several examples of analyses are discussed including process and manufacturing simulations which include the modeling of the crystallization process and the development of residual stresses. Other simulations focus on modeling the welding process itself. One subsection is dedicated to finite element (FE) analyses that were performed to support testing. Another subsection focuses on the modeling of progressive damage and delamination growth including cohesive zone models (CZM), fracture mechanics-based models and customized constitutive models as well as examples where the authors combined approaches in their analyses. The last subsection introduces models that account for strain-rate effects on fracture toughness as well as viscoelastic (VE) and viscoplastic (VP) modeling approaches.

Process Modeling and Manufacturing Simulations

Quantifying the primary and secondary crystalline phases in a material when modelling crystallization kinematics has been studied, most often for unreinforced PEKK [55]. The impact of thermal processing cycles on this is clearly reported, where holding temperature and time are observed to influence the extent and nature of crystallinity developed in the material. Robust models have been developed for the isothermal crystallization cases of PEKK, but further refinement is needed in the case of non-isothermal crystallization kinetics [55]. In the case of CF/PEKK composites, crystallization kinetics studies are minimal. A few of the aforementioned crystallization kinetics models applied to unreinforced PEEK and PEKK have also been implemented to their composite counterparts with some success, however, once again this is less diligent than for neat PEEK and PEKK, and existing models may need some adaptation to account for the inclusion of carbon fibers [55].

Another review [143] focused on the thermo-stamping process found that simulation steps must include both global and local processes which determine the geometry and quality as well as the cost of the manufactured carbon fiber reinforced thermoplastic components [143]. The global process steps provide outside boundary conditions and external environmental conditions for the local process. The various main aspects of the global process have a strong influence on the local process and ultimately the final products. Investigations focused on the local process will provide comprehensive understanding of the evolution of the material characteristics including both physical & chemical behavior and mechanical behavior. Understanding of the critical parameters in the local process and their dependency on the global process will enable the forming numerical simulations to be developed to achieve process optimization. It is important to recognize that the local process and the global process are interconnected. Most research in the literature treated the whole stamping step at a global level, with isothermal cure assumption, which might not reflect the real forming temperature distribution. Consequently, the analysis and simulation of the local process with this global assumption will not achieve satisfactory results. Furthermore, the global and local temperature distribution will influence the forming mechanisms such as the recrystallization of the thermoplastic resin and consequently the deformation behavior. Only limited research using local analyses has been carried out on the crystallization of material in the stamping step, and the complex interaction between formability, temperature and crystallinity is not yet well understood. The advancements in the global process simulations have mainly been focused on the model-specific data interfaces for the information transformation from one simulation step to another during the thermo-stamping process. Most of the studies for the process simulations are focused on the local process during the stamping step since deformation and defects induced during this step are essential to the understanding and optimization of the thermo-stamping process. Review of the advancements of the local process simulation technologies showed the evolution of constitutive modeling for thermo-stamping from early simple non-orthogonal elastic constitutive and the hypo-elastic constitutive models to the recent more

complex hyper-elastic invariants constitutive and the ideal fiber reinforced material based constitutive models. FE strategies have also been developed in line with the multi-scale nature of TPCs. The combination of various constitutive models and the FE strategies have been used in the thermo-stamping process simulations to predict the common forming phenomena and defects of TPCs observed from the experiments. Several specific commercial software has been developed for process simulation, such as AniForm [144] (based on an implicit solution method) and PAM-FORM [145] (based on an explicit solution method), which are suitable for thermo-stamping processes. In addition, in order to fulfill the requirements of common engineering application, commercial FE software Abaqus/Standard® [146] and LS-DYNA® [147] with customer written subroutines are also commonly found in research for thermo-stamping process simulations. Further development efforts regarding rate- and temperature-dependency as well as material state (molten or solid) in numerical models are still required to increase the reliability of the process simulations. Furthermore, it is required to develop some iterative process simulation integrated strategies with the ability to predict the influence of both the global and local aspects on the final quality and manufacturing cost of the TPC products. The integrated strategies can then be used as the necessary numerical tool in an iterative optimization chain [143].

Other researchers developed a complete design and manufacturing scheme for a rubber-formed flap rib [22]. A blank design strategy was created using a FE-based software called PAM-FORM 2G developed by ESI Group [145] to simulate the thermoforming process. The manufacturing and blank were optimized with the aim to minimize composite material while imposing design and manufacturing constraints. This design strategy enables the designer to automatically generate a blank design based on the forming behavior, fiber orientation and clamp positions and types. Designed blank shapes can then be traded-off on product quality and cost aspects. The blank that results in the best product quality at minimal blank surface may actually not always be the most cost-efficient design, as blanks have to be cut from large panels and nesting is critical. Nevertheless, the presented strategy proved to be a valuable tool for reducing cost during rubber forming R&D and production [22].

Modeling crystallization and residual stresses

Early on, researchers developed models to predict the temperature and volume fraction crystallinity distributions in the cross-sectional area of a semicrystalline thermoplastic laminate during processing from the melt [60, 148]. In their work a 2D heat conduction analysis was combined with the calculation of the time-dependent crystallinity profile that is based on the crystallization kinetics model of Velisaris and Seferis which in turn is based on a linear combination of two crystal nucleation and growth processes (dual mechanism) observed experimentally and occurring in parallel. That model had shown good agreement with measurements of crystallinities for both neat and carbon fiber reinforced PEEK samples for a wide range of cooling rates from the melt. The combined model allowed for the prediction of free-edge gradients developing during processing. The model was used to analyze unidirectional 16-ply ACP-2 laminates. It was found that the application of fast cooling rates (2100°C/min, 1200°C/min, 600°C/min) may lead to significant temperature and crystallinity gradients in the vicinity of free edges. This effect was found to be very localized, and it appeared to vanish at a distance of two laminate thicknesses measured inward from the free edge. Moreover, existence of large free-edge gradients during the processing was evident for any surface cooling rate applied. The residual stress state was found to be strongly affected by the temperature and crystallinity gradients occurring during processing (and not only by the steady-state levels) through changes in mechanical properties. Therefore, the results emphasize the importance of the prediction of the free-edge effect developing during processing from the melt of fiber reinforced thermoplastic composites in general, and semicrystalline thermoplastics in particular [60, 148].

Recently, a computational FE model of thermal residual stress was developed for carbon fiber/thermoplastic composites at the microscale and implemented via a user material

subroutine (UMAT) in Abaqus/Standard® [59, 146]. This particular model accounts for cooling-rate effects on crystallinity and stress-free temperature, temperature-dependent elastic modulus, temperature-dependent coefficient of thermal expansion (CTE) of the matrix, and the temperature-independent transversely isotropic properties of the carbon fiber. Results were generated for a model composite, consisting of a single carbon fiber (AS4) embedded in a thin polypropylene film. Single filaments were pre-tensioned in the polymer (PP) melt to induce different levels of residual axial strain as well as maintain straight fibers during cool-down. The residual strain along the length of the fiber was quantified and validated including the shear lag region that develops at the free edge of the sample. Experimentally measured residual strain showed a good correlation with the FE predictions for the applied fiber preloading conditions [59].

Another approach focused of on using molecular dynamics (MD) modeling to predict the thermo-mechanical properties and volumetric shrinkage of PEEK resin as a function of crystallinity content and temperature [58]. Neat PEEK models were created at the molecular level using the open-source LAMMPS (Large-scale Atomic/Molecular Massively Parallel Simulator) MD simulation software package [149]. Once the elastic properties of the molecular models were evaluated using MD simulations, the next higher length scale was used to predict the thermo-mechanical properties of semi-crystalline PEEK as a function of crystallinity and temperature. The semi-crystalline PEEK was modeled using the Generalized Method of Cells (GMC) using the MAC/GMC software package [58]. The results show that accurate predictions of mechanical properties of semi-crystalline PEEK can be obtained using the combination of MD modeling and MAC/GMC. The goal is to be able to predict the residual stress evolution in PEEK composites as a function of processing parameters [58].

Simulations of the welding processes

Several efforts have been made to model the welding processes. During induction heating, the primary heat generation mechanisms of carbon fiber reinforced thermoplastic laminates are joule losses, and junction heating with contact resistance and dielectric hysteresis. These mechanisms are highly affected by the laminate's architecture and the anisotropic properties of each ply. Recently, a static heating model was developed in Altair® Flux® [150] to examine the induction heating mechanisms with anisotropic material properties. Further, the viability of using FE software as a process simulation tool was studied [151]. Three laminate stacking sequences were considered. A FE model of the Joule heating process was studied to compare modeling the electrical and thermal properties of each individual ply with a laminate theory homogenization of the thermal and electrical properties. Two analytic homogenization (HG) approaches and one FE HG approach were studied to examine their efficacy. One of the analytic approaches was based on Athanasopoulos's equation [152] and the other on classical laminate theory [153], while the FE model was built with COMSOL Multiphysics® [154] software. Experimental induction heating of CF/PEKK panels was performed and quantitative (infrared camera) temperature measurements were compared to the FE simulations. Results indicate that the methods and models used in this work are, in most cases, not sufficient. Of the analytical models, the Athanasopoulos model was closest to the experimental results, however it predicts the same resistivity for all three stacking sequences considered, which did not agree with either the COMSOL® HG model or the experimental results. FE homogenization provides an attractive alternative, however even this approach falls short in many cases, overpredicting the temperature for some layups and underpredicting it in others. One challenge is that the base model being used in this work to simulate induction heating has only considered Joule heating, one of the three primary heating mechanisms for induction welding in TPCs. A more advanced model that considers contact resistance and dielectric hysteresis may improve results but would also require homogenization of more material properties. An alternative approach would be to attempt to include other heating mechanisms within a Joule heating model via an effective resistivity [151].

Other researchers used a hybrid FE model for the simulation of induction heating of layered composite plates [87]. Their modelling included the alternating electromagnetic field generated by an alternating current running through a coil, the current densities in the composite plate resulting from the electromagnetic field and the heat generation resulting from the current density distribution. The calculated volumetric heat generation was subsequently used as input for the body forces of a heat transfer problem. The combination of the two codes allowed the simulation of welding a lap-joint between two composite plates. The simulation included an elliptical coil moving over the length of the lap joint. Heat sinks were applied to resemble a practical welding setup [87]. Related research focuses on undesired localized hot spots that can occur during induction welding near the edges of a part, resulting in subpar quality of the joint and an unwanted surface finish (thermal based delamination). To better understand how the hot spots occur, a detailed investigation by analyzing the current flow through the thermoplastic composite laminate layers was performed. The analysis was done using an in-house developmental mixed boundary element (BE) / FE software code, *WelDone* [40]. It was numerically determined that eddy currents follow a 3D current path when the induction coil is in a general centered location. Then when the coil is moved to the edge (half-on and half-off of the plate) a buildup of eddy currents is observed along the edges of the laminate with the dominant eddy current flow direction being out-of-plane. This buildup causes an increase in energy loss, which in-turn increases the volumetric heat generation and results in higher temperatures near edges than observed in a general centered location. These high temperatures exceed the melting temperature and cause surface defects and thermal based delamination, commonly observed at the edges of welded composite specimens [40]. Further research emphasis aimed to reduce the observed edge effects [42]. For the analysis, a multi-physics commercial FE solver *Ansys Maxwell* combined with *Ansys Workbench* was used. The simulations were performed separately with and without a magnetic flux concentrator. The field parameters such as magnetic field intensity (H), induced current density (J) and the volumetric heat generation were evaluated using the electromagnetic analysis capability in *Ansys Maxwell*. The introduction of a concentrator reduced the observed volumetric heat build-up by converging the field lines closer to one another. The subsequent heat transfer analysis using *Ansys Workbench* further highlighted a clear reduction in the overall edge heat propagation upon the addition of the concentrator. The results show that the concentrator provides a better control of the generated magnetic field which in turn helps to manipulate the resulting heat contours. Upon the inclusion of the concentrator, the power supply requirements were also reduced as higher heating rates were achieved for the same process parameters, which opens up the possibility for achieving faster production rates with better quality control [42]. Additional research by the same team focused on the importance of stacking sequence for the magnitude and direction of volumetric heat generation, and the opportunity to influence the volumetric heat generation by adjusting the coil shape to modify the electrical field that is inducing the currents and thus volumetric heat generation [41]. To investigate the effect of the coil shape on volumetric heat generation the in-house developed tool (*WelDone*) was used for the numerical simulation of two 8-ply quasi-isotropic laminates $[45/90/-45/0]_s$ and $[0/90/-45/45]_s$ and four coil shapes. By comparing the volumetric heat generation in two laminates for each coil the effect of the coil shape can be investigated in more detail. For the first three coils the highest volumetric heat was generated in the 0° direction, while the fourth coil generated the most volumetric heat in the 90° direction. Due to the complex out-of-plane behavior of the eddy currents the volumetric heat generation in the thickness direction is on the same order of magnitude as volumetric heat generation in the direction transverse-to-the-fiber. If the stacking sequence is changed, the highest volumetric heat is still generated in the layer aligned with the coil direction. This will also affect the volumetric heat generated in the adjacent layers, therefore the position of the layer aligned with the coil is an important parameter when choosing a coil shape. If it is desired to maximize heat generation at the interface, or symmetry plane then for the first laminate $[45/90/-45/0]_s$ a coil aligned with the 0° direction is best suited. For the second laminate $[0/90/-45/45]_s$, however, optimizing the volumetric heat generation in the 45° layers will require

more than just a coil aligned with the 45° direction. When the coil shape is complex it is difficult to make prediction for which layer is heated the most based solely on the coil shape. It was found that to analyze the effect of the coil shape a more detailed numerical analysis is required [41].

Resistance welding was studied by other researchers who developed a novel optimization tool for determining the optimal process parameters for thermoplastic composites (CF/GF/PPS) [155]. Their numerical tool was based on a transient 2D FE thermal model in FEMLAB that computed the temperature data used in the optimization procedure. In the first stage of the study, thermal analysis was performed that determined the influence of different factors on the temperature in the weld of a lap shear specimen. The results showed that the reinforcement fiber material has a profound influence on the temperature in the weld. Due to a much higher heat transfer coefficient of the carbon fibers in the longitudinal direction, weld temperatures for carbon fiber reinforced materials were significantly lower than weld temperatures of glass fiber reinforced materials welded with the same welding parameters (power level and weld time). The diameter of the wires in the heating element also had impact on the temperature in the weld, with the meshes (steel) with smaller diameters giving comparatively higher weld temperatures. The influence of the thickness of the insulation material (wood) was also studied. It has almost negligible influence on the temperature distribution in the welded material, except for extreme cases when the thickness of the insulation block approaches the thickness of the welded laminate. In the second stage of the study, a MATLAB® [156] optimization tool was used to automatically create theoretical processing windows for different welding configurations and to find the optimal parameter values for minimum energy input. The results showed that the optimal processing windows of carbon fiber reinforced materials were shifted towards higher energy levels, thus confirming the results from the thermal analysis [155].

Finite Element Analysis to Support Testing

The usefulness of single lap shear testing for the characterization of resistance welded thermoplastic composite joints was investigated [90]. In the study, FE analysis and digital image correlation (DIC) measurements were combined to investigate the strain distributions of the joints during testing. Substrates made of glass fiber reinforced PPS (GF/PPS Cetex® 8 harness satin weave glass fiber reinforced PPS (Polyphenylene Sulfide) made by TenCate, Netherlands) were resistance welded using PPS film and different thickness metal meshes. An adhesively bonded joint (3M 9323) was studied for comparison. Shear and peel strain distributions were investigated at the joint overlap area. The effect of the resin fillet and metal mesh on the strain distributions and apparent shear strengths was investigated. Stress/strain analysis of the resistance welded joint was performed by using 2D planar shell elements in Abaqus/Standard® [146]. Linear elastic material properties were used for both substrates and the weld line which was treated as an isotropic material. First, the material properties of the PPS resin were used for the weld line. When using equivalent mechanical properties of the PPS impregnated metal meshes as input to the model, both shear and peel strain concentrations at the overlap edges were diminished, and a closer agreement was found with the DIC results [90]. The results showed that the edges of the resistance welded joints are the weakest areas due to the load eccentricity and the heat transfer related issues during the welding process, and that the use of resin fillets (3M 9323 A/B adhesive) greatly reduces the strain concentrations at the overlap edge. However, it was found difficult to fully characterize the resistance weld quality only from single lap shear testing mainly because both the stress distribution and lap shear strength are influenced by the imperfections of the resistance welding process [90].

The compression after impact (CAI) test of a TPC panel was modeled to predict the behavior and the compressive residual strength [157]. The methodology first used X-ray computed tomography scans to characterize the internal impact-damage region for each ply in

the panel. Second, CAI experiments were used to quantify the unknown stiffness degradation in the damaged region, which will characterize the laminate-level stiffness. Third, the post-impact ply-level stiffness tensor was calculated from the impact-induced laminate-level stiffness. Finally, the damaged ply-level stiffness was assigned to the damaged region in the FE model for CAI predictions. The strain-dependent material constitutive behavior was implemented as a UMAT in Abaqus/Standard® [146]. The results from 3D FE analyses were in good agreement with the experimental data. The numerical results from parametric studies show that width-to-thickness ratio and boundary conditions have a significant effect on the failure load of the plates [157].

A group of researchers used analysis during the design and development of a wing box demonstrator test article and to support related tests on different levels of the building block [108, 110, 111, 132, 158]. The load carrying capabilities of the wing box section were determined considering that the segment of the wing box is located at about 80% of an aircraft's wing semi-span and has a length of about 3 m. Prior to experimental validation, a virtual test (design verification) via FE model of the wing box assembly was undertaken and an analysis was performed to replicate representative in-service loading scenarios and boundary conditions. Two design solutions, a conventional constant stiffness composite layup and variable angle tow (VAT) layup of skin sections were developed with the aim to carry out a comparison between the two approaches. For the virtual tests, two combinations of four-point bending and compression loading were considered in order to replicate the value of the maximum bending moment acting at the most loaded section during two particular flight conditions. To verify that the suggested designs met the requirements in terms of maximum bending moment and maximum strain in the top skin, nonlinear static FE analyses were performed using the commercial software Abaqus/Standard® [146] (S4R shell elements). Primarily, computed strains and displacements obtained from non-linear analyses were used for comparison, which for both load cases considered showed an increased stiffness of the entire wing box due to the VAT layup of the skin section compared to the conventional constant stiffness composite layup [109, 112].

In a related study, the buckling performance of a stiffened panel was evaluated. Laser-assisted tape placement and VAT was used to manufacture the panel using thermoplastic composite tape (Toho Tenax IM7/PEEK), improving manufacturing accuracy and speed. The buckling mode of a stiffened panel was assessed using a three-point bending test fixture to induce compression in the skin. The test was relatively simple to perform compared to traditional pure compression tests, since time-consuming alignment steps were not required prior to testing. In addition, the bending stresses used to induce buckling more closely resemble those in actual aerospace structures compared to the pure compression induced by traditional tests. As above, FE simulations using the commercial software Abaqus/Standard® [146] (S4R shell elements) were used to validate the proposed test concept and to determine the boundary conditions and the panel geometry required to initiate compression buckling. Additionally, a Ritz-based analysis tool was used for linear buckling analysis. A comparison of the buckling mode obtained experimentally and that predicted from numerical models showed good agreement. Future work will focus on further benchmarking the numerical model by direct comparison of the simulation full-field predictions to the experimental data. [113].

Modeling of Progressive Damage and Delamination Growth

Simulations using cohesive zone models

FE analyses were performed including CZM which aimed to determine cohesive laws representative of the fracture behavior of a pure PA polymer (Nylon FX 256) and a composite material reinforced by 15 vol.% short carbon fibers [98]. An inverse procedure was followed by iteratively adjusting the cohesive parameters in order to get the numerical load-displacement curves in agreement with those obtained from three individual DCB tests. A trapezoidal and

trilinear cohesive law were determined appropriate for the pure polymer and the composite, respectively. The average cohesive laws, obtained from correlation with three tests, were subsequently used in numerical simulations and the ensuing load-displacement curves were compared with the experimental curves. In both cases it was concluded that the resulting numerical load-displacement curves replicated the overall trend of the experimental results [98]. A similar procedure was used to simulate the fracture process in DCB, ENF and SLB tests (UD-reinforced polyamide PA6 composite, prepreg tape (CPA635)). In all cases a trapezoidal cohesive law was used for the simulations. The numerical load-displacement and resistance-curves were found to be in agreement with the experimental trends, which demonstrated that the procedure was appropriate in the context of fracture characterization of thermoplastic composites under mixed-mode I + II loading [140, 159].

Simulations using fracture mechanics-based models

On higher levels of the building block, e.g., at structural detail and panel level, researchers found that it is not computationally efficient to model the composite structure in full detail. At this scale the emphasis is on global structural behavior, for example during post-buckling, and the performance of critical interfaces such as the welded skin-stiffener interface are of high importance [160]. Thus, skin-stringer separation was modelled using the Virtual Crack Closure Technique (VCCT) [136] in combination with the Benzeggagh Kenane criteria [136] for mixed-mode interface behavior. The use of VCCT allows for a coarser mesh compared to other interface methods, which is a major advantage when modelling large structures and allows for efficient modelling of skin-stiffener separation, even at the component level. The restriction of VCCT is its requirement for a pre-crack, which normally prevents it from being used for pristine structures. However, the unwelded areas on both sides of the welded joint can be modelled as a pre-crack to limit this restriction. Use is made of a virtual building block approach to ensure the validity of the methodology at each scale and corresponding critical failure mode [160]. The methodology therefore was verified using a model of a DCB specimen and validated on two single-stringer specimens which were experimentally tested by GKN Fokker. The verification and validation steps use the same meshing strategies, element types, and VCCT parameters. Subsequently, for a three-stringer panel, the buckling behavior, damage propagation, and final collapse of the panel were determined with a dynamic implicit analysis. The experimental test to validate the FE analyses were not yet available at the time of publication [130].

Simulations using customized constitutive models

At the lower end of the building, researchers found it appropriate for simulations to take into account the physical mechanisms of damage and nonlinearity at the lamina level through a high-fidelity modelling approach where each ply is discretized using a fiber-aligned meshing technique and behaves according to the constitutive material models [161]. The plies are therefore modelled as separate parts and surface-based general contact is used to facilitate the non-conformal meshes. The constitutive material for the thermoplastic composites model takes into account the 3D stress state and is based on the deformation gradient to account for large shear deformations within the failure modes. The nonlinear elastic-plastic behavior of the matrix is modelled for both in-plane and out-plane shear responses based on Ramberg-Osgood laws. The constitutive material model is implemented in a user-defined subroutine (VUMAT) in Abaqus/Explicit® [146]. Modelling of specimens on the coupon level is automated by means of Python scripting to allow for rapid generation of virtual allowables [161].

Others used an elastic-plastic damage model, which accounts for both the nonlinear behavior and progressive failure of a thermoplastic composite ply, to predict the three-point bend behavior of a thermoplastic matrix composite (AS4/PEEK) [162]. For the intra-laminar failure, they used the Northwestern University damage criteria to capture the damage initiation. For the interlaminar failure, a quadratic-traction criterion was employed to capture the damage initiation in the composite interface. In the interlaminar damage model, the linear softening law was employed to model the damage evolution. An elastic-plastic constitutive model was

employed to capture the nonlinear response of the composite ply. The damage evolution law, based on the energy dissipated during the damage process and linear material softening, was used to predict the evolution of the damage in the composite plies. The developed elastic-plastic damage model was then implemented as a VUMAT in Abaqus/Explicit® [146] and then combined with the Abaqus/Explicit® native cohesive surface model to form a complete FE model to predict the mechanical response and progressive damage of thermoplastic composite laminates. The simulation results, e.g., load response, deformation, and damage morphology, were compared with the experimental results extracted from the three-point bend experiments performed on the composite specimens. The comparison showed that the computational results yielded good agreement to the experimental results [162].

An additional combined elastic-plastic damage model for the progressive failure analysis of composite materials and structures was developed by other researchers [163]. Their model accounts for the irreversible strains caused by plasticity effects and material property degradation due to the damage initiation and development. The strain-driven implicit integration procedure is developed using equations of continuum damage mechanics (CDM), plasticity theory and includes the return mapping algorithm. A tangent operator consistent with the integration procedure was derived to ensure computational efficiency of the Newton-Raphson method in the FE analysis. The algorithm was implemented in Abaqus/Standard® [146] as a user-defined subroutine (UEL). To demonstrate the capability of the proposed model for representing the post-failure regime and to validate its ability to reflect on the plasticity behavior, several analysis were performed using tests reported in the literature for comparison [164], [165]. First, an AS4/PEEK $[\pm 45]_{2s}$ composite laminate subjected to tensile loading was analyzed [165]. The predicted stress–strain curve correlated well with that obtained from the experiment. Second, analyses were performed using data from open hole tension (OHT) tests with specimens made of AS4/PEEK composite $[0/45/90/-45]_{2s}$ [164]. The results obtained from the simulations agreed well with the reported test data [163].

Another constitutive model was implemented into the commercial FE code Abaqus/Standard® [146] using the user subroutine USDFLD. Three in-plane failure modes: fiber breakage, matrix cracking, and fiber/matrix interface debonding were included in this model. Fiber and transverse directions show softening phenomena beyond damage initiation and no plastic strains occur. However, the shear direction behaves elastic-plastically with strain hardening. The model was used to investigate the ultimate tensile failure strength of laminated composites made of AS4/PEEK containing a central circular hole. The effects of hole size and specimen width were studied in detail. By comparing the predicted results with the experimental data, the proposed model showed to be capable of predicting failure strength and load–deflection relations of notched laminated composites [164].

To explicitly model the behavior of the polymer matrix, a material model was developed that characterizes the plastic behavior and damage accumulation in a thermoplastic matrix (PEEK) with dependence on the stress state that the matrix undergoes during loading. All constants required for the stress analysis were taken from the literature and used as input to material models available in Abaqus/Standard® [146]. First, the three-point bending test for the neat PEEK resin was modeled using 3D brick elements with incompatible modes. This analysis showed that the most significant contribution to nonlinearity in stress-strain curves obtained from the flexural test is caused by plastic deformation of the material under a multi-axial stress state, corresponding to values of triaxiality in the range 0.5–0.65. Good correlation of the numerical predictions with the experimental data validated the model and the choice of input parameters. Second, the model was applied to a case of periodic cells of a unidirectional composite with random spacing of fibers subjected to transverse tension loading using fully-integrated 2D plain strain elements. A comparison of the predicted strength values with the typical experimental values was used to validate the proposed criteria. Third, the material model was used for the analysis of interface failure observed during fiber pull-out tests which is modeled using 2D axisymmetric elements. The importance of the triaxiality was demonstrated:

the material near the interface area under plastic deformation exhibits strengthening due to the change of the stress state from shear- to compression-dominated [166].

Simulations using combined models

Researchers investigated welded multi-stringer panels made of CF/LM-PAEK using a combined approach with fracture mechanics-based analysis and first ply failure [143]. The emphasis of the study was on buckling and skin-stringer separation behavior in the post-buckled regime [167]. The multi-stringer panels were designed to approximate the structural behavior of the lower half of the Multi-Functional Fuselage Demonstrator of the *STUNNING* project. The panels have three omega stringers and a length of 500 mm. A three-stringer configuration allows to study the middle stringer in pristine and damaged configurations with minimal influence of the free edges and boundary conditions. The laminated sections were modeled using SC8R continuum shell elements Abaqus/Standard® [146]. The potting material of the test panel was modeled using C3D8R solid elements and the clips and brackets of the fuselage section were modeled using C3D10 tetrahedral elements. The welded joint between the skin and stringer was modelled using VCCT in combination with the Benzeggagh-Kenane (BK) law for mixed-mode failure as discussed above. First ply failure criteria (Tsai-Hill, Tsai-Wu and Hashin) were included in the analysis to check if material failure occurred before skin-stringer separation. The failure of the panel due to skin-stringer separation showed a high level of similarity compared to the full fuselage section, but with a higher number of failure locations. The analysis of both the fuselage section and test panel showed that similar structural behavior to that observed in the fuselage section can be achieved on a lower structural level [167].

In another study, a welded single lap shear joint was designed, manufactured (Solvay AS4D/PEKK-FC), tested and analyzed to predict failure [88]. Failure of welded joints is considered to be similar to the failure of general composite laminates due to the nature of the joining process. The laminate is locally melted and consolidated in a similar manner as consolidating plates in an autoclave process, if the right manufacturing conditions are respected. This means that the welded interface is locally indistinguishable from the bulk material. Therefore, the failure of the welded joint is expected to behave the same as interlaminar damage in the thermoplastic composite material and that a zero-thickness interface can be assumed, which is different from bonded joints that have a non-zero adhesive thickness. The failure mechanisms of the welded joint can therefore be divided into the typical categories of composite failure modes, namely interlaminar and intralaminar damage. Failure of the weld and failure of the ply-to-ply interface of the laminates fall into the interlaminar category. This damage behavior affects the separation between plies, which forms a delamination that can occur under different opening modes. Intralaminar damage considers all the failure modes that occur within each ply such as fiber and matrix failure. The failure of the welded single laps shear joints was analyzed with two distinct modeling approaches using Abaqus/Explicit® [146]. A simplified modeling strategy which only accounts for damage at the weld was compared to a high-fidelity model which can take into account the physical failure mechanisms at the lamina level [88]. In the simple model, the composite sections at the load introduction, which are far from the welded joint, were discretized with through-thickness continuum shell elements (SC8R) and considered only linear-elastic material behavior. The central zone of the joint, also referred to as the damage zone, in the simplified model was also modeled using linear-elastic SC8R elements, and a surface with contact and cohesive surface for the welded interface. A smaller mesh size was used in the damage zone to meet mesh size requirements for cohesive zones. In the high-fidelity model, a ply-by-ply modeling strategy was used in the damage zone, where each ply was discretized as a layer of reduced-integration solid elements (C3D8R). A fiber aligned mesh with an aspect ratio of three (longitudinal direction) to one (transverse direction) was used, following the guidelines given in [161]. The welded interface, as in the simplified model, consisted of a cohesive surface for the weld and a contact definition outside of the weld. The interlaminar model available in ABAQUS/Explicit® [146] was used, while the intralaminar model was implemented in a CDM model through a VUMAT. It was found that the simplified

approach, based on CZM, predicts a very conservative joint strength when unidirectional interlaminar fracture toughness properties are used. The high-fidelity modeling approach, however, provided new insights in the failure behavior of the joint and was able to accurately predict the failure mode. However, predicting the upper bound experimental results was still difficult and some limitations to the numerical methodology were identified. This may include changes in mix mode fracture toughness in the welded region during crack propagation, non-zero through-the-thickness matrix crack angles near the welded interface and not considering frictional effects on the fracture plane. The analysis using the high-fidelity model showed that different material properties for the inter- and intralaminar failure modes have a strong effect on the joint strength and may significantly influence the failure modes. A better understanding of the material properties of the welded joint is still needed and design guidelines may need to consider the welded interface and also the surrounding plies [88].

Others investigated the failure mechanisms of a recently developed butt jointed thermoplastic composite using a combination of CZM and extended FE analysis (XFEM with VCCT) [168]. The laminated skin and the stiffener were made of AS4/PEKK, and the butt joint (filler) was injection molded from 20% short AS4 filled PEKK. The skin and the stiffener were co-consolidated together with the filler to form a hybrid butt joint structure. Observations made during experiments showed that a crack initiated in the filler and then propagated towards the skin-filler interface in less than 33 μs under three-point bending. A 2D FE model (CPE4) created in Abaqus/Standard® [146] was used and the observed failure behavior was simulated using a coupled XFEM-CZM approach. Residual thermal stresses were taken into account in the model. The crack initiation and progression in the filler were predicted using the XFEM (VCCT) and the delamination at the skin-filler interface was modelled using the cohesive surfaces. Good agreement between the experimental results and the numerical predictions was obtained for the butt joint. The predicted stiffness of the specimen, the location of crack initiation and propagation, as well as force drop during delamination were in good agreement with experimental data. The traction at the cohesive surface was found to vary during delamination due to the nature of the mixed-mode behavior of the interface. The mode I opening was found to be dominant at the beginning of the delamination and mode II in-plane shear became more effective during the progression of delamination and near the end of delamination. An increase in G_{Ic} and G_{IIc} input values resulted in larger cohesive zone length with a smaller force drop during delamination and hence a shorter delamination length. The interface strength values had hardly any influence on the simulated delamination length and force drop [168].

Models accounting for strain-rate effects

Accounting for strain-rate effects on fracture toughness

A model taking into account the strain-rate effect of the mode II fracture toughness was developed [49]. First, ENF tests were performed to generate unstable crack growth input parameters. Post-processing the results made it possible to experimentally measure the fracture toughness for high-speed propagation and to identify the strain rate behavior to be implemented into an existing discrete ply model. This model used interface elements which made it possible to simulate both the significant openings of the plies due to matrix cracking and to account for the coupling between the matrix cracking and the interlaminar damage (delamination). Fiber damage was also taken into account by using CDM in the volume elements with a damage criterion based on a simple longitudinal strain criterion onset and an energy dissipation based on the fracture toughness of fiber failure. Second, impact tests on composite specimens (CF/PEEK) with different stacking sequences and different impact energy levels were simulated using the discrete ply model and taking the strain rate effects into account. Results obtained from analysis using Abaqus/Explicit® [146] showed relatively good correlations with experiments. In addition, the impact damage obtained from the analysis of the C/PEEK tests was compared to the analysis results of carbon/epoxy plates which were modeled

without strain rate effects (comparison of numerical results only). This approach was used since the fracture toughness in mode II does not seem to vary significantly with rate for epoxy resin. The carbon/epoxy plate exhibited a slightly smaller delamination size than the carbon/PEEK plate despite the higher static fracture toughness value for PEEK resin. This increased size in the carbon/PEEK plate is caused by the strain rate effects, which considerably reduces the fracture toughness. This reduction may limit the future application of PEEK composite laminates in areas where impact resistant and damage tolerance is required. These observations need to be confirmed by additional studies and different layups including other thermoplastic resins [49].

Viscoelastic and viscoplastic approaches

Semi-crystalline polymeric matrices often exhibit complex viscous effects where both viscoelastic (VE) and viscoplastic (VP) behaviors are combined. Therefore researchers proposed a constitutive model that incorporates viscous behaviors in the mechanical response of semi-crystalline thermoplastic materials [169]. The model is based on three constitutive branches. First, the intermolecular resistance introduces a rate- and temperature-dependent part that is defined by a Neo-Hookean hyperelastic spring and a nonlinear VP dashpot. Second, the resistance of the polymer network introduces a non-linear temperature-dependent hyperelastic part that is defined by a modified eight-chain spring. The third viscous constitutive branch introduces viscoelasticity through a non-linear hyperelastic response which depends on strain rate. The constitutive equations are formulated in finite deformations within a thermodynamically consistent framework and were implemented as a VUMAT for the commercial FE solver Abaqus/Explicit® [146]. The model parameters were taken from experimental data reported in the literature for Ultra-high-molecular-weight-polyethylene (UHMWPE) and high-density polyethylene (HDPE). Subsequently, the model was used to study the influence of viscous contributions and thermo-mechanical coupling on the necking process when semi-crystalline specimens are subjected to large stretching conditions. Numerical predictions show that UHMWPE can undergo higher strain values without neck formation leading to higher ductility with respect to HDPE [169].

To account for VE and VP effects, a thermo-dynamically consistent continuum constitutive model with 10 parameters was developed [170]. The model is specifically designed for amorphous glassy polymers and can predict the mechanical behavior of pure polystyrene obtained in coarse-grained molecular dynamics (MD) simulations under various uniaxial and biaxial loading conditions. The parameters identified based only on two sets of MD simulation data could be validated by a large variety of MD simulation data under different loading conditions. The researchers assumed that plasticity is caused by deformation-dependent intermolecular resistance and thus proposed a constitutive model within the generalized Maxwell framework, but in parallel comprising of an elastic, a VE, and several elastic-visco-plastic (EVP) modules. Regarding the compressibility, the researchers proposed a criterion to assess volumetric inelasticity: the ratio of the dissipated energy in a load cycle due to volume changes to the total dissipated energy. The small ratio justifies neglecting volumetric contributions in the VP constitutive model. This criterion can also be used in constitutive modeling of other slightly compressible materials, both based on MD simulations and experiments. The researchers plan to extend their constitutive model to account for additional inelastic effects, e.g., damage effects and fracture by introducing chain breakage into the MD simulations. In addition, this constitutive model is expected to be used in partitioned-domain multiscale simulations, to investigate the mechanical properties of polymers and polymer-based composites [170].

To describe the behavior of a thermoplastic composite (polybutylene terephthalate with 30 wt.-% short glass fibers) an anisotropic temperature-dependent EVP model was implemented using the available macroscopic material models in the commercial FE solver Ansys [101]. The material model formulations discussed are typically available in most commercial software, and the method requires relatively low computation, which enables robust and efficient simulation of

complex components in an industrial context. The elastic behavior is described by the orthotropic linear elastic model generated through the mean-field homogenization method and the anisotropy in the plastic region by the Hill yield criterion dependent on the fiber orientation. The rate-dependent plasticity is described by the unified visco-plasticity framework of Chaboche [171-172]. To describe the continuous temperature dependency, model parameters are systematically determined as a function of temperature in the range of interest, including regions below and above glass transition temperature. Further, an optimization method based on a genetic algorithm in MATLAB® [156] is adopted for parameter optimization. The optimized model describes the anisotropic material behavior observed in tensile and stress relaxation tests for a wide range of temperatures, specimen orientations, and strain rates. The prediction capability of the model was validated by simulating tensile tests at three intermediate temperatures, which were not included during the initial calibration process [101].

Detailed rate-dependent experimental characterizations were performed to support the development of a VEP damage model to describe the mechanical behavior of continuous fiber reinforced thermoplastic composites [173]. Two different experimental testing methods, suggested by Ladevèze and Kästner, were combined. The Ladevèze method enables the separate determination of the influences from damage and inelastic deformation. The use of relaxation or retardation tests allows the determination of the rate-dependent behavior. This novel testing procedure, so-called stepwise loading-unloading test with relaxation and retardation periods, includes both a continuous stepwise loading and reloading and the imposing of stress-relaxation and strain-retardation periods and enables the determination of the elastic, inelastic and VE portions with only one experimental test. To investigate the complex mechanical behavior and the resulting damage and deformation mechanisms on the microscale, additional experimental diagnostic methods were employed. Based on the experimental results for a continuous glass fiber reinforced polypropylene (GF/PP) composite with non-crimped reinforcement, a VEP damage model was developed to describe the complex mechanical behavior. A damage-plasticity model was improved by using additional spring-dashpot systems for the calculation of the VE overstresses. This mesoscopic model describes the behavior of single plies of a TPC laminate. After the implementation as a user-defined material subroutine into MATLAB® [156] and Abaqus/Explicit® [146] (VUMAT), the model parameter identification and validation was performed. Further, the model validation for different loading rates and the application for structural analysis were demonstrated. The developed model was able to compute the mechanical behavior of the materials and structures and comparisons with respective test results yielded good agreement [173].

A novel approach using a neural network was used to model the creep behavior of a neat polymer (PEEK) response under different temperature conditions. More specifically, a multilayer perceptron neural network was used to model the material under constant shear stress rate excitation at different temperatures. Constant shear stress rate experiments were performed at different temperatures on a rotational rheometer to obtain shear stress-strain measurements which were used to train the neural network and for predictions. The effect of optimal neural network topology and the amount of training data and its distribution in a temperature range on prediction quality were investigated. To demonstrate how well the neural network predicts the material behavior a direct comparison was made between the experimentally determined stress-strain curves at different temperatures and predicted curves. The results showed that based on the proposed optimization criterion, a properly trained neural network can predict polymeric material behavior within the experimental error. Further, the neural network also demonstrated good generalization capabilities and enabled good prediction of the stress-strain curves at temperatures which had not been included in the training [174].

SUMMARY, RECOMMENDATIONS AND OUTLOOK

The opportunities offered by the use of thermoplastic composites in general and challenges encountered in particular were summarized. Further, an overview of thermoplastic materials was presented, manufacturing methods were discussed, and new methods for fastener-less assembly such as welding were introduced. Additionally, representative tests performed on different levels of the building block, ranging from coupon to structural level, were presented. In particular, fracture toughness results for different thermoplastic composite materials were used to demonstrate their superior performance compared to state-of-the-art thermoset composites. Selected examples of analyses were presented including process simulations, the modeling of progressive damage and delamination growth including cohesive zone models, fracture mechanics-based models and customized constitutive models as well as examples where the authors combined approaches in their analyses. Finally, models that account for strain-rate effects on fracture toughness as well as viscoelastic and viscoplastic modeling approaches were introduced. An extensive list of references and appendices with tables supporting the narrative were provided.

In particular, it was found that:

- Processing parameters, such as
  - the lay-up speed and pressure during automated tow placement; and
  - the temperature history during layup, welding, and annealing,

  have significant effects on the crystallinity and subsequently on the strength and fracture toughness of a thermoplastic composite.
  - Slow cooling rates yielded high crystallinity with high strength and lower fracture toughness.
  - Fast cooling rates resulted in reduced crystallinity with low strength and higher fracture toughness.
- Standard test methods developed for thermoset composites were used to obtain material properties.
  - For fracture toughness tests, a wide variety of insert film materials and thicknesses were used to create the initial delamination without yielding conclusive guidance.
  - Investigations on strain rate effects on material properties yielded inconclusive results.
- Analysis tools originally developed for thermoset composites, such as
  - Cohesive zone models;
  - Fracture mechanics-based models (e.g., VCCT); and
  - Progressive damage models,

  were used successfully without major changes.
- Viscoelastic and viscoplastic models were developed and are available should they be required in the future.

Based on the literature review, the following recommendations for future studies are made:

- For each thermoplastic material of interest:
  - the influence of processing parameters on crystallinity and subsequently material properties such as strength and fracture toughness needs to be thoroughly studied and documented; and
  - the influence of the welding process (e.g., the temperature history, the presence of a resistor or susceptor) on the weld performance needs to be studied.
- The limits of existing numerical tools to predict progressive damage in thermoplastics composites needs to be assessed further.

- The limits of current test standards developed for thermoset composites needs to be assessed.
    - Sufficient guidance on type of insert materials and film thicknesses to create the initial delamination in fracture toughness specimens needs to be developed.
    - The significance of strain rate effects needs to be determined.

Overall, a significant amount of progress has been made in the last three and a half decades to mature thermoplastic composites and understand their mechanical behavior. Additional research, however, is required to fully understand their behavior and gain confidence in their performance prior to their application in primary aircraft structures.

ACKNOWLEDGEMENTS

This research was supported by the Hi-Rate Composite Aircraft Manufacturing Project (HiCAM) and the Revolutionary Vertical Lift Technology Project (RVLT) within the Aeronautics Research Mission Directorate (ARMD) as well as the Thermoplastics Development for Exploration Applications (TDEA) within the Game Changing Development (GCD) Program.

The authors would also like to thank Ginger Gardiner and Jeff Sloan of *Composites World* for granting us the kind permission to use Figures 1 through 5 in this report.

The authors would like to recognize Dr. Frank Palmieri (NASA LaRC) and Dr. Sandi Miller (NASA Glenn) for their review and comments regarding processing and manufacturing of thermoplastic composites.

The authors would also like to thank Dr. T. Kevin O'Brien (U.S. Army Research Laboratory/NASA LaRC – retired), Dr. Jeffrey Hinkley (NASA – retired), Dr. Barry D. Davidson (Syracuse University – retired), Dr. Greg Odegard (Michigan Tech), Dr. Lee Nicholson (consultant) and Dr. Lyle Deobald (Boeing – retired) for their eagerness and time to share their experience.

REFERENCES

[1] D. R. Tenney, J. G. Jr. Davis, N. J. Johnston, R. B. Pipes, and J. F. McGuire, “Structural Framework for Flight: NASA’s Role in Development of Advanced Composite Materials for Aircraft and Space Structures,” NASA Langley Research Center, Hampton, VA, USA, NASA/CR–2011-217076, 2011.

[2] Marvin B. Dow and H. Benson Dexter, “Development of Stitched, Braided and Woven Composite Structures in the ACT Program and at Langley Research Center (1985 to 1997) Summary and Bibliography,” NASA, TP-97-206234, 1997.

[3] M. Dow, “The ACEE Program and Basic Composite Research at Langley Research Center (1975-1986),” NASA Langley Research Center, Hampton, VA, USA, NASA-RP-1177, 1987.

[4] S. Trimble, “NASA Seeks Composite Breakthroughs for Next Single-Aisle,” Aviation Week Network. [Online]. Available: https://aviationweek.com/aerospace/nasa-seeks-composite-breakthroughs-next-single-aisle

[5] G. Nehls, “Toray supplies HiCAM project with thermoset, thermoplastic prepreg technologies,” *CompositesWorld*, Jul. 2022.

[6] G. Nehls, “NASA awardees to develop sustainable aviation composite tech,” *CompositesWorld*, Mar. 2023.

[7] Jeff Sloan, “The Learjet 85: Large step out of the autoclave,” *Compos. World*, no. May, 2014.

[8] G. Gardiner, “Welding thermoplastic composites,” *CompositesWorld*, p. 10, 2018.

[9] G. Gardiner, “Consolidating thermoplastic composite aerostructures in place, Part 1,” *CompositesWorld*, p. 15, 2018.

[10] G. Gardiner, “Consolidating thermoplastic composite aerostructures in place, Part 2,” *CompositesWorld*, p. 12, 2018.

[11] M. P. Renieri, S. J. Burpo, L. M. Roundy, and S. M. Todd, “ACT/ICAPS - Thermoplastic Activities,” NASA/CR-198718.

[12] J. A. Hinkley, J. Johnston, and T. K. O’Brien, “Interlaminar fracture toughness of thermoplastic composites,” NASA/TM-1988-100532, 1988.

[13] P. Davies *et al.*, “Round-robin interlaminar fracture testing of carbon-fibre-reinforced epoxy and PEEK composites,” *Compos. Sci. Technol.*, vol. 43, no. 2, pp. 129–136, 1992, doi: https://doi.org/10.1016/0266-3538(92)90003-L.

[14] L. A. Carlsson, J. W. Gillespie, and B. R. Trethewey, “Mode II Interlaminar Fracture of Graphite/Epoxy and Graphite/PEEK,” *J. Reinf. Plast. Compos.*, vol. 5, pp. 170–187, 1986.

[15] R. A. Crick and D. C. Leach, “Interlaminar fracture morphology of carbon fibre/PEEK composites,” *J. Mater. Sci.*, no. 22, pp. 2094–2104, 1987.

[16] A. J. Smiley and R. B. Pipes, “Rate Effects on Mode I Interlaminar Fracture Toughness in Composite Materials,” *Journal of Composite Materials*, vol. 21, no. 7. pp. 670–687, 1987.

[17] R. H. Martin and G. B. Murri, “Characterization of Mode I and Mode II delamination growth and thresholds in graphite/peek composites,” NASA-TM-10057, AVSCOM-TM-88-B-011, 1988.

[18] K. Friedrich, R. Walter, L. A. Carlsson, A. J. Smiley, and J. W. Gillespie, “Mechanisms for rate effects on interlaminar fracture toughness of carbon/epoxy and carbon/PEEK composites,” *J. Mater. Sci.*, vol. 24, no. 9, pp. 3387–3398, Sep. 1989, doi: 10.1007/BF01139070.

[19] T. K. O’Brien and J. A. Hinkley, “Thermoplastic Composites Research at NASA Langley Research Center 1986-1995,” 2021.

[20] J. Sloan, “I want to say two words to you: ‘Thermoplastic tapes’ | CompositesWorld,” *CompositesWorld*, p. 15, 2018.

[21] S. Black, “Reinforced thermoplastics in aircraft primary structure,” *CompositesWorld*, p. 9, 2011.

[22] G. Nino, H. Bersee, and A. Beukers, “Design and Manufacturing of Thermoplastic Composite Ribs Based on Finite Element Analysis,” in *49th AIAA/ASME/ASCE/AHS/ASC Structures, Structural Dynamics, and Materials Conference*, Schaumburg, IL: American Institute of Aeronautics and Astronautics, Apr. 2008. doi: 10.2514/6.2008-2250.

[23] G. Nino, T. Ahmed, and H. Bersee, “Design and Manufacturing of a Multifunctional Thermoplastic Composite Wing Leading Edge,” in *50th AIAA/ASME/ASCE/AHS/ASC Structures, Structural Dynamics, and Materials Conference*, Palm Springs, California: American Institute of Aeronautics and Astronautics, May 2009. doi: 10.2514/6.2009-2613.

[24] G. Nehls, “STUNNING project successfully develops 8.5-meter thermoplastic fuselage skin,” *CompositesWorld*, p. 6, 2021.

[25] G. Gardiner, “Thermoplastic composite demonstrators — EU roadmap for future airframes,” *CompositesWorld*, p. 12, 2018.

[26] G. Gardiner, “Proving out LM PAEK welding for Multifunctional Fuselage Demonstrator,” *CompositesWorld*, p. 31, 2020.

[27] H. Mason, “Moving forward on the Multifunctional Fuselage Demonstrator (MFFD),” *CompositesWorld*, p. 5, 2020.

[28] H. Mason, “Solvay, Leonardo launch joint research lab for thermoplastic composites,” *CompositesWorld,* p. 3, 2021.

[29] E. Clarkson, “VICTREX AETM250 LM PEAK with Hexcel AS4 12k Unitape 34% RC Material Allowables Statistical Analysis Report NCAMP Project Number NPN 072001,” National Institute for Aviation Research, Wichita, KS 67260-0093, NCP-RP-2021-015 N/C, 2022.

[30] R. Andrulonis, R. Lovingfoss, V. Tanoto, and J. Tomblin, “NCAMP Material Specification - Medium Toughness Polyaryletherketone (PAEK) Thermoplastic Toray (Formerly TenCate) Cetex® TC1225 Low Melt (LM) Polyaryletherketone (PAEK) T700 Unidirectional 145 gsm 34% RC,” National Institute for Aviation Research, Wichita, KS 67260-0093, Document No.: NMS 122/1 Revision-February 21, 2020, 2020.

[31] R. Lovingfoss, R. Andrulonis, V. Tanoto, and J. Tomblin, “NCAMP Process Specification - Medium Toughness Polyaryletherketone (PAEK) Thermoplastics Toray (Formerly TenCate) Cetex® TC1225 Low Melt (LM) Polyaryletherketone (PAEK),” National Institute for Aviation Research, Wichita, KS 67260-0093, Document No.: NPS 81225 Revision B, January 21, 2020, 2020.

[32] E. Lian, “Medium Toughness PAEK thermoplastics Toray (Formerly TenCate) Cetex® TC1225 (LM PAEK) T700GC 12K T1E Unidirectional Tape 145 gsm 34% RC Qualification Material Property Data Report,” National Institute for Aviation Research, Wichita, KS 67260-0093, NCAMP Test Report Number: CAM-RP-2019-036 Rev N/C, Feb. 2020.

[33] E. Clarkson, “Medium Toughness PAEK thermoplastics Toray (Formerly TenCate) Cetex® TC1225 (LM PAEK) T700GC 12K T1E Unidirectional Tape 145 gsm 34% RC Material Allowables Statistical Analysis Report,” National Institute for Aviation Research, Wichita, KS 67260-0093, NCAMP Report Number: NCP-RP-2019-011 Rev N/C, 2020.

[34] R. Lovingfoss and M. Mann, “NCAMP Material Specification: High Performance, Low Melt Polyaryletherketone (LMPAEK) Thermoplastic VICTREX AE™ 250, Hexcel AS4 12k Unidirectional 143 gsm 34% RC Type 34, Class 1, Form 1, Grade 143,” National Institute for Aviation Research, Wichita, KS 67260-0093, NMS-125/1-Rev-B, 2022.

[35] R. Lovingfoss and M. Mann, “NCAMP Material Specification: Press Consolidated High Performance, Low Melt Polyaryletherketone (LMPAEK) Thermoplastics (VICTREX AE™ 250),” National Institute for Aviation Research, Wichita, KS 67260-0093, NMS-125-Rev-A, 2022.

[36] R. Lovingfoss, M. Mann, C. Steggall-Murphy, and K. Lasater, “NCAMP Process Specification: High Performance Polyaryletherketone (PAEK) Thermoplastics VICTREX AE™ 250 Low Melt (LM) Polyaryletherketone (PAEK),” National Institute for Aviation Research, Wichita, KS 67260-0093, NPS-81250 Rev. A, 2022.

[37] M. Mann, “VICTREX AETM250 LM PEAK with Hexcel AS4 12k Unitape 34% RC Qualification Material Property Data Report,” National Institute for Aviation Research, Wichita, KS 67260-0093, CAM-RP-2021-025 Rev NC, 2022.
[38] G. Nehls, “NIAR-WSU, Victrex begin NCAMP materials and process qualification for AFP,” *CompositesWorld*, p. 3, 2022.
[39] F. J. van Zanten, H. Mohan, D. Barazanchy, and M. van Tooren, “The Effect of Temperature on the Electric Conductivity for Composite Induction Welding,” in *AIAA SciTech 2022 Forum*, 2022, p. 15.
[40] D. Barazanchy, J. Pandher, and M. J. van Tooren, “The edge-effect in thermoplastic induction welding,” in *AIAA SciTech 2021 Forum*, VIRTUAL EVENT: American Institute of Aeronautics and Astronautics, Jan. 2021. doi: 10.2514/6.2021-1890.
[41] D. Barazanchy, J. Pandher, and M. van Tooren, “The effect of induction welding coil shape on volumetric heat generation,” in *AIAA SciTech 2022 Forum*, American Institute of Aeronautics and Astronautics, 2022, p. 17.
[42] H. Mohan, D. Barazanchy, and M. van Tooren, “Mitigation of edge effects in induction welding by the use of magnetic composite concentrators,” in *AIAA SciTech 2022 Forum*, 2022, p. 19.
[43] G. Nehls, “University of Delaware TuFF composite material shows high potential for UAM,” *CompositesWorld*, p. 9, 2021.
[44] J. Deitzel, D. Heider, R. Crane, and T. Ozdemir, “Stabilization of TuFF Material by Electrospinning of Low Areal Weight TPU Veil Material,” in *Proceedings of the American Society for Composites 36th Technical Conference*, 2021, p. 12.
[45] A. C. Bergan *et al.*, “Thermoplastic Composites as an Enabling Technology for NASA Space Applications - State of the Art Review,” NASA, NASA - TDEA-RPT-001, Dec. 2022.
[46] Z. August, G. Ostrander, J. Michasiow, and D. Hauber, “Recent developments in automated fiber placement of thermoplastic composites,” presented at the SAMPE, 2014, p. 13.
[47] G. Gardiner, M. Bach, S. Maire-Vigueur, J. Raynal, G. Beauduin, and L. Muijs, “Induction Welding for Dustless Assembly of Aircraft Within a Decade,” CompositesWorld Webinar. [Online]. Available: https://www.bigmarker.com/gardner-business-media-inc-w1/Induction-Welding-for-Dustless-Assembly-of-Aircraft-Within-a-Decade?bmid=373b416cfe25
[48] G. P. de Araujo, M. V. Donadon, G. Salerno, and R. de C. M. Sales, “Temperature Effects on the Mechanical Behaviour of PAEK Thermoplastic Composites Subjected to High Strain Rates Under Compression Loading,” *Compos. Struct.*, vol. 261, p. 113299, Apr. 2021, doi: 10.1016/j.compstruct.2020.113299.
[49] C. Bouvet, J. Serra, and P. G. Perez, “Strain rate effect of mode II interlaminar fracture toughness on the impact response of a thermoplastic PEEK composite,” *Compos. Part C Open Access*, vol. 2, p. 100031, Oct. 2020, doi: 10.1016/j.jcomc.2020.100031.
[50] P. G. Perez, C. Bouvet, A. Chettah, F. Dau, L. Ballere, and P. Pérès, “Effect of unstable crack growth on mode II interlaminar fracture toughness of a thermoplastic PEEK composite,” *Eng. Fract. Mech.*, vol. 205, pp. 486–497, Jan. 2019, doi: 10.1016/j.engfracmech.2018.11.022.
[51] B. Vieille *et al.*, “Kerosene flame behaviour of C/PEKK composite laminates: Influence of exposure time and laminates lay-up on residual mechanical properties,” *Compos. Part B Eng.*, vol. 222, p. 109046, Oct. 2021, doi: 10.1016/j.compositesb.2021.109046.
[52] G. Gardiner, “Thermoplastics in Aerospace Composites Outlook, 2014-2023,” *CompositesWorld*, p. 9, 2014.
[53] G. Gardiner, “Thermoplastic composites: Primary structure?,” *CompositesWorld*, p. 11, 2011.
[54] C. Red, “Thermoplastics in Aerospace Composites Outlook, 2014-2023,” CompositesWorld. [Online]. Available: https://www.compositesworld.com/articles/the-outlook-for-thermoplastics-in-aerospace-composites-2014-2023

[55] H. Pérez-Martín, P. Mackenzie, A. Baidak, C. M. Ó Brádaigh, and D. Ray, “Crystallinity studies of PEKK and carbon fibre/PEKK composites: A review,” *Compos. Part B Eng.*, vol. 223, p. 109127, Oct. 2021, doi: 10.1016/j.compositesb.2021.109127.
[56] D. Baker, “Mechanical Property Characterization and Impact Resistance of Selected Graphite/PEEK Composite Materials,” NASA, Langley Research Center, Hampton, VA, USA, NASA-TM-102769, 1991.
[57] M. Wynn and N. Zobeiry, “A Fast Method for Evaluating Effects of Process Parameters on Morphology of Semi-Crystalline Thermoplastic Composites,” in *Proceedings of the American Society for Composites 36th Technical Conference*, 2021, p. 10.
[58] K. Kashmari, P. Deshpande, S. Patil, S. Shah, M. Maiaru, and G. M. Odegard, “Prediction of PEEK Resin Properties for Processing Modeling Using Molecular Dynamics,” in *Proceedings of the American Society for Composites 36th Technical Conference*, 2021, p. 19.
[59] N. K. Parambil, B. R. Chen, J. M. Deitzel, and J. W. Gillespie, “A methodology for predicting processing induced thermal residual stress in thermoplastic composite at the microscale,” *Compos. Part B Eng.*, vol. 231, p. 109562, Feb. 2022, doi: 10.1016/j.compositesb.2021.109562.
[60] M. M. Domb and J. S. Hansen, “Development of free-edge effect during processing of semicrystalline thermoplastic composites,” *AIAA J.*, vol. 32, no. 5, pp. 1029–1033, May 1994, doi: 10.2514/3.12090.
[61] L. Cadieu, J. B. Kopp, J. Jumel, J. Bega, and C. Froustey, “A fracture behaviour evaluation of Glass/Elium150 thermoplastic laminate with the DCB test: Influence of loading rate and temperature,” *Compos. Struct.*, vol. 255, p. 112907, Jan. 2021, doi: 10.1016/j.compstruct.2020.112907.
[62] L. Cadieu, J. B. Kopp, J. Jumel, J. Bega, and C. Froustey, “Temperature effect on the mechanical properties and damage mechanisms of a glass/thermoplastic laminate,” *J. Compos. Mater.*, vol. 54, no. 17, pp. 2271–2282, Jul. 2020, doi: 10.1177/0021998319894383.
[63] J. A. Hinkley, W. D. Bascom, and R. E. Allred, “Interlaminar Fracture in Carbon Fiber/Thermoplastic Composites,” *MRS Proc.*, vol. 170, p. 351, 1989, doi: 10.1557/PROC-170-351.
[64] C. T. Sun and Y. Rui, “Orthotropic elasto-plastic behavior of AS4/PEEK thermoplastic composite in compression,” *Mech. Mater.*, vol. 10, no. 1–2, pp. 117–125, Nov. 1990, doi: 10.1016/0167-6636(90)90022-8.
[65] T. Hayashi and T. Ishikawa, “CF/modified-PEEK composites for aircraft,” in *Proceedings of the 2019 International Conference on Composite Materials*, Melbourne, Australia, 2019, p. 6.
[66] R. Velthuis, “Induction Welding Technology - Joining Fiber Reinforced Thermoplastic Polymer (composites) for Aerospace Applications,” in *54th International Astronautical Congress of the International Astronautical Federation, the International Academy of Astronautics, and the International Institute of Space Law*, Bremen, Germany: American Institute of Aeronautics and Astronautics, Sep. 2003. doi: 10.2514/6.IAC-03-I.3.06.
[67] A. Offringa, “Thermoplastic Composites tutorials,” CAMX 2019. [Online]. Available: https://tprc.nl/news/thermoplastic-composites-tutorials
[68] T. Spahr, “An Introduction to the Polyether Ketone Ketone (PEKK) Co-Polymer,” 2015.
[69] G. Gardiner, “PEEK or PEKK in future TPC aerostructures?,” *CompositesWorld*, p. 7, 2018.
[70] G. Gardiner, “PEEK vs. PEKK vs. PAEK and Continuous Compression Molding,” *CompositesWorld*, p. 10, 2018.
[71] G. Gardiner, “First Toray LM-PAEK laminate for Clean Sky MECATESTERS project,” *CompositesWorld*, p. 3, 2019.
[72] S. K. Bhudolia, P. Perrotey, and S. C. Joshi, “Mode I fracture toughness and fractographic investigation of carbon fibre composites with liquid Methylmethacrylate thermoplastic matrix,” *Compos. Part B Eng.*, vol. 134, pp. 246–253, Feb. 2018, doi: 10.1016/j.compositesb.2017.09.057.

[73] S. K. Bhudolia, G. Gohel, K. F. Leong, and S. C. Joshi, “Damping, impact and flexural performance of novel carbon/Elium® thermoplastic tubular composites,” *Compos. Part B Eng.*, vol. 203, p. 108480, Dec. 2020, doi: 10.1016/j.compositesb.2020.108480.
[74] R. Shrestha, J. Simsiriwong, M. Lugo, and N. Shamsaei, “Fatigue Behavior and Modeling for Thermoplastics,” in *56th AIAA/ASCE/AHS/ASC Structures, Structural Dynamics, and Materials Conference*, Kissimmee, Florida: American Institute of Aeronautics and Astronautics, Jan. 2015. doi: 10.2514/6.2015-0895.
[75] Li, Zhao, Li, Yang, and Wang, “Flexural Properties and Fracture Behavior of CF/PEEK in Orthogonal Building Orientation by FDM: Microstructure and Mechanism,” *Polymers*, vol. 11, no. 4, p. 656, Apr. 2019, doi: 10.3390/polym11040656.
[76] M. Mokhtari, E. Archer, N. Bloomfield, E. Harkin-Jones, and A. Mcilhagger, “Melt-Blended Multifunctional PEEK/Expanded Graphite Composites,” *Front. Mater.*, vol. 8, p. 724958, Sep. 2021, doi: 10.3389/fmats.2021.724958.
[77] L. Ye and K. Friedrich, “Mode I interlaminar fracture of co-mingled yarn based glass/polypropylene composites,” *Compos. Sci. Technol.*, vol. 46, no. 2, pp. 187–198, 1993, doi: https://doi.org/10.1016/0266-3538(93)90174-F.
[78] L. Ye, K. Friedrich, J. Kästel, and Y.-W. Mai, “Consolidation of unidirectional CF/PEEK composites from commingled yarn prepreg,” *Compos. Sci. Technol.*, vol. 54, no. 4, pp. 349–358, Jan. 1995, doi: 10.1016/0266-3538(95)00061-5.
[79] K. R. Hart, R. M. Dunn, and E. D. Wetzel, “Increased fracture toughness of additively manufactured semi-crystalline thermoplastics via thermal annealing,” *Polymer*, vol. 211, p. 123091, Dec. 2020, doi: 10.1016/j.polymer.2020.123091.
[80] L. Raps, A. R. Chadwick, I. Schiel, and I. Schmidt, “CF/LM-PAEK: Characterisation and sensitivity to critical process parameters for automated fibre placement,” *Compos. Struct.*, vol. 284, p. 115087, Mar. 2022, doi: 10.1016/j.compstruct.2021.115087.
[81] F. Sacchetti, W. J. B. Grouve, L. L. Warnet, and I. F. Villegas, “Effect of cooling rate on the interlaminar fracture toughness of unidirectional Carbon/PPS laminates,” *Eng. Fract. Mech.*, vol. 203, pp. 126–136, Nov. 2018, doi: 10.1016/j.engfracmech.2018.02.022.
[82] I. Esguerra-Arce, M. I. Martín, A. Pérez-Pastor, and V. García-Martínez, “Evolution of crystallinity with multiple lamination steps in high performance thermoplastic composites by in-situ consolidation process,” in *Proceedings of the 2019 International Conference on Composite Materials*, Melbourne, Australia, 2019, p. 7.
[83] F. Sacchetti, “Interlaminar toughness of fusion bonded thermoplastic composites,” PhD, University of Twente, Enschede, The Netherlands, 2017. doi: 10.3990/1.9789036543781.
[84] N. L. Batista, K. Anagnostopoulos, E. Cocchieri Botelho, and H. Kim, “Influence of crystallinity on interlaminar fracture toughness and impact properties of polyphenylene sulfide/carbon fiber laminates,” *Eng. Fail. Anal.*, vol. 119, p. 104976, Jan. 2021, doi: 10.1016/j.engfailanal.2020.104976.
[85] A. Beehag and L. Ye, “Role of cooling pressure on interlaminar fracture properties of commingled CF/PEEK composites,” *Compos. Part Appl. Sci. Manuf.*, vol. 27, no. 3, pp. 175–182, Jan. 1996, doi: 10.1016/1359-835X(95)00027-Y.
[86] S. Mall, G. E. Law, and M. Katouzian, “Loading Rate Effect on Interlaminar Fracture Toughness of a Thermoplastic Composite,” *J. Compos. Mater.*, vol. 21, no. 6, pp. 569–579, Jun. 1987, doi: 10.1177/002199838702100607.
[87] M. Holland and M. J. Van Tooren, “Macroscopic modelling of induction heating of thermoplastic composites using computational electromagnetism,” in *AIAA SciTech 2020 Forum*, Orlando, FL: American Institute of Aeronautics and Astronautics, Jan. 2020. doi: 10.2514/6.2020-2274.
[88] B. H. A. H. Tijs, M. H. J. Doldersum, A. Turon, J. E. A. Waleson, and C. Bisagni, “Experimental and numerical evaluation of conduction welded thermoplastic composite joints,” *Compos. Struct.*, vol. 281, p. 114964, Feb. 2022, doi: 10.1016/j.compstruct.2021.114964.
[89] G. Gardiner, “New horizons in welding thermoplastic composites,” *CompositesWorld*, p. 10, 2018.

[90] H. Shi, I. Fernandez Villegas, and H. Bersee, “An investigation on the strain distribution of resistance welded thermoplastic composite joints,” in *53rd AIAA/ASME/ASCE/AHS/ASC Structures, Structural Dynamics and Materials Conference*, Honolulu, Hawaii: American Institute of Aeronautics and Astronautics, Apr. 2012. doi: 10.2514/6.2012-1448.
[91] J. W. van Ingen, J. E. A. Waleson, A. Offringa, and M. Chapman, “Double curved thermoplastic orthogrid rear fuselage shell,” in *SAMPE Europe Conference*, Nantes, France, 2019, p. 11.
[92] T. Zhao *et al.*, “Enhancing weld attributes in ultrasonic spot welding of carbon fibre-reinforced thermoplastic composites: Effect of sonotrode configurations and process control,” *Compos. Part B Eng.*, vol. 211, p. 108648, Apr. 2021, doi: 10.1016/j.compositesb.2021.108648.
[93] I. F. Villegas and R. van Moorleghem, “Ultrasonic welding of carbon/epoxy and carbon/PEEK composites through a PEI thermoplastic coupling layer,” *Compos. Part Appl. Sci. Manuf.*, vol. 109, pp. 75–83, Jun. 2018, doi: 10.1016/j.compositesa.2018.02.022.
[94] T. Zhao, C. Rans, I. Fernandez Villegas, and R. Benedictus, “On sequential ultrasonic spot welding as an alternative to mechanical fastening in thermoplastic composite assemblies: A study on single-column multi-row single-lap shear joints,” *Compos. Part Appl. Sci. Manuf.*, vol. 120, pp. 1–11, May 2019, doi: 10.1016/j.compositesa.2019.02.013.
[95] A. Yousefpour, M. Hojjati, and J.-P. Immarigeon, “Fusion Bonding/Welding of Thermoplastic Composites,” *J. Thermoplast. Compos. Mater.*, vol. 17, no. 4, pp. 303–341, Jul. 2004, doi: 10.1177/0892705704045187.
[96] “Additive Manufacturing,” Electroimpact. [Online]. Available: https://www.electroimpact.com/3d/overview.aspx
[97] “NIAR - Capabilities and Equipment,” NIAR - Learn More. [Online]. Available: https://www.wichita.edu/industry_and_defense/NIAR/Laboratories/atlas/about-us-atlas.php
[98] J. Fonseca, I. A. Ferreira, M. F. S. F. de Moura, M. Machado, and J. L. Alves, “Study of the interlaminar fracture under mode I loading on FFF printed parts,” *Compos. Struct.*, vol. 214, pp. 316–324, Apr. 2019, doi: 10.1016/j.compstruct.2019.02.005.
[99] P. Malnati, “Short carbon fiber compounds expand reach of thermoplastic composites,” *CompositesWorld*, p. 9, 2021.
[100] R. Gaitzsch, M. Koerdt, H. Bertling, S. Scholl, T. Schäfer, and A. S. Herrmann, “Characterisation of bond strength in overmoulded high-performance thermoplastic composites,” in *Proceedings of the 2019 International Conference on Composite Materials*, Melbourne, Australia, 2019, p. 12.
[101] H. Xu, M. Kuczynska, N. Schafet, F. Welschinger, and J. Hohe, “Modeling the anisotropic temperature-dependent viscoplastic deformation behavior of short fiber reinforced thermoplastics,” *Compos. Sci. Technol.*, vol. 213, p. 108958, Sep. 2021, doi: 10.1016/j.compscitech.2021.108958.
[102] G. Gardiner, “Manufacturing the upper half of the Multifunctional Fuselage Demonstrator (MFFD),” *CompositesWorld*, p. 14, 2021.
[103] R. Akkerman, M. Bouwman, and S. Wijskamp, “Analysis of the Thermoplastic Composite Overmolding Process: Interface Strength,” *Front. Mater.*, vol. 7, no. 27, 2020.
[104] F. Neveu, “Manufacturing and impact behaviour of aeronautic overmolded grid-stiffened thermoplastic carbon plates,” *Compos. Struct.*, p. 16, 2022.
[105] K. Mason, “Thermoplastic primary aerostructures take another step forward,” *CompositesWorld*, p. 11, 2019.
[106] J. Koenig, “Innovation Takes Off,” presented at the Clean Sky 2 -Information Day dedicated to the 9th Call for Proposal Partners, Brussels, Belgium.
[107] A. Offringa, “NASA PMC CoP Thermoplastic Composites session - materials, technologies, applications and current developments,” presented at the NASA PMC CoP session, NASA, 2021.

[108] V. Oliveri *et al.*, “Design, Manufacture and Test of an In-Situ Consolidated Thermoplastic Variable-Stiffness Wingbox,” *AIAA J.*, vol. 57, no. 4, pp. 1671–1683, Apr. 2019, doi: 10.2514/1.J057758.
[109] V. Oliveri *et al.*, “Design of a unitized thermoplastic composite out-of-autoclave three-bay wingbox demonstrator,” in *AIAA SciTech 2021 Forum*, VIRTUAL EVENT: American Institute of Aeronautics and Astronautics, Jan. 2021. doi: 10.2514/6.2021-0919.
[110] D. Peeters, G. J. Clancy, V. Oliveri, R. O’Higgins, D. Jones, and P. M. Weaver, “Thermoplastic Composite Stiffener Design with Manufacturing Considerations,” in *2018 AIAA/ASCE/AHS/ASC Structures, Structural Dynamics, and Materials Conference*, Kissimmee, Florida: American Institute of Aeronautics and Astronautics, Jan. 2018. doi: 10.2514/6.2018-0479.
[111] G. J. Clancy, D. Peeters, V. Oliveri, D. Jones, R. O’Higgins, and P. M. Weaver, “Steering of Carbon Fiber/Thermoplastic Pre-preg Tapes using Laser-Assisted Tape Placement,” in *2018 AIAA/ASCE/AHS/ASC Structures, Structural Dynamics, and Materials Conference*, Kissimmee, Florida: American Institute of Aeronautics and Astronautics, Jan. 2018. doi: 10.2514/6.2018-0478.
[112] G. Zucco, M. Rouhi, O. Vincenzo, E. Cosentino, R. O’Higgins, and P. M. Weaver, “DESIGN OF A COMPOSITE PANEL WITH CONTINUOUS TOW STEERING AROUND AN ELLIPTICAL CUT-OUT,” in *American Society for Composites 2021*, Destech Publications, Inc., Sep. 2021. doi: 10.12783/asc36/35768.
[113] R. Telford *et al.*, “Enhanced Buckling Performance of a Stiffened, Variable Angle Tow Thermoplastic Composite Panel,” in *2018 AIAA/ASCE/AHS/ASC Structures, Structural Dynamics, and Materials Conference*, Kissimmee, Florida: American Institute of Aeronautics and Astronautics, Jan. 2018. doi: 10.2514/6.2018-0480.
[114] James G. Ratcliffe and William M. Johnston Jr, “Influence of Mixed Mode I-Mode II Loading on Fatigue Delamination Growth Characteristics of a Graphite Epoxy Tape Laminate,” in *Proceedings of the American Society for Composites 29thTechnical Conference*, 2014.
[115] Gretchen B. Murri, “Evaluation of Delamination Onset and Growth Characterization Methods Under Mode I Fatigue Loading,” NASA/TM-2013-217966, 2013.
[116] T. Kevin O’Brien, William M. Johnston, and Gregory Toland, “Mode II Interlaminar Fracture Toughness and Fatigue Characterization of a Graphite Epoxy Composite Material,” NASA/TM-2010-216838, 2010.
[117] J. R. Reeder, “3D Mixed-Mode Delamination Fracture Criteria—An Experimentalist’s Perspective,” presented at the American Society for Composite Technical Conference, 2006, p. 17.
[118] Q. V. Bui, “A Modified Benzeggagh-Kenane Fracture Criterion for Mixed-mode Delamination,” *J. Compos. Mater.*, vol. 45, no. 4, pp. 389–413, Feb. 2011, doi: 10.1177/0021998310376105.
[119] P. P. Camanho, C. G. Davila, and M. F. de Moura, “Numerical Simulation of Mixed-Mode Progressive Delamination in Composite Materials,” *J. Compos. Mater.*, vol. 37, no. 16, pp. 1415–1438, 2003, doi: 10.1177/0021998303034505.
[120] J. R. Reeder, “A Bilinear Fracture Criterion for Mixed-Mode Delamination,” *ASTM STP 1206*, pp. 303–322, 1993.
[121] J. R. Reeder and J. H. Crews, “Mixed-mode bending method for delamination testing,” *AIAA J.*, vol. 28, no. 7, pp. 1270–1276, 1990, doi: 10.2514/3.25204.
[122] T. K. O’Brien and H. Martin, “Results of ASTM round robin testing for mode I interlaminar fracture toughness of composite materials,” NASA, NASA Langley Research Center, NASA/TM-1992-10422, 1992.
[123] F. Sacchetti, W. J. B. Grouve, L. L. Warnet, and I. F. Villegas, “Effects of release media on the fusion bonding of carbon/PEEK laminates,” *Compos. Part Appl. Sci. Manuf.*, vol. 94, pp. 70–76, Mar. 2017, doi: 10.1016/j.compositesa.2016.11.028.
[124] G. C. Christopoulos and S. A. Paipetis, “Interlaminar Fatigue Crack Propagation in Mode I of Carbon Fiber/PEEK Composites,” *Adv. Compos. Lett.*, vol. 2, no. 1, p. 096369359300200, Jan. 1993, doi: 10.1177/096369359300200101.

[125] J. W. Gillespie, L. A. Carlsson, and A. J. Smiley, “Rate-dependent mode I interlaminar crack growth mechanisms in graphite/epoxy and graphite/PEEK,” *Compos. Sci. Technol.*, vol. 28, no. 1, pp. 1–15, Jan. 1987, doi: 10.1016/0266-3538(87)90058-3.
[126] K. Shirasu, J. Tsuyuki, R. Higuchi, S. Onodera, and T. Okabe, “Experimental and numerical study on open-hole tension/compression properties of carbon-fiber-reinforced thermoplastic laminates,” *J. Compos. Mater.*, vol. 56, no. 14, pp. 2211–2225, Jun. 2022, doi: 10.1177/00219983221096880.
[127] R. Frassine and A. Pavan, “Viscoelastic effects on the interlaminar fracture behaviour of thermoplastic matrix composites: I. rate and temperature dependence in unidirectional PEI/carbon-fibre laminates,” *Compos. Sci. Technol.*, vol. 54, pp. 193–200, 1995.
[128] R. Fracasso, M. Rink, A. Pavan, and R. Frassine, “The effects of strain-rate and temperature on the interlaminar fracture toughness of interleaved PEEK/CF composites,” *Compos. Sci. Technol.*, vol. 61, pp. 57–63, 2001.
[129] H. Setiawan, “Rate effects on mode I fracture toughness of polymeric carbon fibre composites,” PhD Thesis, Imperial College, London, UK, 1996.
[130] K. S. van Dooren, E. Labans, and C. Bisagni, “Analysis and testing of a thermoplastic composite stiffened panel under compression,” in *Proceedings of the 2019 International Conference on Composite Materials*, Melbourne, Australia, 2019, p. 7.
[131] “Toray Cetex® TC1225 LMPAEK,” Toray Advanced Composites, Product Data Sheet, 2020.
[132] A. K. Bandaru, G. J. Clancy, D. Peeters, R. O’Higgins, and P. M. Weaver, “Interface Characterization of Thermoplastic Skin-Stiffener Composite Manufactured using Laser-Assisted Tape Placement,” in *2018 AIAA/ASCE/AHS/ASC Structures, Structural Dynamics, and Materials Conference*, Kissimmee, Florida: American Institute of Aeronautics and Astronautics, Jan. 2018. doi: 10.2514/6.2018-0481.
[133] J. C. Fish, M. L. Vitlip, S. P. Chen, and K. S. Shin, “Interlaminar fracture characteristics of bonding concepts for thermoplastic primary structures,” *AIAA J.*, vol. 30, no. 6, pp. 1602–1608, Jun. 1992, doi: 10.2514/3.11107.
[134] M. W. Czabaj and B. D. Davidson, “Determination of the mode I, mode II, and mixed-mode I–II delamination toughness of a graphite/polyimide composite at room and elevated temperatures,” *J. Compos. Mater.*, vol. 50, no. 16, pp. 2235–2253, 2016, doi: 10.1177/0021998315602945.
[135] J. Wilk, “Applicability of mode II interlaminar fracture toughness testing methods for characterization of thermoplastic laminates with woven fabric reinforcements,” *Eng. Fract. Mech.*, vol. 216, p. 106533, Jul. 2019, doi: 10.1016/j.engfracmech.2019.106533.
[136] M. L. Benzeggagh and M. Kenane, “Measurement of mixed-mode delamination fracture toughness of unidirectional glass/epoxy composites with mixed-mode bending apparatus,” *Compos. Sci. Technol.*, vol. 56, no. 4, pp. 439–449, 1996.
[137] T. Q. Li, M. Q. Zhang, K. Zhang, and H. M. Zeng, “The dependence of the fracture toughness of thermoplastic composite laminates on interfacial interaction,” *Compos. Sci. Technol.*, vol. 60, no. 3, pp. 465–476, Feb. 2000, doi: 10.1016/S0266-3538(99)00147-5.
[138] H. Wafai, A. Yudhanto, G. Lubineau, R. Yaldiz, and N. Verghese, “An experimental approach that assesses in-situ micro-scale damage mechanisms and fracture toughness in thermoplastic laminates under out-of-plane loading,” *Compos. Struct.*, vol. 207, pp. 546–559, Jan. 2019, doi: 10.1016/j.compstruct.2018.09.046.
[139] M. Arhant, E. Lolive, T. Bonnemains, and P. Davies, “Fatigue crack growth properties of carbon-polyamide 6 thermoplastic composites using a multi-ΔG control method,” *Eng. Fract. Mech.*, vol. 252, p. 107825, Jul. 2021, doi: 10.1016/j.engfracmech.2021.107825.
[140] J. P. Reis, M. F. S. F. de Moura, R. D. F. Moreira, and F. G. A. Silva, “Pure mode I and II interlaminar fracture characterization of carbon-fibre reinforced polyamide composite,” *Compos. Part B Eng.*, vol. 169, pp. 126–132, Jul. 2019, doi: 10.1016/j.compositesb.2019.03.069.
[141] A. J. Smiley and R. B. Pipes, “Rate sensitivity of mode II interlaminar fracture toughness in graphite/epoxy and graphite/PEEK composite materials,” *Compos. Sci. Technol.*, vol. 29, no. 1, pp. 1–15, 1987, doi: https://doi.org/10.1016/0266-3538(87)90033-9.

[142] R. Frassine, M. Rink, and A. Pavan, “Viscoelastic effects on the interlaminar fracture behaviour of thermoplastic matrix composites: II. Rate and temperature dependence in unidirectional PEEK/carbon-fibre laminates,” *Compos. Sci. Technol.*, vol. 56, no. 11, pp. 1253–1260, Jan. 1996, doi: 10.1016/S0266-3538(96)00084-X.
[143] H. Chen, S. Li, J. Wang, and A. Ding, “A focused review on the thermo-stamping process and simulation progresses of continuous fibre reinforced thermoplastic composites,” *Compos. Part B Eng.*, vol. 224, p. 109196, Nov. 2021, doi: 10.1016/j.compositesb.2021.109196.
[144] “Composite forming simulations | AniForm,” ANIFORM - VIRTUAL FORMING. [Online]. Available: https://aniform.com
[145] ESI Group, “PAM-COMPOSITES: Composite Simulation Software,” PAM-COMPOSITES Composite Simulation Software. [Online]. Available: https://www.esi-group.com/products/pam-composites
[146] “Abaqus Analysis User’s Guide - Abaqus 2021,” DS Simulia Corp., Providence, RI, USA., 2021.
[147] “LS-DYNA® Keyword user’s manual. Volume I, LS-DYNA R13,” Livermore Software Technology (LST), an ANSYS Company, Sep. 2021.
[148] M. Domb, “Development of free-edge effect during the processing of fibre-reinforced semicrystalline thermoplastic composites,” in *34th Structures, Structural Dynamics and Materials Conference*, La Jolla, CA, U.S.A.: American Institute of Aeronautics and Astronautics, Apr. 1993. doi: 10.2514/6.1993-1348.
[149] LAMMPS, “LAMMPS Molecular Dynamics Simulator.” [Online]. Available: https://www.lammps.org/
[150] Altair, “Altair® Flux® Applications,” Altair® Flux®. [Online]. Available: https://altair.com/flux-applications
[151] W. Seneviratne, J. Tomblin, J. J. C. Teoh, N. A. Smith, and B. L. Saathoff, “Induction Heating of CF/PEKK Laminates Using Homogenization Techniques,” in *Proceedings of the American Society for Composites 36th Technical Conference*, 2021, p. 12.
[152] N. Athanasopoulos and V. Kostopoulos, “Calculation of an Equivalent Electrical Conductivity Tensor for Multidirectional Carbon Fiber Reinforced Materials,” in *Progress in Electromagnetics Research Symposium*, Moscow, Russia.
[153] Stephen W. Tsai and H. Thomas Hahn, *Introduction to Composite Materials*. Technomic Publishing Co., Inc., 1980.
[154] COMSOL, “COMSOL - Software for Multiphysics Simulation,” COMSOL - Software for Multiphysics Simulation. [Online]. Available: https://www.comsol.com
[155] D. Stavrov, G. Nino, and H. Bersee, “Process Optimization for Resistance Welding of Thermoplastic Composites,” in *47th AIAA/ASME/ASCE/AHS/ASC Structures, Structural Dynamics, and Materials Conference*, Newport, Rhode Island: American Institute of Aeronautics and Astronautics, May 2006. doi: 10.2514/6.2006-2246.
[156] MathWorks®, “MATLAB - Math. Graphics. Programming.,” MATLAB. [Online]. Available: https://www.mathworks.com/products/matlab.html
[157] T. Lu, X. Chen, and H. Wang, “Predicting compression-after-impact behavior of thermoplastic composite laminates by an experiment-based approach,” *Compos. Sci. Technol.*, vol. 213, p. 108952, Sep. 2021, doi: 10.1016/j.compscitech.2021.108952.
[158] G. Zucco *et al.*, “Static Test of a Thermoplastic Composite Wingbox Under Shear and Bending Moment,” in *2018 AIAA/ASCE/AHS/ASC Structures, Structural Dynamics, and Materials Conference*, Kissimmee, Florida: American Institute of Aeronautics and Astronautics, Jan. 2018. doi: 10.2514/6.2018-0482.
[159] J. P. Reis, M. F. S. F. de Moura, R. D. F. Moreira, and F. G. A. Silva, “Mixed mode I + II interlaminar fracture characterization of carbon-fibre reinforced polyamide composite using the Single-Leg Bending test,” *Mater. Today Commun.*, vol. 19, pp. 476–481, Jun. 2019, doi: 10.1016/j.mtcomm.2019.05.006.
[160] B. Tijs, K. Dooren, and C. Bisagni, “Development of a Numerical Framework for Virtual Testing to Support Design of a Next Generation Thermoplastic Multifunctional Fuselage,” in *II European Conference on Multifunctional Structures*, CIMNE, 2020. doi: 10.23967/emus.2020.005.

[161] O. Falcó, R. L. Ávila, B. Tijs, and C. S. Lopes, “Modelling and simulation methodology for unidirectional composite laminates in a Virtual Test Lab framework,” *Compos. Struct.*, vol. 190, pp. 137–159, Apr. 2018, doi: 10.1016/j.compstruct.2018.02.016.
[162] H. Liu *et al.*, “Modelling damage in fibre-reinforced thermoplastic composite laminates subjected to three-point bend loading,” *Compos. Struct.*, vol. 236, p. 111889, Mar. 2020, doi: 10.1016/j.compstruct.2020.111889.
[163] J. F. Chen, E. V. Morozov, and K. Shankar, “A combined elastoplastic damage model for progressive failure analysis of composite materials and structures,” *Compos. Struct.*, vol. 94, no. 12, pp. 3478–3489, Dec. 2012, doi: 10.1016/j.compstruct.2012.04.021.
[164] R.-H. Maa and J.-H. Cheng, “A CDM-based failure model for predicting strength of notched composite laminates,” *Compos. Part B Eng.*, vol. 33, no. 6, pp. 479–489, Sep. 2002, doi: 10.1016/S1359-8368(02)00030-6.
[165] M. C. Lafarie-Frenot and F. Touchard, “Comparative in-plane shear behaviour of long-carbon-fibre composites with thermoset or thermoplastic matrix,” *Compos. Sci. Technol.*, vol. 52, no. 3, pp. 417–425, Jan. 1994, doi: 10.1016/0266-3538(94)90176-7.
[166] B. N. Fedulov, A. A. Safonov, M. M. Kantor, and S. V. Lomov, “Modelling of thermoplastic polymer failure in fiber reinforced composites,” *Compos. Struct.*, vol. 163, pp. 293–301, Mar. 2017, doi: 10.1016/j.compstruct.2016.11.091.
[167] K. S. V. Dooren and C. Bisagni, “Design and Analysis of Thermoplastic Welded Stiffened Panels in Post-Buckling,” in *Proceedings of the American Society for Composites 36th Technical Conference*, 2021, p. 12.
[168] I. Baran, L. L. Warnet, and R. Akkerman, “Assessment of failure and cohesive zone length in co-consolidated hybrid C/PEKK butt joint,” *Eng. Struct.*, vol. 168, pp. 420–430, Aug. 2018, doi: 10.1016/j.engstruct.2018.04.089.
[169] D. Garcia-Gonzalez, S. Garzon-Hernandez, and A. Arias, “A new constitutive model for polymeric matrices: Application to biomedical materials,” *Compos. Part B Eng.*, vol. 139, pp. 117–129, Apr. 2018, doi: 10.1016/j.compositesb.2017.11.045.
[170] W. Zhao, M. Ries, P. Steinmann, and S. Pfaller, “A viscoelastic-viscoplastic constitutive model for glassy polymers informed by molecular dynamics simulations,” *Int. J. Solids Struct.*, vol. 226–227, p. 111071, Sep. 2021, doi: 10.1016/j.ijsolstr.2021.111071.
[171] J. L. Chaboche, “Thermodynamic formulation of constitutive equations and application to the viscoplasticity and viscoelasticity of metals and polymers,” *Int. J. Solids Struct.*, vol. 34, no. 18, pp. 2239–2254, 1997.
[172] J. L. Chaboche, “A review of some plasticity and viscoplasticity constitutive theories,” *Int. J. Plast.*, vol. 24, no. 10, pp. 1642–1693, 2008.
[173] M. Zscheyge, R. Böhm, A. Hornig, J. Gerritzen, and M. Gude, “Rate dependent non-linear mechanical behaviour of continuous fibre-reinforced thermoplastic composites – Experimental characterisation and viscoelastic-plastic damage modelling,” *Mater. Des.*, vol. 193, p. 108827, Aug. 2020, doi: 10.1016/j.matdes.2020.108827.
[174] A. Aulova, A. Oseli, and M. Bek, “Neural networks for predicting the temperature-dependent viscoelastic response of PEEK under constant stress rate loading,” *Polym. Test.*, vol. 100, p. 107233, Aug. 2021, doi: 10.1016/j.polymertesting.2021.107233.
[175] V. Zinnecker, C. M. Stokes-Griffin, and P. Compston, “Laser-assisted thermoplastic tape placement: Effects of thermal history and placement speed on wedge peel strength of CF/PA6,” in *Proceedings of the 2019 International Conference on Composite Materials*, Melbourne, Australia, 2019, p. 8.
[176] H. Uematsu *et al.*, “Fracture properties of quasi-isotropic carbon-fiber-reinforced polyamide 6 laminates with different crystal structure of polyamide 6 due to surface profiles of carbon fibers,” *Compos. Part Appl. Sci. Manuf.*, vol. 154, p. 106752, Mar. 2022, doi: 10.1016/j.compositesa.2021.106752.
[177] M. Akamatsu, T. Ohori, T. Hayashi, and J. Takahashi, “Investigation of the delamination behavior on carbon fiber tape reinforced thermoplastics,” in *Proceedings of the 2015 International Conference on Composite Materials*, Copenhagen, Denmark, 2015, p. 8.

[178] A. Choudhary and I. Fernandez, “Robotic Sequential Ultrasonic Welding of Thermoplastic Composites: process Development and Testing,” in *Proceedings of the American Society for Composites 36th Technical Conference*, 2021.
[179] F. Sacchetti, W. J. B. Grouve, L. L. Warnet, and I. F. Villegas, “Effect of resin-rich bond line thickness and fibre migration on the toughness of unidirectional Carbon/PEEK joints,” *Compos. Part Appl. Sci. Manuf.*, vol. 109, pp. 197–206, Jun. 2018, doi: 10.1016/j.compositesa.2018.02.035.
[180] F. Sacchetti, W. J. B. Grouve, L. L. Warnet, and I. Fernandez Villegas, “Interlaminar fracture toughness of 5HS Carbon/PEEK laminates. A comparison between DCB, ELS and mandrel peel tests,” *Polym. Test.*, vol. 66, pp. 13–23, Apr. 2018, doi: 10.1016/j.polymertesting.2017.12.005.
[181] J. A. Daniels, A. N. Palazotto, and R. S. Sandhu, “Failure characteristics in thermoplastic composite laminates due to an eccentric circular discontinuity,” *AIAA J.*, vol. 29, no. 5, pp. 830–837, May 1991, doi: 10.2514/3.10663.
[182] B. Vieille, J.-D. Gonzalez, and C. Bouvet, “Fracture mechanics of hybrid composites with ductile matrix and brittle fibers: Influence of temperature and constraint effect,” *J. Compos. Mater.*, vol. 53, no. 10, pp. 1361–1376, May 2019, doi: 10.1177/0021998318802613.
[183] “Tenax-E TPWF PEEK-HTA40 Product Datasheet,” Teijin, Product Data Sheet, 2020.
[184] G. J. Clancy, R. O’Higgins, and P. M. Weaver, “Spreading of Carbon Fiber/Thermoplastic Pre-preg Tapes,” in *AIAA SciTech 2020 Forum*, Orlando, FL: American Institute of Aeronautics and Astronautics, Jan. 2020. doi: 10.2514/6.2020-0481.
[185] R. Sitohang, W. Grouve, L. Warnet, S. Koussios, and R. Akkerman, “An experimental approach to reproduce in-plane fiber waviness in thermoplastic composites test coupons using a reverse forming method,” *J. Compos. Mater.*, vol. 56, no. 4, pp. 561–574, Feb. 2022, doi: 10.1177/00219983211026734.
[186] D. M. Hoang and S. V. Hoa, “Effect of Processing Parameters on the Widths and Thicknesses of Thermoplastic Composites Made by Automated Fiber Placement,” in *Proceedings of the American Society for Composites 36th Technical Conference*, 2021, p. 9.
[187] G. Pedoto, J.-C. Grandidier, M. Gigliotti, and A. Vinet, “Coupling between thermal ageing/degradation and creep behavior of PEKK and C/PEKK composites above the glass transition temperature,” *Compos. Part Appl. Sci. Manuf.*, vol. 153, p. 106717, Feb. 2022, doi: 10.1016/j.compositesa.2021.106717.
[188] G. Pedoto, “Characterization and modelling of the thermomechanical and ageing behavior of PEKK and C/PEKK composites for aircraft applications at high temperatures (above the glass transition temperature),” Ph.D. Thesis, Ecole Nationale Supérieure de Mécanique et Aéronautique - ENSMA, Poitiers, France, 2020.
[189] L. Ye, A. Beehag, and K. Friedrich, “Mesostructural aspects of interlaminar fracture in thermoplastic composites: Is crystallinity a key?,” *Compos. Sci. Technol.*, vol. 53, no. 2, pp. 167–173, Jan. 1995, doi: 10.1016/0266-3538(95)00015-1.
[190] J. Tancrez, “Damage and fracture mechanisms in thermoplastic-matrix composites in relation to processing and structural parameters,” *Compos. Sci. Technol.*, vol. 56, no. 7, pp. 725–731, 1996, doi: 10.1016/0266-3538(96)00013-9.
[191] H. Wafai *et al.*, “In situ micro-scale high-speed imaging for evaluation of fracture propagation and fracture toughness of thermoplastic laminates subjected to impact,” *Compos. Struct.*, vol. 210, pp. 747–754, Feb. 2019, doi: 10.1016/j.compstruct.2018.11.092.
[192] W. Fang, X. Yang, X. Xu, W. Li, and Q. Li, “Quasi-static and low-velocity impact responses of polypropylene random copolymer composites with adjustable crystalline structures,” *Compos. Part B Eng.*, vol. 224, p. 109139, Nov. 2021, doi: 10.1016/j.compositesb.2021.109139.
[193] D. Meyer, P. Carnevale, H. Bersee, and A. Beukers, “New Affordable Reinforced Thermoplastic Composite for Structural Aircraft Applications,” in *50th AIAA/ASME/ASCE/AHS/ASC Structures, Structural Dynamics, and Materials*

Conference, Palm Springs, California: American Institute of Aeronautics and Astronautics, May 2009. doi: 10.2514/6.2009-2337.
[194] S. Black, “Thermoplastic composites in flight ... for decades,” *CompositesWorld*, 2016, [Online]. Available: https://www.compositesworld.com/articles/thermoplastic-composites-in-flight-for-decades
[195] J. W. van Ingen, A. Buitenhuis, M. van Wijngaarden, and F. Simmons, “Development of the Gulfstream G650 induction welded thermoplastic elevators and rudder,” in *Proceedings of the international SAMPE symposium and exhibition*, Seattle, WA, USA, 2010.
[196] S. Black, “Thermoplastic composite wings on the horizon?,” *CompositesWorld*, 2016, [Online]. Available: https://www.compositesworld.com/articles/thermoplastic-composite-wings-on-the-horizon
[197] A. Offringa, D. Myers, and A. Buitenhuis, “Redesigned A340-500/600 Fixed Wing Leading Edge (J-Nose) in Thermoplastics,” presented at the 46th International SAMPE Symposium, Long Beach, CA, USA, 2001, p. 331` – 343.
[198] J. Sloan and S. Black, “Plant Tour: Fokker Aerostructures: Hoogeveen, Netherlands,” *Compos. World*, 2015, [Online]. Available: https://www.compositesworld.com/articles/fokker-aerostructures-hoogeveen-the-netherlands
[199] G. Gardiner, “Thermoplastic composites welding advances for more sustainable airframes,” *Compos. World*, 2022.
[200] H. Mason, “GKN Aerospace thermoplastic composites featured on Bell V-280 Valor,” *CompositesWorld*, 2019, [Online]. Available: https://www.compositesworld.com/news/gkn-aerospace-thermoplastic-composites-featured-on-bell-v-280-valor
[201] “Thermoplastic composites gain leading edge on the A380,” *CompositesWorld*, 2006.
[202] S. Black, “Thermoplastic composites technology: A view from Europe,” *CompositesWorld*, 2015, [Online]. Available: https://www.compositesworld.com/articles/thermoplastic-composites-technology-a-view-from-europe
[203] G. Gardiner, “Thermoplastic composites: Inside story,” *CompositesWorld*, 2009.
[204] J. W. Gillespie, L. A. Carlsson, R. B. Pipes, R. Rothschilds, B. Trethewey, and A. Smiley, “Delamination growth in composite materials,” NASA, NASA/CR-1986-176416, 1986.
[205] J. W. Gillespie, L. A. Carlsson, R. B. Pipes, R. Rothschilds, B. Trethewey, and A. Smiley, “Delamination growth in composite materials,” NASA, NASA/CR-1986-178066, 1986.
[206] P. Czarnocki, “Experimental Comparison of Interlaminar Toughness of Carbon/PEEK, Carbon/Expoxy and Glass/Epoxy composites,” *J. Theor. Appl. Mech. Mecganik Teoretyczna Stosow.*, pp. 443–453, 1995.
[207] S. Stelzer, A. J. Brunner, A. Argüelles, N. Murphy, G. M. Cano, and G. Pinter, “Mode I delamination fatigue crack growth in unidirectional fiber reinforced composites: Results from ESIS TC4 round-robins,” *Eng. Fract. Mech.*, vol. 116, pp. 92–107, Jan. 2014, doi: 10.1016/j.engfracmech.2013.12.002.
[208] L. C. M. Barbosa, D. B. Bortoluzzi, and A. C. Ancelotti, “Analysis of fracture toughness in mode II and fractographic study of composites based on Elium® 150 thermoplastic matrix,” *Compos. Part B Eng.*, vol. 175, p. 107082, Oct. 2019, doi: 10.1016/j.compositesb.2019.107082.
[209] S. M. Bayazeid, K.-L. Poon, B. Subeshan, M. Alamir, and E. Asmatulu, “Recovery of impact-damaged carbon fiber–reinforced composites using induction heating,” *J. Compos. Mater.*, vol. 56, no. 4, pp. 605–618, Feb. 2022, doi: 10.1177/00219983211058796.
[210] G. Dai, L. Zhan, C. Guan, and M. Huang, “The effect of moulding process parameters on interlaminar properties of CF/PEEK composite laminates,” *High Perform. Polym.*, vol. 32, no. 7, pp. 835–841, Sep. 2020, doi: 10.1177/0954008320903768.

[211] L. A. Carlsson, C.-G. Aronsson, and J. Bäcklund, “Notch sensitivity of thermoset and thermoplastic laminates loaded in tension,” *J. Mater. Sci.*, vol. 24, no. 5, pp. 1670–1682, May 1989, doi: 10.1007/BF01105690.
[212] D. Orlino and N. Caravasos, “Affordable thermoplastic structures (for U.S. Army helicopter tailboom design),” in *36th Structures, Structural Dynamics and Materials Conference*, New Orleans, LA, U.S.A.: American Institute of Aeronautics and Astronautics, Apr. 1995. doi: 10.2514/6.1995-1420.
[213] Ronald Krueger, “A summary of benchmark examples and their application to assess the performance of quasi-static delamination propagation prediction capabilities in finite element codes,” *J. Compos. Mater.*, vol. 49, no. 26, pp. 3297–3316, 2015, doi: Published online before print December 2, 2014, doi: 10.1177/0021998314561812.
[214] O. Falcó, R. L. Ávila, B. Tijs, and C. S. Lopes, “Modelling and simulation methodology for unidirectional composite laminates in a Virtual Test Lab framework,” *Compos. Struct.*, vol. 190, pp. 137–159, Apr. 2018, doi: 10.1016/j.compstruct.2018.02.016.
[215] P. J. Minguet and T. K. O’Brien, “Analysis of Composite Skin/Stringer Bond Failures Using a Strain Energy Release Rate Approach,” in *The Tenth International Conference on Composite Materials*, vol. I, A. Poursartip and K. Street, Eds., 1995, pp. 245–252.

APPENDIX A – OVERVIEW OF THERMOPLASTIC COMPOSITE MATERIALS

Table A-I. Selection of thermoplastic composite materials.

Fiber	Matrix	Material name	Commercial name/vendor	Comments	Source
Polyamid matrix-based composites					
CF	PA 12 (Nylon FX 256)	CF15	Fillamentum©	short carbon fibers (15 vol.%), with approximately 100 μm in length and 10 μm diameter, both obtained in filament form	[98]
CF	PA 6		CPA635 supplied from Jonam Composites - UK	unidirectional prepreg tape	[140, 159]
CF	PA 6		CFR-TP-PA6-CF60-01	unidirectional prepreg from Celanese with a fiber volume fraction of 48% and a ply thickness of 125 μm	[139, 175]
CF/GF	PA 6/PA 66			semi-finished product information and related literature for thermo-stamping process	[143]
T700, TR50	PA 6			PA 6 film was selected as the matrix polymer to prepare the prepreg sheets. Two types of PAN-based fibers T700 and TR50 were used.	[176]
CF	PA 6			Chopped carbon fiber tape reinforced thermoplastics made of randomly oriented carbon fiber tapes. Ultra-thin UD prepreg sheet (44 μm) was used which was manufactured by compression molding.	[177]

Fiber	Matrix	Material name	Commercial name/vendor	Comments	Source
Polyaryletherketone matrix-based composites					
T700	PAEK	TC1225/ T700GC 12K T1E UD Tape	Toray (formerly TenCate)		[30-33]
T700	PAEK	TC1225 LM PAEK	Cetex TC1225 LM PAEK	PAEK polymer from Victrex. LM PAEK has much better flow versus PEKK and PEEK. It also can be processed at higher speeds than PEKK and PEEK	[8, 70, [71, 80, 178]
T300 JB 3K 5HS		Cetex® TC1225	Toray (formerly TenCate)	5HS fabric	[48, 100]
Polyetherimide matrix-based composites					
AS4-3K	PEI		TenCate Advanced Composites	UD carbon-fiber prepregs	[127]
Polyetheretherketone matrix-based composites					
T300 JB 3K	PEEK 150		Cetex TC1200 produced by TenCate		[83, 123, 179]
T300 JB 3K	PEEK		PEEK powder coated semi-preg supplied by TenCate	Carbon fiber bundles with an equal amount of bundles in the warp and weft direction (5HS woven fabric)	[83, 180]
AS4	PEEK	ACP-2		21.5 – 23.8% crystallinity, 64% fiber volume fraction	[17]
AS4	PEEK	ACP-2	ICI Fiberite Corp	62% fiber volume fraction	[14, 18, 125, 141]
AS4	PEEK	ACP-2	ICI Fiberite Corp	60% - 64% fiber volume fraction	[13, 15, 124]
AS4-3K	PEEK		BASF		[142]
AS4	PEEK		CYTEC		[162]
AS4	PEEK	ACP-2	ICI Fiberite Corp	Hercules AS4 fiber in Victrex PEEK matrix, 68% fiber volume fraction	[181]
Tenax®-E HTA40 E13 3K 200tex	PEEK	Tenax®-E TPWF PEEK-HTA40	Teijin	PEEK powdered woven fabric made of high tenacity CF and TP matrix	[182, 183]
Tenax®-E HTS45 24K)/PEEK	PEEK		Teijin		[184]

Fiber	Matrix	Material name	Commercial name/vendor	Comments	Source
Polyetheretherketone matrix-based composites					
CF	PEEK		Tenax®-E thermoplastic unidirectional prepreg PEEK IMS65	processed by automated tape placement.	[108]
AS4	PEEK		Cetex® TC1200 Toray Advanced Composites	UD CF/PEEK tapes, 59% fiber volume fraction	[185]
AS4	PEEK	ACP-2	CYTEC (SOLVAY Group)	Raw material comes in as a roll of tow with nominal width of 0.25 inch and nominal thickness of 0.005 inch.	[186]
IM7	PEEK			UD	[49, 50]
IM7	PEEK		Victrex PEEK	UD	[129]
IM7	PEEK			UD prepreg tape Toho Tenax IM7	[113]
AS4-3K-RC40	PEEK		BASF	Commingled yarn supplied by BASF. The fiber yarn consists of a 60:40 wt% mixture of carbon fibers (AS4, Hercules) and PEEK fibers (150G, 25-40 μm in diameter).	[78]
CF	PEEK			PEEK film and bidirectional plane weave graphite cloth	[86]
T300 JB 3K	PEEK			5HS woven fabric, hot press	[135]
T300	PEEK		EniChem	UD and 8HS fiber impregnated with thermoplastic'. The product is available as a flexible continuous tow of PEEK with embedded carbon fibers, having a diameter of about 0.2 mm.	[128]
CF	PEEK		VICTREX® PEEK 90HMF40	Injection molding compound is PEEK filled with 40 wt.% short carbon fibers.	[100]

Fiber	Matrix	Material name	Commercial name/vendor	Comments	Source
Polyetherketoneketone matrix-based composites					
CF	PEKK	Cetex TC1320	TenCate		[70]
CF	PEKK	Cetex TC1320	Novaspire from Solvay		[70]
CF	PEKK		PEKK polymer (Kepstan® 7003 PT from ARKEMA) and polyacrylonitrile-based UD carbon fibers provided by Porcher Industry		[51]
CF	PEEK				[42, 82, 130]
AS4	PEKK				[88, 168]
AS4C	SC PEKK 7002			28% max crystallinity	[187, 188]
Polyimides matrix-based composites					
T650	PI	T650-35/HFPE-II-52 8HS fabric		8HS fabric	[134]
PolyMethyl-MethAcrylate matrix-based composites					
CF	PMMA		C-Ply™ 200 and 400 g/m^2 from CHOMARAT and Elium® 280 from ARKEMA	NCF bi-angle ply C-Ply™	[72]
GF	PMMA		Elium® 150 from ARKEMA	UD GF plies (400g/m^2) resin infused with PMMA. Fiber volume fraction 50%	[61]
Polypropylene matrix-based composites					
GF	PP		Toyobo Co., Japan	Co-mingled yarn, 50:50 wt% mixture of the two components	[77, 189]
GF	PP			Short glass fiber	[190]
GF	PP			UD tape, 41-45% fiber volume fraction	[138, 191]
GF	PP			UD and multi-layered weft- knitted fabric with non-crimped alignment of the reinforcement fibers	[173]
GF ERS240-T959	K7100		Hebei Inc., China (fiber); Yanshan Petrochemical Co., Ltd., China (matrix)		[192]

Fiber	Matrix	Material name	Commercial name/vendor	Comments	Source
Polypropylene matrix-based composites					
AS4	PP		ExxonMobil isotactic PP, Hexcel AS4	Continuous ~200 mm long carbon fibers (7μm diameter) used to make single-fiber model composites	[59]
TR50S	PP			45% volume fraction	[177]
Polysulfone matrix-based composites					
	PPS	Ryton	Solvay		[70]
	PPSU	Radel R	Solvay		[70]
CF	PPS	Cetex TC1100	Prepreg - TenCate	Prepreg - 34% matrix content by weight, 33.3% crystallinity	[81, 83]
CF/PW			Hexcel PW fabric, Curbell Plastics PPS plastic sheets.	60% volume fraction	[84]
CF/5HS	PPS		Cetex® made by TenCate	5HS woven carbon PPS semipregs	[22, 193]
GF/8HS	PPS		Cetex® made by TenCate	8HS glass fabric	[23, 90]
CF/5HS	PPSS		TenCate	5H woven carbon PPSS prepregs	[193]

Table A-II. Flying structural parts made of thermoplastic composites.

Description	Manufacturer	Material	Manufacturing Process	Size	Date Introduced	Notes	Reference
Lockheed Martin F-22 Raptor landing gear		TPCs			1980s		[194]
Lockheed Martin F-22 Raptor weapons-bay door	GKN Fokker	TPCs			1980s		[194]
Fairchild Dornier 328, Fo 50 ice protection plate	GKN Fokker	Sandwich - carbon fabric TPC facesheets. Kevlar/ PEI	Laser cutting of contour and holes, thermofolding edges, hot dimpling holes, ultrasonic welding of injection pads on rear. Ultem 2300 injection molded window frame is welded onto laminate.		1990s	Protects fuselage from ice flung from propellors.	[67]
Fokker cargo hold cover	GKN Fokker	Glass/PEI 2-2 twill Fabric	Stamp formed continuous fibers.		1990s		[67]
Gulfstream G5 first primary structure	GKN Fokker		Thermoplastic skins bonded to honeycomb		1995		[54, 67]
Airbus 340 wing leading edge access panels	GKN Fokker	Carbon/PPS	Co-consolidated. Metal inserts installed inside hats during the forming process.		2002		[54]
Airbus A350 brackets	GKN Fokker	Carbon/PPS	Stamp formed clips and cleats bolted to skins and frames		2002	The Airbus 350-XWB has over 8,000 TPC brackets.	[67]

Description	Manufacturer	Material	Manufacturing Process	Size	Date Introduced	Notes	Reference
Airbus A380 wing leading edge	GKN Fokker	Glass/PPS, layed-up using singe plies of 8-harness semipreg.	Automated stamp forming and trimming. Eliminated shimming. Skin is laid up first and then ribs are resistance welded to the skin. Spars are mechanically fastened because can't apply the required pressure to both parts during fusion.	9.84 ft to 13.1 ft	Since 2007	>800 ribs and stiffeners per aircraft. Low-cost, continuous fiber reinforced parts. The joined skin and rib parts and weld strip have the same thermoplastic matrix and don't require rivets.	[54, 67]
Gulfstream G500, G600, G650 and G650 ER rudder and elevators - GKN Fokker	GKN Fokker	Carbon/PPS fabric	Butt-joint co-consolidated stiffeners. Final assembly by induction welding using KVE equipment. G650 ribs made in press, beams and skins made with autoclave and incorporates induction welding.	1.2 x 0.7 m torsion box	2008	Seven-year development program. 20% cost/10% weight savings compared with carbon/epoxy due to post-buckled skin design (allow buckling at 70% limit load with stable substructure). G650 - 2010.	[67,195]
Boeing Phantom Eye (UAV) rudder		TPCs fabric	Induction welding		2011		[8]
Airbus 400 cockpit floor	Dahar	Carbon/PEEK			Reported in 2014.		[54, 67]
Boeing 787 brackets		Carbon/PPS			Reported in 2014.	Over 10,000 per aircraft. Provided by Daher.	[54]
Gulfstream 450, 550, 650 floor panels	GKN Fokker	Similar to Airbus. T300/PEI. Ultrasonic spot welding to attached injection molded inserts.	Part of structure is primary structure. Folded edges and welded inserts.		Reported in 2014	Still use metallic fasteners at locations where welding is not possible due to inadequate access or insufficient structurally.	[21, 53-54]
Lockheed Martin C-130 Hercules		Graphite TPC	Ultrasonic welding		Reported in 2014		[54]

Description	Manufacturer	Material	Manufacturing Process	Size	Date Introduced	Notes	Reference
Lockheed Martin Desert Hawk III (UVA) propellers		TPCs			Reported in 2014		[54]
Fokker 50 outer wing trailing edge	GKN Fokker	Carbon/PEI skin			Reported in 2016	Used instead of Carbon/epoxy to sustain heat from the nearby engine exhaust.	[196]
Airbus A340 and A380 inboard leading edges (J-nose)	GKN Fokker	Glass/PPS	Skin is co-consolidated. Ribs are stamp formed and attached to skin with resistance welding using PPS coated stainless steel mesh.		Reported in 2017	20% weight reduction. Welding reduced shimming with tooling used to push the part while its soft to take up the assembly tolerance.	[67, 197-198]
Airbus 220 Wing Fuel Tank Access Doors	Aviacomp	TPCs fabric	Uses induction welding.		Reported in 2018		[71]
Fokker 50 main landing gear doors	GKN Fokker	Carbon/PPS	Assembled with Resistive welding using a PPS coated stainless steel mesh resistive element.		Reported in 2018		[199]
Leonardo (AgustaWestland) AW169 helicopter horizontal tail leading edge	GKN Fokker	Carbon/ PPS	Two omega sections butted between flat skins to produce a full span torsion box. Skin joined to omega sections in hot co-consolidation process. Consolidated leading edges with pre-formed ribs. Thermofolded trailing edges with press-formed ribs.	9.75 ft - 2 ft chord and depth 6 inches	Reported in 2018	JEC 2013 innovation award. 15% lighter than previous design.	[25]

Description	Manufacturer	Material	Manufacturing Process	Size	Date Introduced	Notes	Reference
Bell V280 ruddervator		Carbon/PPS			2019		[200]
Airbus 340-600 ribs and angle brackets	GKN Fokker	Carbone/PPS				Used on keel beam and ailerons.	[54]
Airbus Beluga floor panels	GKN Fokker		Inserts - TP injection molded and UT welded into place.				[201]
Bell V280 experimental aircraft stabilizer access panels		Recycled Carbon/PPS prepreg				60-75% cost reduction. Mechanical properties are much lower than the virgin materials and so limited to potential nonstructural applications.	[200]
Boeing Apache avionics bays panels	GKN Fokker	Carbon/PEI Laminate	Stamp formed.			Cost-reduction initiative.	[202]
Dassault F6X rudder and elevators	GKN Fokker	Similar materials/process as Gulfstream 450, 550, and 650		Skin Thickness is about 1 mm.			[71]
Fokker floor panels	GKN Fokker	Sandwich construction - Glass/PEI. Epoxy adhesive. Nomex core.	Top skin folded over panel edge. Facesheet and core bonded with conventional epoxy adhesive.			Allows for a smooth floor. Prevents carts from getting "snagged".	[203]
Gulfstream rudder trailing edge	GKN Fokker	Toray carbon fiber fabric	A flat laminate is folded around a heated rod.	7 ft long		50% cost savings compared to thermosets. Quality of folded area is low.	[195]

Description	Manufacturer	Material	Manufacturing Process	Size	Date Introduced	Notes	Reference
Lockheed Martin Hawk III (UVA) fuselage protection plates		Glass/PPS					[67]
Lockheed Martin C-130 Hercules	GKN Fokker	Graphite TPC	Ultrasonic welding				[67]
Lockheed Martin - additional uses	GKN Fokker					F-35 flaperons, F-35 ifod, F-16 flaperons, PAC-3 cannisters, F-35 Wiring System, F-35 arresting gear, F-16 landing gear parts.	[67]
Sikorsky UH-60 Black Hawk and CH-53K King Stallion helicopter floors	Sikorsky, Automated Dynamics, DRS Technologies and Fiberforge	TPCs		CH-53K floor: 8.5 ft x 44 ft.		25% cost savings compared with aluminum design.	[53-54]

APPENDIX B - TESTING OF THERMOPLASTIC COMPOSITES ON DIFFERENT LEVELS OF THE BUILDING BLOCK

Table B-I. Coupon testing.

Test	Fiber/Matrix	Material	Comments	Source
Material characterization tests - Flexure tests				
	CF/PA6		JIS K 7017	[176]
	CF/PEEK		ASTM D-790	[78, 85]
	CF/PEEK		ASTM D7264	[162]
	CF/PEEK		ISO 178:2003	[75]
	CF/PPS and PPSS		ASTM D-7264	[193]
	GF/PP		ASTM D-790	[192]
Fracture tests				
CELS	T300/PEEK	Cetex	5HS	[83, 180]
	T300JB-3K/PEEK		5HS	[135]
DCB - static	CF/PA			[139-140]
	AS4/PEEK	ACP-2	UD	[117, 119, 122, 125, 133, 139, 204-205]
	AS4-3K/PEEK		BASF	[142]
	CF/PEEK	Cetex TC1200		[83, 123, 179]
	T300/PEEK	Cetex	5HS	[180]
	T300/PEEK		UD and 8HS	[128]
	CF/PEEK		UD Ciba Geigy	[206]
	CF/PEEK			[86, 132]
	IM7/PEEK	Victrex		[129]
	CF/PEI			[127]
	CF/PI			[134]
	CF/PPS			[81]
	GF/PMMA	Elium 150		[61]
	GF/PP			[77, 138, 189]
DCB - fatigue	C/PA		UD	[139]
	AS4/PEEK	ACP-2	5 Hz; R=0.1; 0.5, Paris Law, growth onset and thresholds	[17]
	AS4/PEEK		3-10 Hz; R=0.1; Paris Law	[207]
Double Torsion	CF/PEI	Ultem 1000	G_{Ic}	[127]
	CF/PEEK	Victrex 15OP	G_{Ic}	[142]
EDT	CF/PC			[12]
	CF/PI			[12]

Test	Fiber/Matrix	Material	Comments	Source
ENF - static	CF/PA			[140]
	AS4/PEEK	ACP-2	UD	[14, 117, 119, 133, 139, 141, 204, 205]
	CF/PEEK	Suprem and Toho Tenax	ASTM D7905	[132]
	CF/PEEK		UD Ciba Geigy	[206]
	IM7/PEEK		UD $[0]_{32}$	[49-50]
	T300/PEEK		UD and 8HS	[128]
	T300JB-3K/PEEK		5HS	[135]
	CF/PI			[134]
	CF/PMMA	Elium® 150 plain weave fabric	VARTM	[208]
	CF/PPS			[84]
	GF/PP			[138]
ENF - fatigue	CF/PEEK	ACP-2	5 Hz; R=0.1; 0.5, Paris Law, growth onset and thresholds	[17]
ELS	CF/PEEK	ACP-2		[13]
MMB	CF/PEEK	ACP-2		[117-121]
Mandrel peel	T300/PEEK	Cetex 5HS		[83-180]
SENB	AS4/PEEK			[137]
	CF/GF/PEEK	Tenax®-E HTA40 3K – PEEK 5HS woven plies prepreg and GF/PEEK prepreg	Hybrid CF fabric and glass	[182]
	GF/PP			[138]
SENT	CF/GF/PEEK	Tenax®-E HTA40 3K – PEEK 5HS woven plies prepreg and GF/PEEK prepreg	Hybrid CF fabric and glass	[182]
SLB	CF/PA			[134]
	CF/PI			[159]
Wedge peel test	C/PA			[175]

Test	Fiber/Matrix	Material	Comments	Source
Impact tests				
	CF/PA6			[176]
	CF/PEEK			[50, 209]
	CF/PPS			[84]
	GF/PP			[191, 192]
SHPB	T300 JB 3K/PAEK	Cetex® TC1225 woven fabric (5-HS)	Energy absorption	[48]
Shear tests				
ILSS	CF/PEEK	Suprem and Toho Tenax,	ASTM D2344	[110, 132]
	CF/PEEK		Chinese standard (JC/T 773-2010)	[210]
	CF/PPS		ASTM D2344	[84]
In-plane shear	GF/PP		Multi-layered weft-knitted fabric, DIN EN ISO 14129	[173]
Iosipescu shear	CF/PEEK			[56]
SBS	CF/PEEK			[75, 83, 123]
Tension tests				
	CF/PEEK		UD, QI, cross-ply and fabric flat specimens 10 x 1.0 in similar to ASTM D3039 - 8000 pounds per minute	[56]
	CF/PEEK			[209]
	CF/PEKK		UD $[0]_8$ and QI plates tested after exposure to Kerosene flame (fire) for 5, 10 and 15 minutes	[51]
	CF/PPS, CF/PPSS		ASTM D-3039	[193]
	GF/PP		ASTM D-3039	[192]
	GF/PP		Multi-layered weft-knitted fabric, DIN EN ISO 527	[173]

Table B-II. Sub-element level testing.

Test	Fiber/Matrix	Material	Comments	Source
Bending tests				
3PB	AS4/PEEK		The hybrid butt jointed skin-stiffener specimens were cut from a panel into small pieces width 14.9 mm, nominal length 70 mm span 57 mm.	[168]
Compression tests				
CAI	CF/PEEK		UD, QI, cross-ply and fabric flat panels 5 x 10 in - 8000 pounds per minute. Flat specimens 1.5 x 2.25 in - 8000 pounds per minute	[56]
CAI	CF/TP		Test and analysis approach development comparison	[157]
		ACP-2	Specimen with imbedded through-the-width delamination. UD layup $[0]_{64}$ chosen to provide correlation with results from UD DCB, ENF and CLS test.	[204-205]
Curved Beam tests				
	TPS50/PP		UD 25 ply specimens	[177]
	CCT/PA6		Chopped CF tape	[177]
	CF/PEEK	Suprem and Toho Tenax	ASTM D6415	[110]
Single-Lap Shear (SLS)				
SLS	CF/PAEK		LM-PAEK SLS test developed at DLR	[80]
	CF/PAEK		SLS-test to characterize the weld	[178]
	AS4D/PEKK-FC		ASTM D3165 to characterize the weld	[88]
	CF/PPS		DIN EN 1465 – SLS test to characterize the weld	[66]
	GF/PPS		Cetex® 8 harness satin weave glass fiber reinforced PPS, ASTM D1002	[90]

Test	Fiber/Matrix	Material	Comments	Source
Tension tests				
Uniaxial tension	AS4/PEEK		$[\pm45]_{2s}$	[165]
OHT	AS4/PEEK	ACP-2	$[0]_{16}$, $[90]_{16}$, $[\pm45]_{4s}$, $[0/\pm45/90]_{2s}$ eccentric open hole tension	[181]
	AS4/PEEK		$[0/45/90/-45]_{2s}$	[163]
	AS4/PEEK		$[0/45/90/-45]_{2s}$, $[0/90_2/0]_{2s}$, $[\pm45]_{4s}$	[164]
	AS4/PEEK	ACP-2		[211]
CEN	AS4/PEEK	ACP-2		[211]
DEN	AS4/PEEK	ACP-2		[211]
	CF/PEKK		Butt joint pull-off	[168]
Fire exposure				
	CF/PEKK	PEKK polymer (Kepstan® 7003 PT from ARKEMA) and Polyacrylonitrile UD CF provided by Porcher Industry	UD $[0]_8$ and QI $[0/+45/-45/90]_S$ - kerosene flame exposure (thermal aggression of 116 kW/m^2 and 1100°C for 5-10-15min) and residual mechanical behavior	[51]

Table B-III. Element level testing.

Specimen	Fiber/Matrix	Comments	Source
Hat-stiffener	IM7/ITX	Y-Frame Element using fastener-less single diaphragm/co-consolidation process. Frame pull-off test.	[11]
	CF/PEEK – Suprem and Toho Tenax6	An omega-shaped stiffener was made using a novel manufacturing approach using winding and laser-assisted tape placement (LATP) to lay up the specimen.	[110]
Blade-stiffener	IM7/ITX	Element made using fastener-less single diaphragm/co-consolidation process. Frame pull-off test.	[11]
	T300/PAEK 5HS (laminate) and PEEK with 40 wt.% short fibers (for over-molding)	Over-molded stiffener (rib). Melt temperature, packing pressure, injection speed, number of gates as well as the time of insert residing in mold before injection was varied. Some of the manufacturing parameters showed no significant effect; others largely affected the response of the pull-off test.	[100]
Lug-element	AS4/PEEK-ACP-2	Tensile test for analysis validation	[11]
Tube	CF/ Elium® 150 resin	Tubes made of woven CF and Elium® 150 resin in B-RTM process. Volume fraction of 55–56%. Carbon/Elium® composites under low-velocity impact have shown higher peak load and major energy absorbing capability compared to carbon/epoxy tubes. Impact test results with Elium® composite have shown interlaminar failure, matrix cracks, and crack bifurcation features whilst epoxy composite tube has shown highly localized and catastrophic failure.	[73]

Table B-IV. Higher level testing (sub-component, component and sub-structure).

Item	Fiber/Matrix	Comments	Source
Rotorcraft tailboom	CF/TP	A three-foot-long, two-foot-diameter cylindrical shell was fiber-placed (in-situ consolidation) and ballistically tested. Based on test results two configurations (16-ply and 10-ply skin) were developed for further study. Both configurations had the same type and number of frames (4) and longerons (6). The 10-ply-minimal skin thickness configuration additionally had crack arrestors (6 straps).	[212]
Multifunctional rudder leading edge	CF/PEI	A heat emitting layer made of Satin 8H glass fabric with unidirectionally interwoven 316 stainless steel fibers formed the top ply. Further, a copper mesh to improve erosion was placed on top of the laminate mode of CETEX Carbon/PEI which was consolidated and thermoformed.	[23]
Demonstrator leading edge	CF/PPS	Demonstrator leading edge section for A 330-200 welded by means of induction heating. Demonstrator consists of CF/PPS with an Atlas 1/4-weave. No welding aid was needed because the CF-fabric is conductive itself and can melt the PPS within seconds.	[66]
Wing box	CF/PEEK	The demonstrator wing box is 750 mm long and wide, which is representative of a section between two ribs. The height was 240 mm. The hat stiffeners and spars are integrated into the top and bottom panels of the wing box resulting in a single-piece blended structure with no fasteners or joints. CF/PEEK tows are used for ATP manufacturing. The proposed design has been virtually verified via high fidelity FE analysis.	[108-112, 132, 158]
Stiffened panel	IM7/PEEK - Toho	The stiffened panel (600 mm by 320 mm) was manufactured via tow steering. A 3-point bending test fixture was used to induce compression to the skin. The test was relatively simple to perform compared to traditional pure compression tests, as no critical and time-consuming alignment steps were required prior to testing. The test method was designed using FE models, experimentally validated, and the results were compared against a numerical model (based on the Ritz approach) and FE analysis.	[113]
Three-stringer panel	LMPEAK	Analysis and testing of three-hat-stringer panel (556 mm width by 500 mm length) under compression. The length of the panels is according to the maximum welding length possible. A combined numerical and experimental methodology is in development to evaluate the strength of the welded joint between skin and stringer.	[167]
Three-stringer panel	CF/PEKK FC and GF/PEEK FC	The stiffened panel is 495.3 mm long and 344.8 mm wide. Three stringers with a non-symmetric design have a spacing of 152.4 mm. An artificial	[130]

		delamination (40-mm Teflon insert) was created between the skin and the middle stringer. The delamination is extended to 70 mm in a testing machine and propagation is modeled using VCCT.	
Aircraft horizontal tail demonstrator	Solvay APC (PEKK-FC)/ AS4D	manufactured by GKN Fokker	[70]
Fuselage panel	CF/LM PAEK - TenCate	Fuselage panel with integrated stiffeners. Press-formed omega and butt-jointed T-stringer elements that were welded to the AFP manufacture skin.	[70]
Torsion box demonstrator	CF/TP	Design uses rib stiffeners co-consolidated with the AFP skin	[25]
Fuselage demonstrator	CF/TP	Developed and produced by GKN Aerospace's Fokker business, features fully welded frames using butt jointed orthogrid technology	[25, 105]
Engine pylon upper spar	CF/PEEK	A 6m-long, 28mm-thick spar produced by NLR made using AFP but consolidated in an autoclave	[25]
Multifunctional fuselage demonstrator	CF/PEEK CF/LM PAEK	Multifunctional Fuselage Demonstrator (MFFD) (8m long, 2m diameter), is one of three full-scale demonstrators within the Large Passenger Aircraft (LPA) Innovative Aircraft Demonstration Programs (IADPs)	[24-27, 106]

APPENDIX C – SELECTED MATERIAL DATA

Table C-I. Elastic constants for baseline thermoset composite materials.

	IM7/8552 [213]	**AS4/8552** [214]	**IM6/3501-6** [215]	**T300/1076** [213]	**C12K/R6376** [213]
E_{11} – GPa	161	137.1	144.7	139.4	146.9
E_{22} – GPa	11.38	8.8	9.65	10.16	10.6
E_{33} – GPa	11.38		9.65	10.16	10.6
ν_{12}	0.32	0.314	0.3	0.3	0.33
ν_{13}	0.32	0.314	0.3	0.3	0.33
ν_{23}	0.45	0.487	0.45	0.436	0.33
G_{12} – GPa	5.5	4.9	5.2	4.6	5.45
G_{13} – GPa	5.2	4.9	5.2	4.6	5.45
G_{23} – GPa	3.9		3.4	3.54	3.99

Table C-II. Elastic constants for selected thermoplastic composite materials.

	AS4/PEEK [163]	**PEEK IMS65** [108]	**IM7/PEEK**[49]	**LM-PAEK TC1225** [167]	**AS4D/PEKK-FC** [88]
E_{11} – GPa	127.6	135.0	150	116.8	138.3
E_{22} – GPa	10.3	7.54	9	9.1	10.4
E_{33} – GPa					
ν_{12}	0.32	0.3	0.3	0.36	0.316
ν_{13}					
ν_{23}					0.487
G_{12} – GPa	6.0	5.0	5	4100	5.19
G_{13} – GPa					5.19
G_{23} – GPa					

Table C-III. Fracture toughness data for baseline thermoset composite materials.

Material	G_{Ic} kJ/m^2	G_{IIc} kJ/m^2	η	Comments	Source
IM7/8552	0.212	0.774	2.1	Baseline state of the art carbon fiber/epoxy	[114-116]
AS4/3501-6	0.0818	0.554	1.75	Epoxy with AS4 fiber	[117]
IM7/E7T1	0.161	2.05	2.35		[117]
IM7/977-2	0.306	1.68	1.39		[117]
IM7/977-2	0.298			DCB	[129]
T300/1076	0.17	0.494	1.62		[213]
C12K/R6376	0.341	1.286	3.39		[213]

Table C-IV. Fracture toughness data for selected thermoplastic composite materials.

Material	G_{Ic} kJ/m^2	G_{IIc} kJ/m^2	η	Comments	Source
AS4/PEEK (ACP-2)	0.949	1.35	0.63		[117, 119]
AS4/PEEK (ACP-2)	0.948	1.273	0.456		[118]
AS4/PEEK (ACP-2)	0.969	1.719	2.284		[118-119]
AS4/PEEK (ACP-2)	0.8304	1.251	-		[120]
AS4/PEEK (ACP-2)	1.3	2.5	-		[121]
AS4/PEEK (ACP-2)	1.182			DCB $G_{Ic, NL}$	[122]
C/PEEK - Cetex TC1200	1.27			DCB	[83, 123]
C/PEEK UD Ciba Geigy	2.0			DCB 2 mm/min ENF 1 mm/min	[206]
AS4/PEEK-ICI ACP-2	1.56			DCB $[0]_{26}$ Crosshead rate 0.25 mm/min COD rate 0.02-1.6 m/s 10^{-10}	[125, 204-205]
AS4/PEEK-ICI ACP-2		1.8 {1.84}		ENF $[0]_{26};[0]_{40}$ Crosshead rate 0.25 mm/min Sliding velocity 2.86 m/s 10^{-9}	[14, 204-205]
AS4/PEEK-ICI ACP-2	1.315 1.546 (G_{IR})			DCB $[0]_{24}$ 1 mm/min	[124]
AS4/PEEK-ICI ACP-2	1.404			DCB $[0]_{24}$	[13]
AS4-3K-PEEK BASF	2.6			DCB UD 30% crystallinity, crosshead rate 3.2 mm, crack speed 10^{-6} m/s	[142]

Material	G_{Ic} kJ/m^2	G_{IIc} kJ/m^2	η	Comments	Source
T300 FIT /PEEK.	1.98			DCB $[0]_{14}$ crack speed 3.3 10^{-11} m/s	[128]
IM7/PEEK		0.6 – 1.3		ENF $[0]_{32}$	[49-50]
IM7/PEEK Victrex	1.83			DCB crosshead rate 2 mm/min	[129]
AS4-3K-PEI	1.7			DCB $[0]_{16}$ 10^{-5} m/s	[127]
CF/PA 6	3.44			DCB $[0]_{40}$	[139]
C/PPS - Cetex TC1100	0.95			DCB – press consolidated; cooling rate 5°C/min, 33.3% crystallinity	[81, 83]
CF/PEKK	1.41	1.9	2.3		[130]
AS4D/PEKK-FC Solvay	0.7(G_c)	1.45(G_c)			[88]